# Multilayer Design for Increased Toughness of CrN-based Coatings




**Doctoral Thesis**

**Dipl.-Ing. Manfred Schlögl**

Department of Physical Metallurgy and Materials Testing
Montanuniversität Leoben

Leoben, December 2012

This work was supported by the Austrian Science Fund
in the framework of START Project Y371.

*Affidavit:*
I declare in lieu of oath, that I wroth this thesis and performed the associated research myself, using only literature cited in this volume.

Leoben, December 2012

Manfred Schlögl

# Acknowledgements

First of all, I want to express my sincere gratitude and appreciation to my supervisor **Paul H. Mayrhofer** for his endless support and trust. Thank you for pushing and motivating me during the thesis always at the right times. I am grateful to the opportunity to have learned from you how to act as a great boss. Despite your new challenges at the TU Wien, the associated efforts and troubles you had during the transfer, you always found time for supporting the whole group in our scientific work. Thanks for being such a great teacher and friend.

I am grateful to **Jörg Paulitsch** for being a great "Co-Supervisor" and primarily for being a good friend. Thank you for your great support during this thesis and all the endless discussions during countless tennis games.

I also want to thank **Jozef Keckes** for many scientific discussions and his support especially during the micro-mechanical test experiments. You provided me with an access to the equipment at, and the knowledge from all the experts of, the Erich Schmid Institute hence turning this thesis into a really exciting thing for me.

I cannot leave out from these acknolwdgements my Diploma Student, **Bernhard Mayer**, and my student co-workers **Heribert Marihart** and **Annika Vieweg** for their excellent experimental work providing a lot of important results for this thesis. In the line with them I want to express my personal thanks to **Bruno Krajnc** for enthusiastic discussions during the development of the rotating substrate holder, called "Hendlgriller".

I am also grateful to all my former and present colleagues at the thin film group, but also the "Substrate Group" at the Department of Physical Metallurgy and Materials Testing in Leoben, for making the last three years so enjoyable and so much fun for me. Special thanks to, **Robert Hollerweger**, **David Holec**, **Corinna Sabitzer**, **Helmut Riedl**, **Christian Koller** and **Christoph Kirchlechner** for their encouragement in science but also in life!

Special thanks to my “Three Musketeers”, **Christopher Pöhl**, **Christoph Lerchbacher** and **Matthias Nöhrer**. I am grateful for your friendship and for supporting me all situations of my life during my study. I will never forget all the countless hours I have spent with you, especially at the “Admiral”. Your friendship I would never want to miss!
“*One for All, All for One!*”

Ein ganz besonderes “Danke” gilt meiner **Familie** die mich in allen Lebenslagen immer unterstützte. Ihr wusstet mich aufzurichten, zu bremsen, zu ermutigen und habt mir trotz meines turbulenten Lebens zuhause immer einen Ort der Ruhe und Entspannung gegeben. Vielen Dank!

# Contents

Chapter 1

# Introduction

The success of our society is strongly linked to the development of new materials. Moreover, due to the growing awareness regarding environmental and economic issues, research and development of highly potential materials become more attractive than ever before. However, one of the most difficult parts is to find a material covering all the different requirements needed in high end applications. Therefore many scientists start to combine materials having different properties, e.g. good thermal and oxidation behavior, high hardness and toughness, good electrical and thermal conductivity. Such combinations extend the possibilities for the industry producing materials with a specific property profile. In addition assembling the materials in such a way as to have attributes not offered by any one material alone can be achieved by different architectural designs. Figure 1.1 demonstrates combinations of different configurations which allow superimposition of their properties and the creation of "new materials" with tailored properties.

Nevertheless, the protection of bulk materials by coatings is well known for a long time. Especially ceramic hard coatings such as nitrides ranging from a few nanometers to several micrometers which were synthesized by physical vapor deposition (PVD) or chemical vapor deposition (CVD) techniques extend the life time of numerous components, decreasing the costs for the users and take care of the environment. Particularly, transition metal nitrides, such as CrN are widely used for various industrial applications because of their outstanding properties like high thermal stability, oxidation resistance and abrasion resistance.

In general a trend from macro-scaled towards nano-scaled materials could be observed during the last decades. This allows new design concepts for stabilizing materials in their metastable phases within a stable matrix, by e.g. in two or three dimension configurations (multilayers, precipitates, nanocomposites). Multilayer coatings having a single layer thickness in the size of lattice parameters are well known as a superlattice [2] and become more important in the nanostructure community in the last decades. The characteristic of these coatings are simply explained by a hardness profile with a sharp super hardness peak and excellent wear

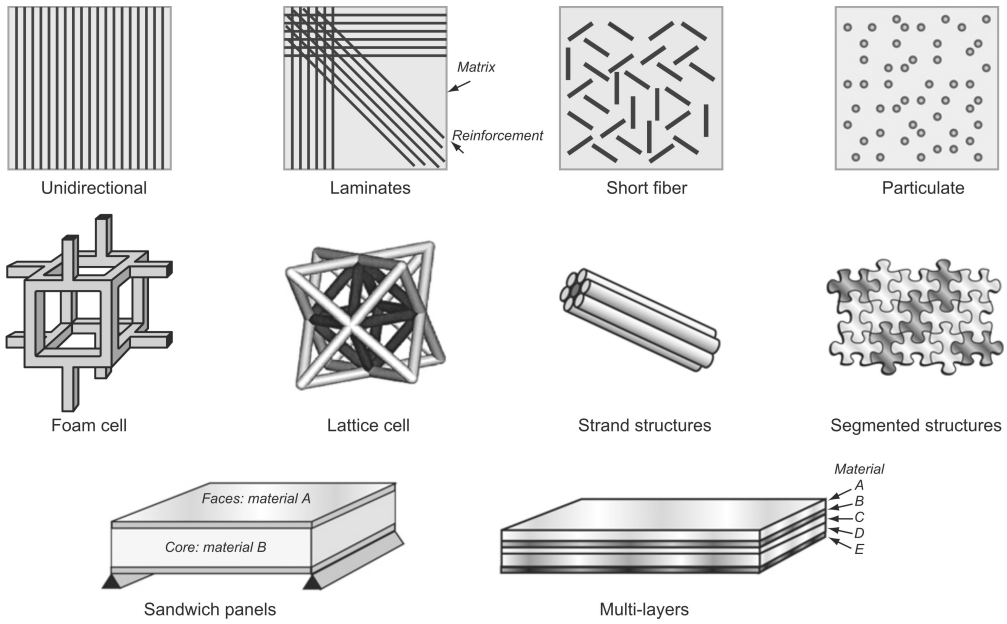


Figure 1.1: Different architectured material configurations and connectivity options [1].

and oxidation resistance when having fully cubic stabilized structure [3].

CrN/AlN superlattice coatings are well known to fulfill these requirements which have been reported to be mainly influenced by the AlN layer thickness [4, 5]. Therefore publication I and II are devoted to both individual layer thicknesses, of CrN and AlN within CrN/AlN superlattice coatings and their influence on structure and morphology. Moreover, the effect of different structure on hardness and thermal stability were discussed in detail featured by high resolution transmission electron microscopy (HRTEM), differential scanning calorimetry (DSC), thermal gravimetric analyzes (TGA), nanoindentation and X-ray diffraction (XRD) measurements.

Recent studies showed tremendous improvement of thermal behavior when stabilizing AlN in its metastable cubic structure within single ternary Cr–Al–N thin films. Further incorporation of the reactive trace element yttrium improves the oxidation behavior and increase the hardness as it promotes grain refinement. While these previous studies concentrate on the cubic stabilization of AlN in single layered Cr–Al–N and Cr–Al–Y–N thin films, publication III is devoted to the stabilization of metastable cubic AlN in a layered architectural design. Here the cubic stabilization of AlN in CrN/AlN, CrAlN/AlN and CrAlYN/AlN multilayers and the effect of the different structure in AlN layers on mechanical and thermal behavior were investigated in detail.

One of the major challenges for coating materials especially when having ceramic bonding character (mixed ionic and covalent) are their brittleness which often limit their usage in numerous applications. The interaction of such brittle coatings with notch sensitive bulk

materials such as gamma titanium aluminide ($\gamma$-TiAl) based alloys has considerable risks for components in e.g. aero engines.

Interfaces in a multilayer structure provide obstacles for the crack propagation and contribute to increased fracture toughness by different interface mechanisms, e.g. crack splitting and deflection. In addition a stress induced transformation within CrN/AlN multilayers of metastable cubic stabilized AlN in its stable wurtzite phase is connected with a volume expansion of 26% and suggest promising results for the fracture behavior. Hence, publication IV is related to the investigation of the influence of fully cubic stabilized AlN as well as mixed wurtzite and cubic structured AlN layers within CrN/AlN multilayer coatings on the fracture behavior. The results were discussed in detail by comparing with the fracture behavior of monolithic CrN coatings. The successful development of the fracture toughness of such brittle ceramic coatings depends on the fracture mechanism and the crack path. Therefore micro-mechanical tests such as bending, tensile, compression and nanoindentation have become a frequently used technique to determine the fracture behavior of different materials in a micro-scaled range. Within this thesis compression, bending and tensile tests were used to provide various perspectives for the investigation of the fracture mechanism of CrN/AlN multilayer coatings whereby publication IV is only related to compression tests.

The following chapters give a short introduction to the fundamental materials of this thesis, CrN and AlN in single as well as multilayer architecture and state of the art regarding their hardness, thermal stability and fracture toughness. Furthermore, an extensive description of in-situ fracture tests in a micro-scaled range is provided which gives a significant contribution to the field of fracture toughness of hard ceramic coatings.

Chapter 2

# Background and Motivation

## 2.1 Hard Ceramic Coatings

Hard ceramic coatings can be distinguished by their bonding character (metallic, covalent and ionic) and their corresponding change in properties as shown in Fig. 2.1 [6–8], and by their hardness as they can be classified in "normal" hard (> 20 GPa), "super-hard" (< 40 GPa) or "ultra-hard" (< 80 GPa) coatings [9].

Carbides, borides, nitrides and oxides have been used in the last decades for aerospace, tools, molds and dies due to their outstanding properties [6]. Especially transition metal nitrides (TMN) exhibit properties like wear and corrosion resistance, high hardness, thermal stabil-

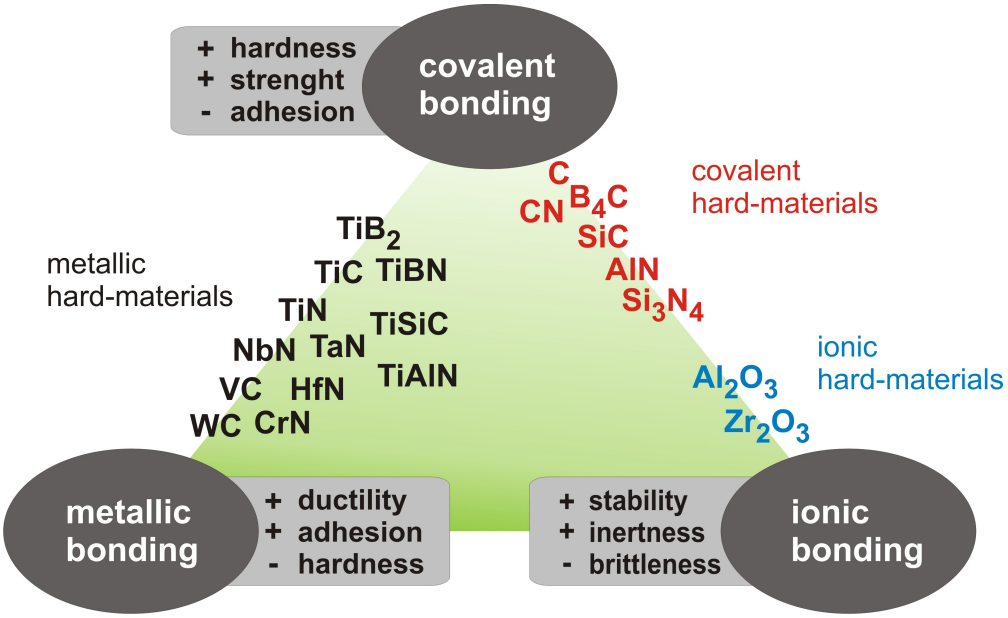


Figure 2.1: Classification of hard ceramic coatings according to their bonding character and their change in properties (modified after [6–8]).

ity and electrical conductivity increasing the life time of many components [10, 11]. These attractive properties can be adjusted during growth in plasma-assisted vapor conditions by varying grain size and defect density [10]. Hence nanostructured materials and microstructural changes for such hard coatings become more important and are well established [12, 13]. In addition, excellent mechanical properties of ceramic coatings can be attributed to the mixture of metallic, covalent and ionic bonding character [6]. Due to the ever growing demand on improved properties TMNs such as CrN and TiN were developed by partial substitution of the transition metal with Al resulting in $Cr_{1-x}Al_xN$ and $Ti_{1-x}Al_xN$ having superior properties compared to their binary nitrides [14–19]. Moreover, recent studies focused on the synthesis of multinary coating systems by the incorporation of additional elements like Nb, Ta and Y.

Based on the architectural coating design of nanocomposite materials having excellent hardness, separated TMN phases in layered structure (multilayer) were found to create new opportunities of the usage of ceramic hard coatings [20–23].

## 2.2 CrN Based Coatings

The binary phase diagram of Cr–N shown in Fig. 2.2 is characterized by intermetallic hexagonal $Cr_2N$ and CrN phases in the solid state. Depending on the temperature, CrN is indicated by orthogonal ($T \lesssim 265$ K) and cubic (B1) structure modifications [25]. As this work is focused on face-centered cubic structured CrN special attention is given to the NaCl modifi-

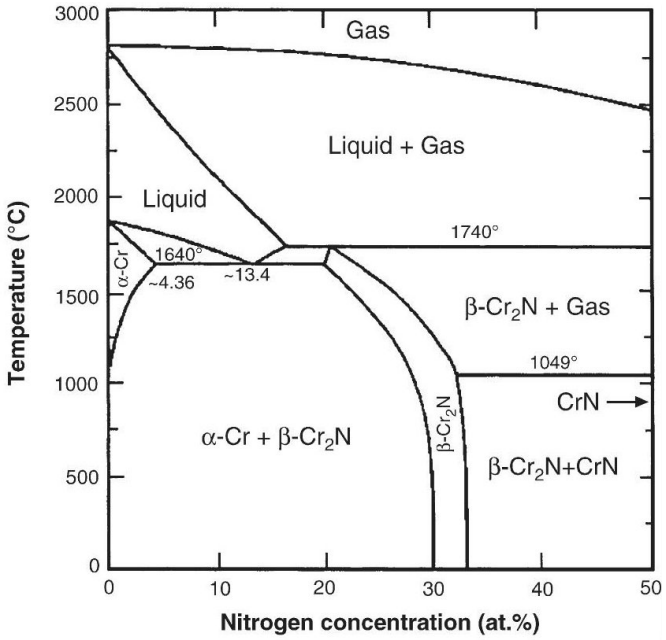


Figure 2.2: Binary phase diagram Cr–N [24].

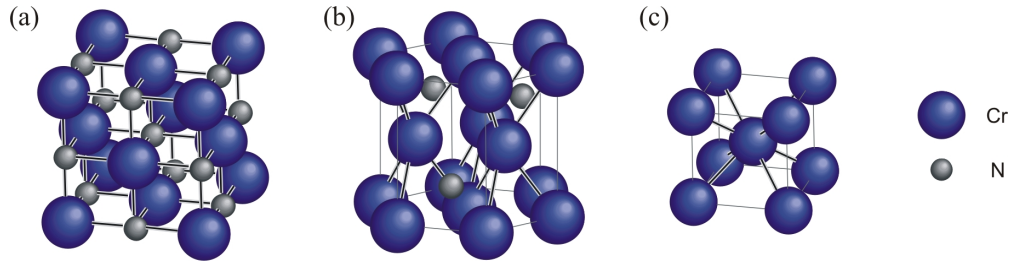


Figure 2.3: Schematic of the lattice structure of a) NaCl structured CrN, b) hexagonal $Cr_2N$ and c) bcc Cr [34].

cation having lattice parameter of $a = 4.140$ Å [26]. Such a structure configuration is shown in Fig. 2.3a where the nitrogen is placed at the octahedral interstitial sites of a face centered cubic lattice formed by Cr atoms. Together, Cr and N form a NaCl type lattice. CrN exhibits mainly metallic bonding character with ionic and covalent binding contributions [27]. The compositional range of CrN is very small and decomposition depends on the nitrogen partial pressure as can be seen in Ref. [28]. In general the decomposition temperature at atmospheric pressure varies from 400 °C to 1000 °C [19, 29–31]. As shown by Mayrhofer *et al.* [30] annealing of CrN in inert atmosphere leads to decomposition into $Cr_2N$ with $N_2$ release at temperatures ranging from 1000–1250 °C. This hexagonal closed packed structure is indicated by randomly arranged N-atoms within the interstitial sites of the Cr-matrix [32], see Fig. 2.3b ($a = 4.752$ Å, $c = 4.429$ Å [33]). Further annealing to higher temperatures result in dissociation of $Cr_2N$ into the body-centered cubic (bcc) Cr (Fig. 2.3c) and $N_2$ [30].

CrN hard coatings are well known for their good oxidation resistance, high hardness (24 GPa, [35]), chemical inertness and wear resistance [16, 36–38]. The combination of all of these properties is highly attractive for applications in tooling, automotive, aerospace and decorative industries [31, 39]. Nowadays, increased mechanical and thermal properties of monolithically grown CrN coatings can be achieved by alloying with different elements [16, 40, 41].

## 2.3 AlN Coatings

AlN exists in a stable hexagonal close packed wurtzite-type (B4) crystal structure having lattice parameter $a = 3.1114$ Å and $c = 4.9792$ Å [42] (see Fig. 2.4a). This modification exhibit covalent binding character with ionic contributions [6, 17] and a high thermal resistance against decomposition up to 2800 °C. AlN is also able to exist in a metastable high pressure cubic modification having a face centered cubic NaCl (B1) structure with a lattice parameter of $a = 4.05$ Å [43] (see Fig. 2.4b). Figure 2.4c displays the cubic ZnS-structure (B3) which can be epitaxial stabilized for some nanometers [44, 45].

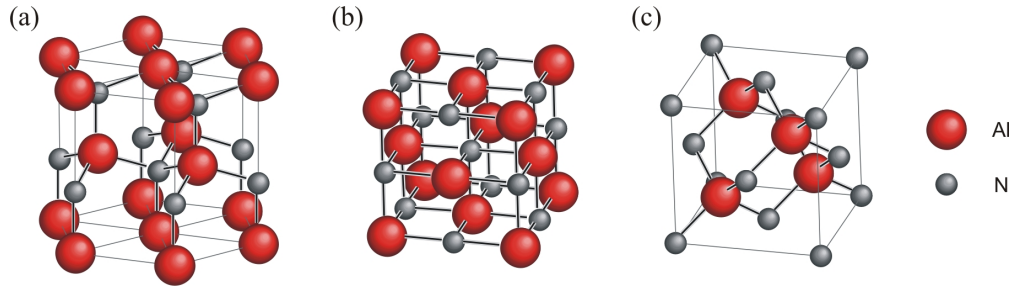


Figure 2.4: Possible crystal lattice structures of AlN. a) wurtzite, b) NaCl and c) ZnS type [34].

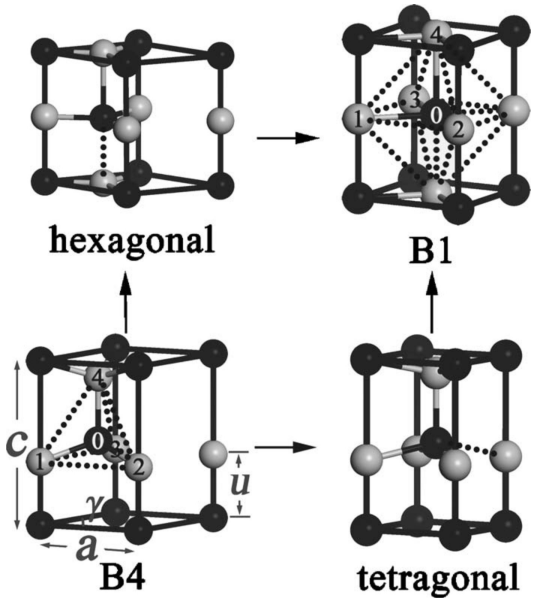


Figure 2.5: Schematic representations of B4 → B1 phase transformation along the hexagonal and tetragonal path. The dark and gray balls indicate N and Al atoms, respectively [46].

By means of high pressure the wurtzite B4 structure can be transformed into the NaCl (B1) structure. Cai and Chen [46] summarized different models of the transformation paths from the wurtzite (B4) to the rocksalt (NaCl) structure (B1) by two different mechanisms as shown schematically in Fig. 2.5. These hexagonal and tetragonal paths are two stage processes in which the hexagonal path is the energy-favored transition path for the AlN [47]. Such a transformation was observed to occur by a sudden movement of Al and N atoms [47]. *Ab initio* calculation by Mayrhofer, Willmann, and Reiter [19] and Mayrhofer, Music, and Schneider [17] reveal an $\sim 1.26$ times larger specific volume of h-AlN compared to c-AlN.

AlN is well known for good insulating properties, a high breakdown field, low diffusivity for dopants and high thermal conductivity of around 2 W cm$^{-1}$ K$^{-1}$ [48]. Due to its wide band gap of 6.2 eV [48] the most interest on AlN is given on its potential for electrical and optical applications such as semiconductors and lasers [49, 50].

## 2.4 CrN/AlN Multilayer

Research and development of multilayered structured hard coatings since the 1980s has become increasingly important. Especially multilayer coatings consisting of two different assembled materials upgrade the properties of monolithically grown coatings. These improvements can be obtained in compounds consisting of metal/ceramic or ceramic/ceramic layers [51–56]. In such multilayer systems the layer thickness, the number of layers and consequently the number of interfaces as well as the condition (sharpness) of these interfaces characterize the properties of the coatings. In addition the crystallographic relationship between the layers and the base layer to the substrate is one of the most influencing parts within a multilayer system. As generally the most important properties-improvements are obtained for multilayer coatings with epitaxial grown layers this has to be taken into account at the beginning of developing a multilayer system. Such growth mechanisms depend on the difference in lattice parameter and the ability of the lattice to adjust for small misfits. The lattice mismatch is attributed to the crystallographic relationship of different crystal structures of adjacent materials which is well known as hetero-epitaxy. In contrast to homo-epitaxy where the crystal structure of the materials are identical and the lattice parameters are perfectly matched, the lattice-mismatch in hetero-epitaxially grown coatings results in coherency strains [57].

Nowadays, significant improvements in terms of hardness [58], oxidation resistance [59], wear and corrosion resistance [60], toughness [61] and tribological properties [2] have been extensively reported for multilayer coatings where the layer thickness is in the range of a few nanometers forming a superlattice structure. Such low layer thickness configuration is also used for CrN/AlN multilayers having increased thermal and mechanical properties compared to their monolithic coatings.

This work focuses on the CrN/AlN superlattice system having cubic CrN layers and different modification of AlN layers. Recent studies reveal a critical AlN layer thickness of $\sim 3$ nm to have either cubic or wurtzite structure. Nevertheless, the critical size can be influenced by the density of misfit dislocations at the interface of CrN and AlN layers where the interface is more incoherent and the film becomes more relaxed. Figure 2.6 represents a schematic image for (a) fully coherent (epitaxial), (b) semicoherent and (c) incoherent (non-epitaxial) interfaces.

For the fully coherent grown coatings (Fig. 2.6a) the cubic CrN operate as template for the AlN and stabilize it in its metastable cubic structure. These coatings are indicated by a coherently matched interface and a hetero-epitaxial growth. The overall CrN/AlN multilayer coatings with layer thicknesses in the range of a few nanometers exhibit NaCl structure. Lower lattice parameter for c-AlN ($a = 4.05$ Å [43]) compared to c-CrN ($a = 4.149$ Å [26]) induce tensile stresses for AlN and compressive stresses for CrN at the interface [63].

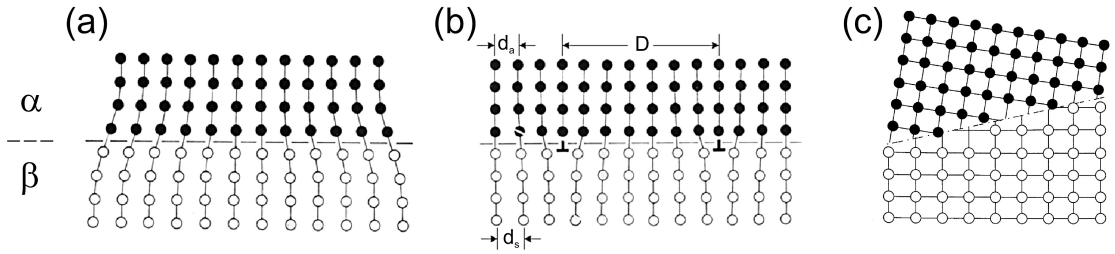


Figure 2.6: Schematic of (a) coherent interfaces with slight lattice mismatch, (b) semi-coherent interface and (c) in-coherent [62].

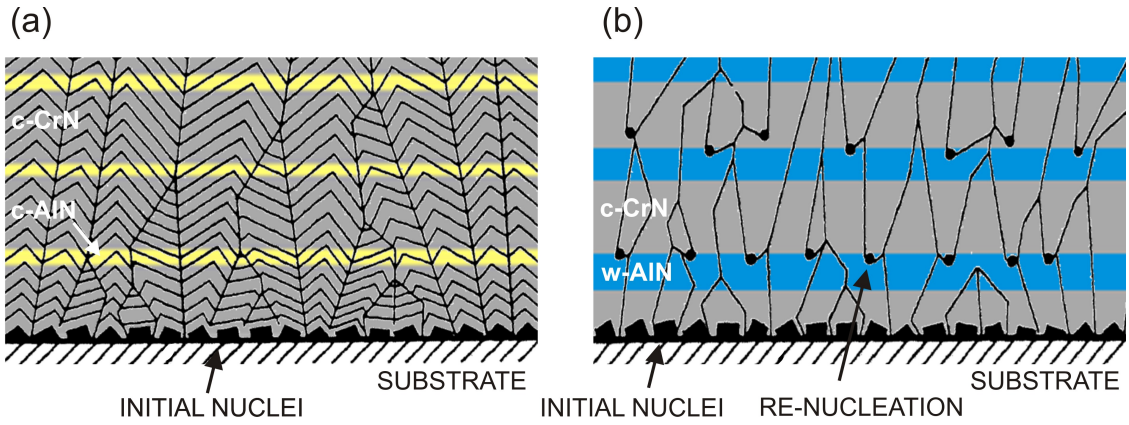


Figure 2.7: Schematic of the different crystal structure in CrN/AlN multilayers with (a) cubic AlN layers and (b) wurtzite AlN layers (modified after [64]).

These stress fields at the interface can change the physical properties and affect the fracture behavior as described in section 3.1.

AlN layers passing the critical layer thickness cannot be stabilized in the metastable cubic structure and transform into the stable wurtzite form. This transformation interrupts the epitaxial growth in CrN/AlN multilayers resulting in semicoherent (Fig. 2.6b) or incoherent (Fig. 2.6c) interfaces. Hence pronounced columns in the growth direction as promoted by epitaxial grown CrN/AlN layers (see Fig. 2.7a) are inhibited due to re-nucleation of the cubic CrN layers at the interfaces (Fig. 2.7b).

### 2.4.1 Hardening Effects in CrN/AlN Superlattice Coatings

The combination of two nitride hard coatings such as CrN and AlN within a layered superlattice structure has been shown to exhibit super hardness values above 40 GPa [4]. This increase in hardness can be explained by several hardening mechanisms based on the concept of nanocrystalline materials including image forces on dislocations, dislocation motion in an alternating strain field, the supermodulus effect and the Hall-Petch effect [21]. Especially nanocomposites composed of at least two different phases with coherent boundaries in the

nanoscale regime impede grain boundary sliding and strengthen the material. As dislocation motion is required for plastic deformation, density and mobility of dislocations have to be decreased. This can be achieved by decreasing grain size and consequently increased grain boundary density. A good approach for this strengthening mechanism related to hardness and grain size is described by the well known Hall-Petch relation

$$H = H_0 + kD^{-1/2} \tag{2.1}$$

where $H$ is the resulting hardness, $D$ is the grain size, $H_0$ is the hardness of the material with large grains and $k$ is a material constant [65]. The model used for polycrystalline bulk materials is based on the theory that dislocations are hindered at the grain boundaries, pile up and initiate a dislocation source in an adjacent grain. Many publications were found using this Hall-Petch relationship for multilayers by replacing the grain size with the multilayer period. Nevertheless this is a rough assumption for superlattice coatings with bilayer periods $< 20$ nm as only few dislocations are present compared to monolithically grown coatings. This makes it necessary to extend the model and consider in addition to the number of dislocation loops in a given layer, effects of a mismatch in slip plane orientation, lattice mismatch between the layers, image forces on dislocations, the dislocation core spreading into the interface, structural differences between the layers and the difference in stacking fault energies. A detailed description of the modified Hall-Petch model elaborated by Anderson et al. can be found in [66–69]. In general, the model describes the dependence of the hardness on the bilayer period.

Several theoretical contributions explained the mechanical properties of multilayer coatings by the Peach-Koehler image forces created by the different dislocation line energies in each layer [21, 70–74]. Multilayer structured materials having different shear moduli within each layer would require additional stress to move dislocations over layers [75]. Dislocation moving towards the interface were rejected when located in the elastically softer layer and attracted when located in the stiffer one [72]. Within CrN/AlN multilayer coatings the c-CrN layers exhibit lower shear modulus than c-AlN hence higher forces would be required for dislocation to overcome the interface [4]. As the minimum stress required for the formation of new dislocations is related to the distances between the pinning points small layer thickness within a multilayer impede the activation of dislocation sources (such as Frank-Read source) [76]. This decreases the density of dislocations and avoids the generation of new ones which contributes to plastic deformation. In contrast, multilayers having increased layer thickness will force the formation of dislocations and enable large distances which are not contributing to a hardening mechanism [77]. However multilayers having very thin layers exhibit also a high density of interfaces which interact and decrease the stress needed for the motion of dislocations across the boundaries [3]. Hence the highest hardness can be reached for a multilayer system when the optimal layer thicknesses have been found to hinder dislocation motion across boundaries without dislocation motion in the layers [21, 77].

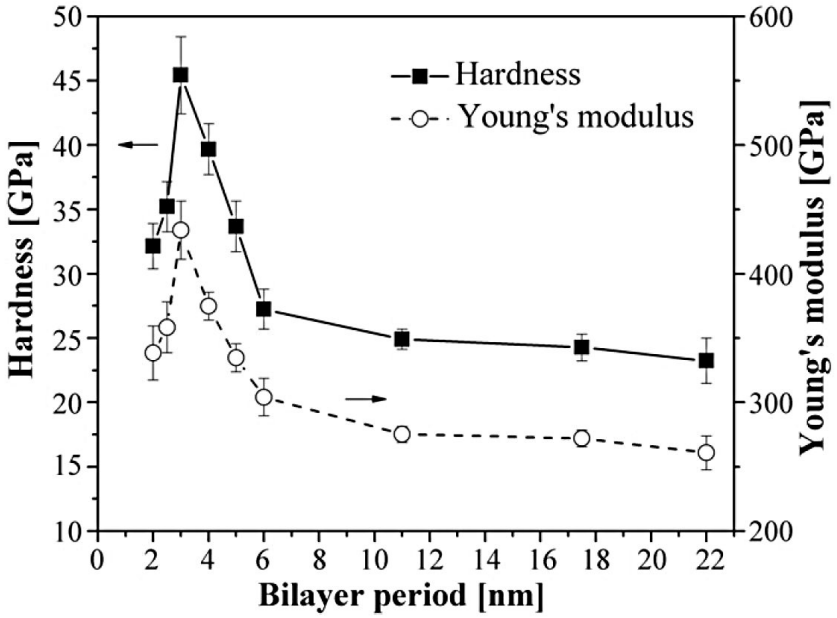


Figure 2.8: Hardness and Young modulus profile of CrN/AlN superlattice coatings measured by nanoindentation [4].

Figure 2.8 demonstrates the sensitivity of the previous mentioned hardening effects on the bilayer period in CrN/AlN superlattice coatings, published by Lin et al. [4]. The hardness and Youngs modulus profile is characterized by a sharp peak with a super hardness of 45 GPa when having a fully cubic structure at a $\Lambda$ of 3.0 nm. In contrast to the work presented in publication I, the epitaxial stabilization of cubic AlN is only reported to be affected by the AlN layer thickness while different CrN to AlN layer ratios have not been considered [78].

### 2.4.2 Thermal Stability of CrN/AlN Multilayer and Superlattice Coatings

Thermal stability of thin films controls life-time of coated tools hence process costs which are essential for a successful implementation in industry can be reduced [11]. Nowadays hard nitride coatings were used to protect materials in forming and machining applications which are exposed to temperatures exceeding 1000 °C during operation. The increased demand of thermal behavior on monolithically nitride coatings such as CrN and TiN limit their usage and force to develop coatings with smart architectural design [79]. Multilayer structured coatings combining different materials allow the formation of tailored properties and become more important for the industry [11]. These properties can be adjusted in a very easy way just by changing their individual layer thickness which can be attributed to the different microstructure evolution during film growth. Thermal stability of multilayer coatings is also influenced by the individual layer thickness as shown by Tien et al. [80].

Especially CrN/AlN multilayer exhibit increased oxidation behavior when decreasing the individual layer thickness of the coatings. Even though structural and mechanical properties of CrN/AlN superlattice coatings are investigated in numerous works, a detailed literature research showed only few explorations about the thermal behavior of such coatings. Lin *et al.* [81] observed poor oxidation resistance when annealing up to 1100 °C in air for the CrN/AlN multilayer coating containing wurtzite AlN. However, CrN and AlN distinguished by good oxidation resistance due to formation of $Cr_2N$ and $Al_2O_3$ respectively suggest increased thermal stability for CrN/AlN multilayer coatings compared to single CrN coating which is confirmed by Tien and Duh [82] and Tien, Duh, and Lee [83] when annealing up to 900 °C in air and vacuum environments. This increased thermal stability of multilayer coatings is based on the numerous interfaces which act as obstacles for the inward and outward diffusion of ion species while monolithically grown coatings provide pathways for the diffusion. Especially dissolving into $Cr_2N$ and finally Cr can be retard as the nitrogen release is inhibited by the interface [4].

In contrast to most other studies which deal with thermal analyzes of multilayer coatings mainly in air up to a maximum temperature of 1100 °C publication II deals with the thermal behavior of CrN/AlN multilayer coatings in He and vacuum atmosphere up to 1500 °C. The influence of c- and w-AlN layers which is connected with a different structural growth mode, as shown in section 2.4, on thermal behavior is discussed using differential scanning calorimetry (DSC) combined with thermal gravimetric analyzes (TGA), nanoindentation and X-ray diffraction (XRD) after annealing.

Chapter 3

# Methodical Approach

## 3.1 Fracture Toughness in Multilayer Coatings

The fracture toughness is defined by the stress intensity factor $K_{IC}$ at which a crack starts to propagate in the material. Numerous evaluation methods for this value using fracture stress, coating thickness and crack length were published elsewhere [84–87]. Nevertheless, an exact measurement of the crack length is needed, which is in general difficult for small materials [88]. As this work is mainly devoted to the mechanisms of increased fracture toughness in multilayers, the evaluation of $K_{IC}$ is not explained in more detail.

Since many decades nature has inspired many researchers by their biological structures of humans, animals and plants with excellent protection measures against hard requirements, for e.g. fracture toughness. Such protective properties of biological species exhibiting extraordinarily high toughness and strength have been found in fine-scaled layered mollusk shells. There a combination of alternating softer and (brittle) hard phase maximize the critical stress intensity required for crack propagation.

The fracture toughness of multilayers can be adjusted by their individual layer thickness, the number of interlayers and the combination of the material. Moreover, multilayer coatings can also be designed based on one material with different microstructures. Hence multilayer design becomes more important due to their versatile possibilities of adjusting high potential coatings having high strength and toughness. Therefore Stoudt, Ricker, and Cammarata [74], Springer and Catlett [89], and Movchan *et al.* [90] to name a few investigated hierarchical microstructure of alternating layers in metal/metal, metal/ceramic and ceramic/ceramic multilayer configurations, respectively.

As schematically shown in Fig. 3.1 several mechanisms in a multilayer designed coating as blunting of the crack tip by plastic deformation [91, 92], deflection of the crack path near the

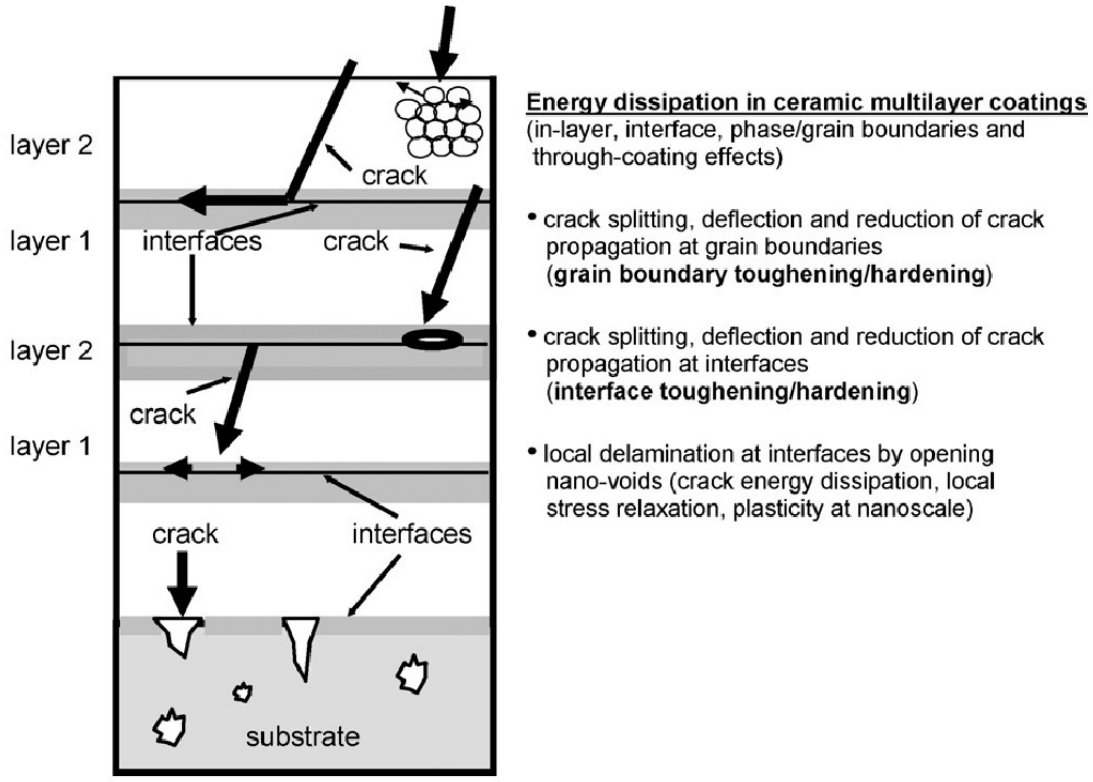


Figure 3.1: Schematic toughening and strengthening mechanism in ceramic multilayer coatings according to Stueber [94].

interfaces due to differences in elasticity or morphology [93] can inhibit the crack propagation through the multilayer.

Another attempt to improve the toughness of ceramic coatings was made by the incorporation of ceramic particles into a nanocomposite compound. Such toughening mechanism using $Y_2O_3$ for the stabilization of tetragonal $ZrO_2$ provide excellent flexural strength and fracture toughness at room temperature due to the stress-induced phase transformation from tetragonal to monoclinic zirconia [95–98].

Based on this knowledge, for this work the effect of a combination of a multilayer architecture and a stress induced phase transformation on the fracture behavior within a CrN/AlN multilayer system has been investigated.

The crack mechanism illustrated in Fig. 3.2 shows the initiation and the propagation of the crack in a CrN/c-AlN and CrN/w-AlN multilayer coating. As already mentioned in section 2.3 AlN provides a metastable cubic phase which transforms with an increase in volume of 26% to the stable wurtzite phase. During the crack propagation in the CrN/c-AlN multilayer at the free surface generated at the crack edges the cubic AlN cannot be stabilized anymore and transforms into the stable wurtzite phase. This transformation and changing

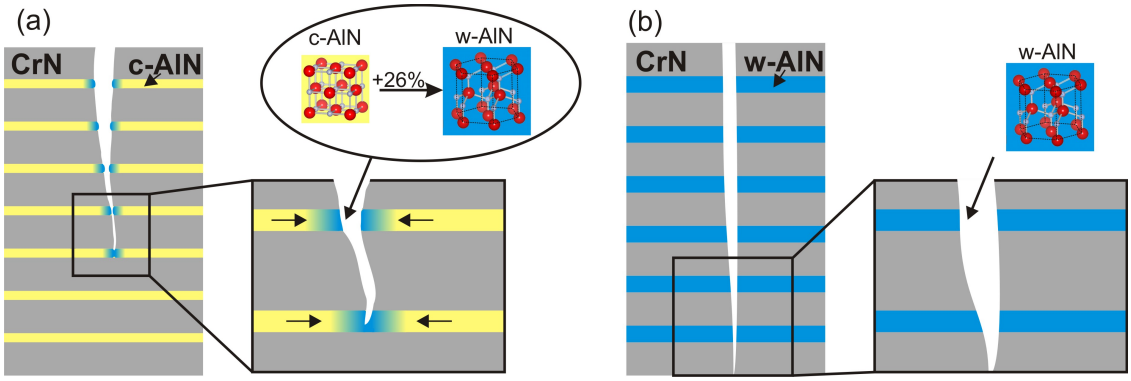


Figure 3.2: Schematic of the crack mechanism in (a) CrN/c-AlN and (b) CrN/w-AlN multilayer coatings.

in volume can induce toughening mechanisms influencing the fracture behavior by crack deflection and absorbing crack energy. In contrast, the crack propagation in CrN/w-AlN multilayer coatings cannot be influenced by a phase transformation and the crack proceeds immediately through the coating as soon as the crack is initiated as discussed in publication IV in more detail.

## 3.2 Coating Preparation

The coatings were deposited by a reactive magnetron sputtering system using an AJA Orion 5 lab-scaled deposition plant, see Fig. 3.3. This system is characterized by a computer-controlled shutter system which enables multilayer coatings in the range of few nanometers. Hence, multilayer coatings can be produced in two different ways, either switching on and off the targets or opening and closing the shutters. Furthermore two dc generators and one rf generator can be used to power two 2 inch and one 3 inch gun which are located in circular array at the bottom of the chamber. The different substrates used (Si, $Al_2O_3$, MgO, Fe- and Cu-foil) were fixed on a rotating substrate holder (6 inch diameter) at the top of the chamber which can be heated up to 800 °C. Furthermore, substrate etching as well as dense coating morphology was achieved by rf-biasing of the substrates. The CrN/AlN multilayer and superlattice coatings within this work were prepared starting and ending with the CrN layer. The multilayer coatings (publications III and IV) were prepared with 20 alternating layers having an AlN volume fraction of 3% (cubic) and 9% (wurtzite), respectively. For all superlattice coatings (publications I and II) a total thickness of $\sim 1.5$ µm was obtained by varying the number of layers from 250 ($\Lambda = 12.0$ nm) to 1580 ($\Lambda = 1.9$ nm).

Special attention was paid on the development of a substrate holder which enables the rotation of samples on their own axis (Fig. 3.4). The driving force for the rotation of the substrate clamps was achieved by the original propeller (also used for the rotation of the

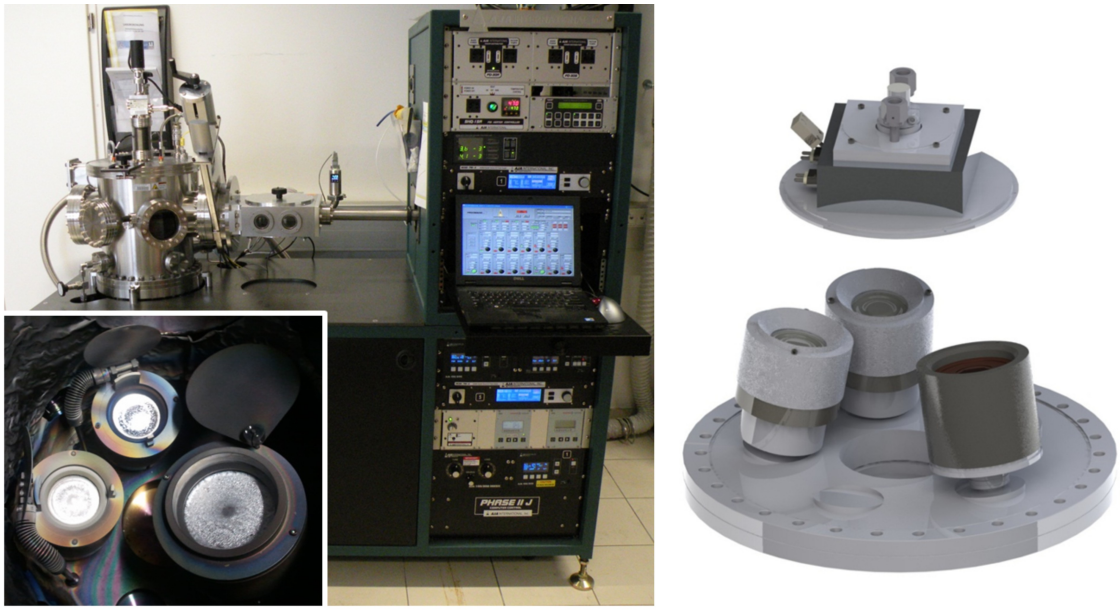

Figure 3.3: (a) AJA Orion 5 deposition plant equipped with a load lock system and a computer controlling unit. (b) Schematic of the sputter gun and sample holder arrangement within the chamber.

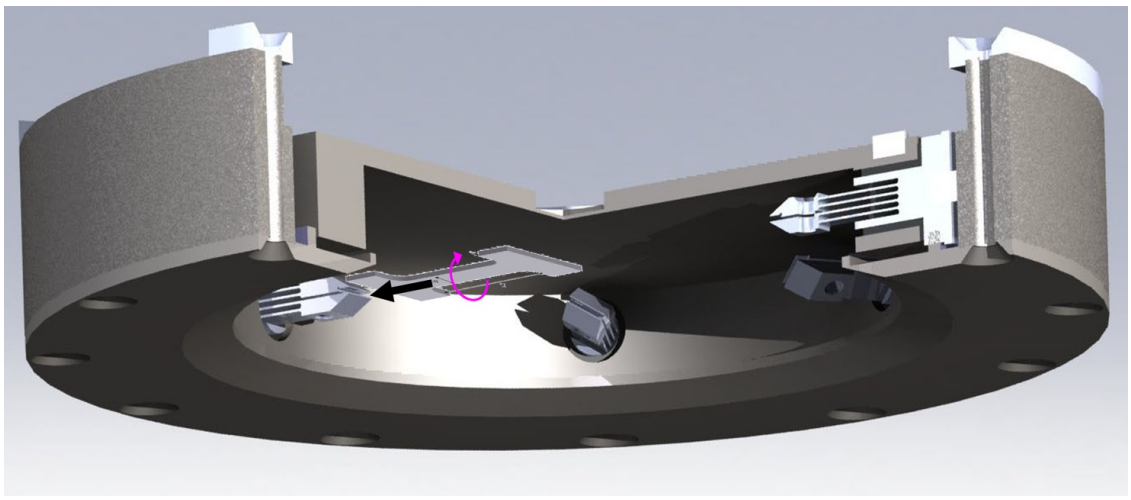

Figure 3.4: Substrate holder for the AJA Orion 5 developed for the deposition of 3-dimensional samples.

"1-dimensional" substrate holder) at the center of the chamber. This rotating moment is transferred by means of a fixed gear ring located at the outermost diameter of a fixed shell and boosts the gear wheel which is connected to the clamps of the substrate. In addition to the rotation of the samples on their own axis the samples are now also able moving 360° within the chamber over all usable targets. This enables deposition of multinary coatings on round substrates and double-sided depositions on flat substrates for e.g. tensile tests and bending tests.

## 3.3 Structural and Chemical Investigations

### 3.3.1 XRD

X-ray diffraction analyzes of powdered and as deposited thin films were conducted in the Bragg-Brentano configuration with high-angle (HAXRD) and low-angle (LAXRD) mode using a Bruker AXS D8 and D500 diffractometer equipped with a Cu-$K_\alpha$ radiation source ($\lambda = 1.54056$ nm).

In this thesis this non-destructive structural characterization technique was used for phase identification and stress analysis. The bilayer period ($\Lambda$) of the small layered superlattice coatings were determined in the LAXRD mode by using the modified Bragg equation:

$$\Lambda = \frac{m\lambda}{2\sin\theta} \tag{3.1}$$

where $m$ is the order of the reflection in the LAXRD pattern, $\lambda$ is the X-ray wavelength of Cu ($\lambda(K_\alpha) = 0.15406$ nm), $\theta$ is the position of the Bragg diffraction angle, and $\Lambda$ is the bilayer period. Similar to LAXRD the bilayer period in HAXRD mode can be calculated according to formula:

$$\sin\theta_\pm = \theta_B \pm \frac{m\lambda}{2\Lambda} \tag{3.2}$$

where $m$ is the order of the satellite peak, $\lambda$ the wavelength of the X-ray beam, $\theta_B$ half of diffraction angle of the main Bragg peak, $\theta_\pm$ half of the angle position of the satellite peak, and $\Lambda$ the resulting bilayer period. Detailed descriptions and settings of the bilayer evaluation by X-ray analyzes can be found in literature [21, 99].

### 3.3.2 SEM

The morphology, structure and overall thickness of the coatings deposited on silicon substrates were investigated on fracture cross-sections using a Zeiss EVO 50 microscope operating with an acceleration voltage of 20 kV. Fracture tests during bending and compression mode and fracture images were conducted in a Zeiss, XB1540 and Zeiss, LEO 982, respectively. Chemical compositions of the films were determined by energy-dispersive X-ray (EDX) analysis.

### 3.3.3 TEM

Detailed structural investigations of the coatings by transmission electron microscope (TEM) were executed in a Phillips CM12 microscope, operated at 25 kV and 120 kV, respectively, as well as by high resolution transmission electron microscopy (HRTEM) using a Tecnai F20 operating at 200 kV. Prior to the TEM investigations the coated Si substrates were mechanically polished to around 50 µm in thickness and ion etched using a GATAN precision

ion polishing system PIPS, with an incident angle of 4° and an acceleration voltage of 3.5–4 kV.

Crystallographic identification of the coatings was evaluated after selected area electron diffraction (SAED) by means of the Gatan DigitalMicrograph Software (Vers. 3.7.1.).

## 3.4 Thermal Analyzes

Phase transformation and thermal resistance were conducted on grinded powder by differential scanning calorimetry (DSC) in combination with thermal gravimetric analyzes (TGA) in a SETSYS Evolution TMA (Setaram instrumentation) calorimeter. The measurements were accomplished in He atmosphere at temperatures up to 1500 °C with a heating rate of 20 °C/min. Additionally annealing of powdered coatings were executed in a Reetz vacuum furnace (HTM Reetz GmbH, base pressure $< 5 \cdot 10^{-4}$ Pa).

## 3.5 Mechanical Investigations

### 3.5.1 Nanoindentation

The hardness of the coatings was measured using a CSIRO ultra micro indentation system equipped with a three-sided pyramid Berkovich tip. For every sample 20 indents were conducted in load controlled mode ranging from 20 to 10 mN in steps of 0.5 mN to allow reliable statistics. The resulting indentation depth was kept below $\sim$ 10% of the overall coating thickness which minimizes the influence of the substrate [100]. The values were obtained by evaluating the unloading segment of the indentation curve after the Oliver and Pharr method [101]. Detailed description on indentation and data evaluation can be found in literature [100, 102].

### 3.5.2 Fracture Tests

Numerous testing methods have been developed to evaluate the fracture behavior of hard ceramic coating systems (e.g. TiC, TiN, CrN and CrAlN), such as tensile tests [103–105], four-point bending tests [88, 106–108], indentation tests [92, 109], scratch tests [110] and double-cantilever beam tests [85]. The fracture characterization of coatings in the micro scale is accompanied by small test specimens providing only a small specific volume of consideration. Such a small specific test volume is connected to a high sensitivity for possible faults during the test. Hence, substrate effects, impact velocity, loading speed, contact area and the contact position of the indenter on the sample and the alignment of the sample during the test have to be taken into account when selecting suitable tests for the evaluation.

Moreover, coatings having different architectural coating design need to be loaded from the corresponding direction to generate cracks at the most informative part of the sample. Especially fracture investigations in multilayer coatings having layer thickness in the range of few nanometers provide numerous effects during fracture, as e.g. interfacial fracture, delamination, crack deflection and crack stop, to name a few and require extensive considerations. As this study focused on the crack behavior and crack propagation influenced by c-AlN layers and w-AlN layers within CrN/AlN multilayer coatings in-situ compression, bending and tensile tests inducing different strain states on the compound were conducted and explained in more detail in the next paragraphs.

### Sample Preparation

Fracture studies dealing with the investigation of samples in the micro scale needs an extensive preparation. In order to determine reliable fracture values for each specific test approach a proper sample preparation has to be found. As we want to exclude effects of substrates on the fracture behavior of the multilayers and avoid also uncontrolled damage of the substrate to the coating interface an etching process was used to prepare free-standing coatings. Therefore, the selected areas were etched by a stirred potassium hydroxide (30 wt.%) aqueous solution for 1 h at 60 °C. After chemical etching, the specimens were cleaned in distilled water and ethanol. The final step of preparation was accomplished by using a focused ion beam (FIB) workstation. Here depending on the different fracture tests cantilever and pillars providing different geometries were prepared from free-standing coatings as described in the respective chapters.

### Compression Tests

The influence of cubic and wurtzite structured layers in CrN/AlN multilayers on the fracture behavior was investigated by in-situ compression tests using a field emission scanning electron microscope (Zeiss, LEO 982). For representative fracture stress values numerous micro-pillars ($2 \times 1 \times 1$ µm$^3$) from the free-standing coatings shown in Fig. 3.5 were prepared and tested. The pillars were loaded using a conical diamond microindenter (ASMEC, UNAT) with a punch diameter of 20 µm. As shown in Fig. 3.5 the fracture behavior of the multilayer coatings was observed from the top, looking on the surface of the top layer of the coating (CrN layer) and the side view providing the observation of both, the surface of the top layer and the stacked layers with their interfaces. During the tests the loading speed was kept constant at 85 nm/s for the pillars observed from the top view but 5 nm/s for the pillars observed from the side view in order to get more information about the role of the interface during cracking. The generated load–displacement curves of the coating pillars were calculated to engineering stress–displacement values according to [111].

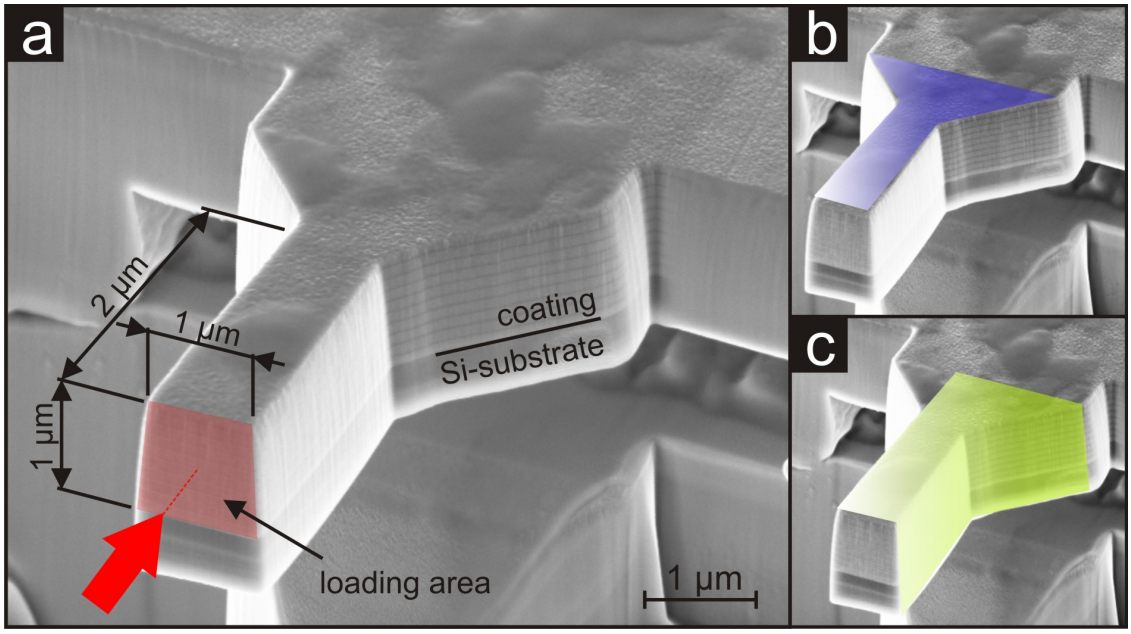


Figure 3.5: (a) SEM micrograph of CrN/w-AlN multilayer pillar prepared by FIB milling having dimensions of $2 \times 1 \times 1$ µm$^3$. The loading area is marked in red. (b) Top view and (c) side view of the coatings prepared by FIB milling.

The tests clearly demonstrate higher fracture stresses for the CrN/c-AlN multilayers compared to the monolithically grown CrN and CrN/w-AlN multilayers. Moreover, stress versus displacement curves are linear elastic until fracture occurs for all coatings investigated. The multilayer coatings with cubic stabilized AlN layers inhibit crack propagation while the fracture pattern of w-AlN containing coatings are characterized by shearing at the interface, as presented in paper 5.2. This behavior can be attributed to a phase transformation of c-AlN to w-AlN by a volume increase of 26% as mentioned in section 3.1.

As shown schematically in Fig. 3.6 loading of CrN/w-AlN multilayer coatings (a) induces tensions between the layers which lead to an opening within the weak bonded incoherent interfaces [62]. Hence, shearing off the interfaces within this cracked part in the coating can be observed. In contrast, loading of CrN/c-AlN multilayer coatings (b) induces also tensions at the interface but promotes also stress-induced-phase-transformation of the metastable cubic AlN structure to the stable wurtzite AlN structure providing increased volume. This avoids dissociation of the CrN and AlN layers and sustains the coating for higher loads.

### Bending Tests

In-situ bending tests of free-standing mico-cantilevers with dimensions of $1 \times 1 \times 8$ µm$^3$ were conducted using a Leo, XB1540 equipped with a picoindenter (Hysitron PI-85). Detailed information about the preparation of such micro-cantilevers can be found in [112]. The test was executed in load controlled mode. In order to avoid bending of the free-standing coating

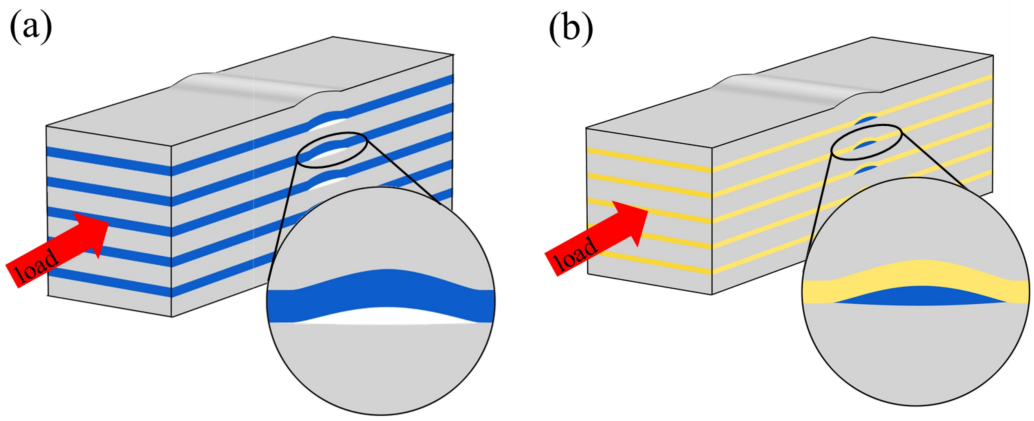


Figure 3.6: Schematic of compression tests of (a) CrN/w-AlN (without phase transformation) and (b) CrN/c-AlN (interface closing mechanism due to phase transformation) multilayer coatings.

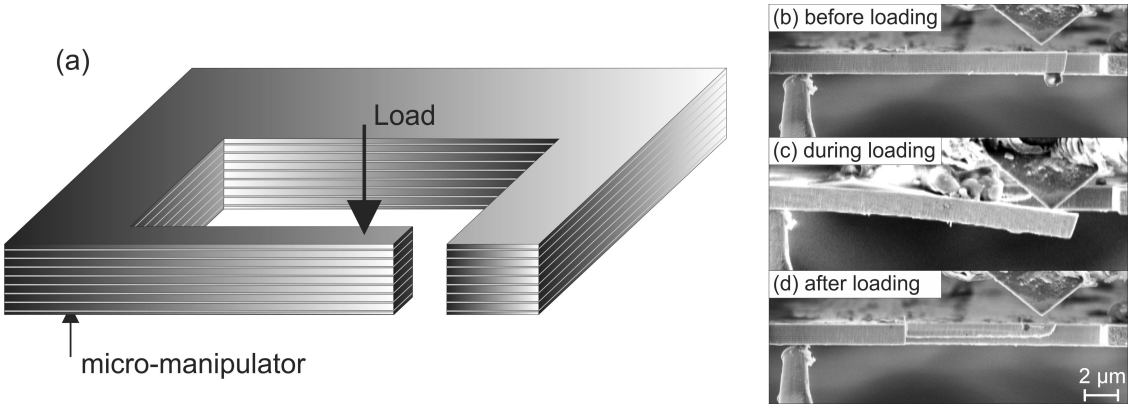


Figure 3.7: (a) Schematic image of the bending test alignment. SEM images of CrN/w-AlN multilayer cantilever (b) before, (c) during and (d) after loading.

a micro-manipulator pulling against the onset of the pillar was used to stabilize the system against contortion, as shown schematically in Fig. 3.7. During loading, the cantilevers were observed from the side view providing the layer structure and the interfaces of the multilayers. Figure 3.7 displays SEM images of the cantilever before (b), during (c) and after (d) the test. Although the scanning speed during the test was set to high frequencies no crack formation and propagation could be observed as the crack energy of formation seems to be higher than the energy needed for crack propagation. Therefore, in future experiments a definite surface defect in form of a pre-crack (notch) has to be introduced.

Load and displacement of the indenter were recorded during the bending experiments enabling the determination of the fracture stress. The measurements shown in Fig. 3.8 reveal increased fracture stresses for the CrN/c-AlN ($\sim$ 4000 MPa) than for the CrN/w-AlN

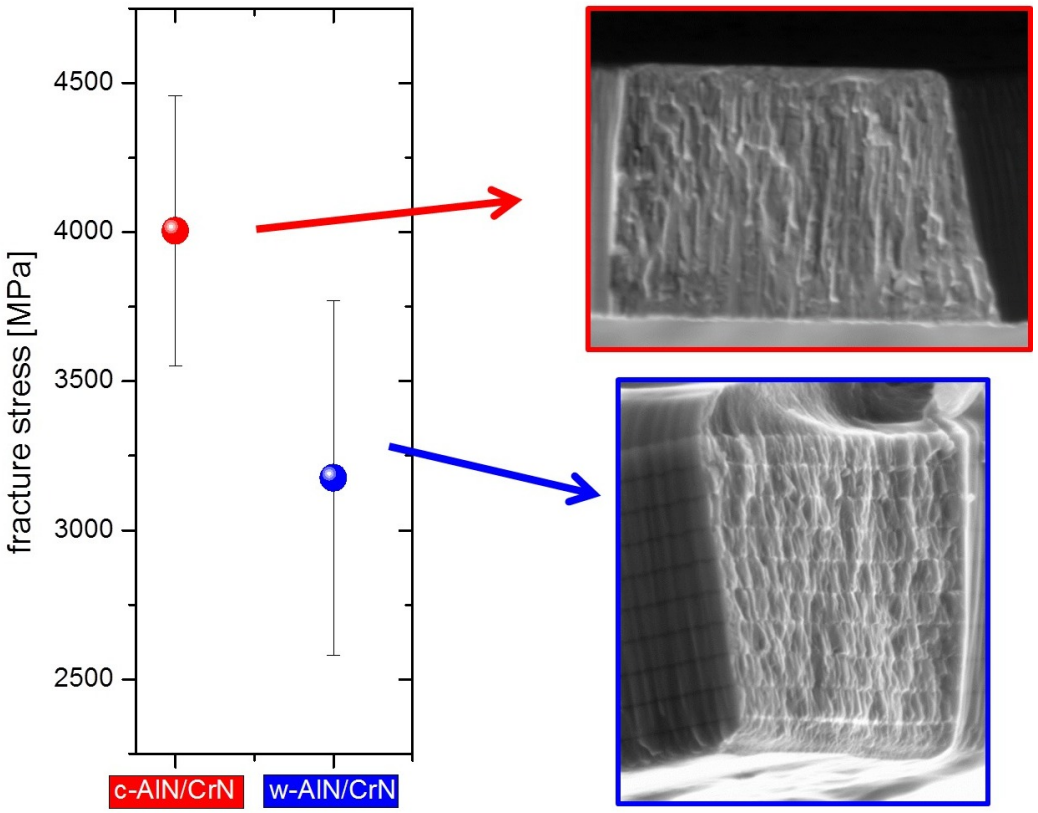


Figure 3.8: Fracture stress of CrN/c-AlN (red) and CrN/w-AlN (blue) with their corresponding fracture pattern after bending test.

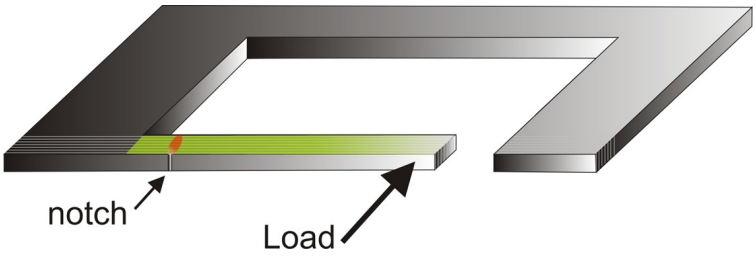


Figure 3.9: Schematic drawing of the in-situ bending test alignment in TEM. The interface structure provided for investigations is marked in green and red, respectively.

($\sim$ 3300 MPa) multilayer. The fracture patterns after the tests exhibit no significant differences.

To demonstrate phase transformation of c-AlN into w-AlN in the CrN/AlN multilayer coatings during loading detailed investigations of in-situ bending tests within a TEM are in preparation. Figure 3.9 shows, that the cantilever has to be prepared in a way to provide the layer structure from the top view for the in-situ bending tests (marked by green and red areas). Furthermore, the sample has to be prepared very thin to be suitable for transparent investigations which will be performed by focused ion beam.

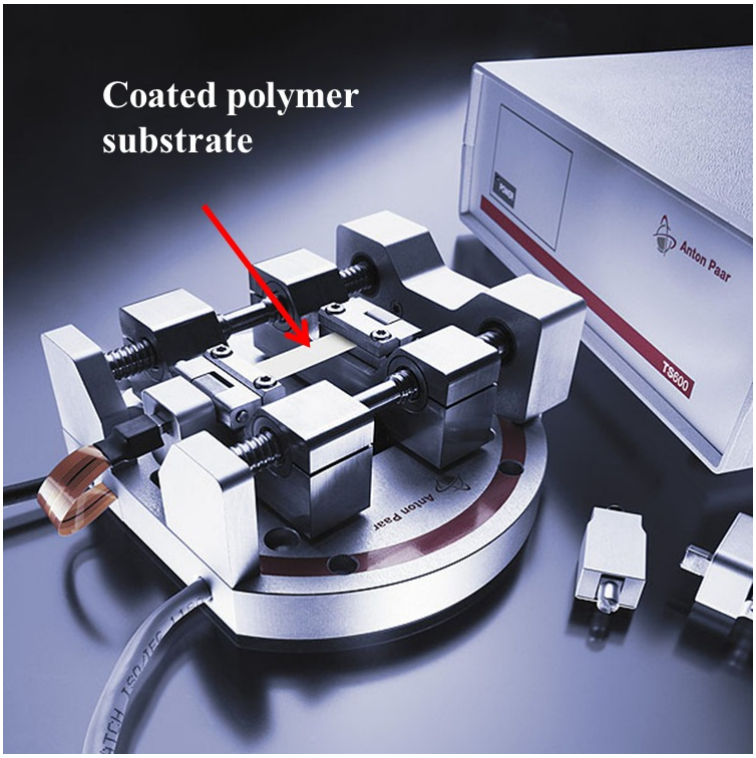


Figure 3.10: Anton Pharr tensile stage TS 600.

### Tensile Tests

For detailed investigations of the crack path CrN/AlN multilayer coatings having cubic and wurtzite AlN structure were analyzed after tensile tests. Here the coatings were deposited on polymer substrates at lower temperatures ($T_{\mathrm{dep}} = 200\,^{\circ}\mathrm{C}$) compared to the coatings tested in bending and compression mode ($T_{\mathrm{dep}} = 470\,^{\circ}\mathrm{C}$). During deposition, the thin substrate was fixed at the ends to avoid twisting due to residual stresses of the coating.

The coated polymer samples with an origin length of $\sim 23$ mm were climbed and strained in an Anton Paar Tensile Stage TS 600, see Fig. 3.10.

During the test, the top view image of the strained coating was recorded in steps of 1, 2, 4, 6, 8, 10, 12, 14, 16, and 18% of elongation by means of a light optical microscope which were then correlated to the recorded strain–elongation curve, compare Figs. 3.11 and 3.12, respectively. Since residual stresses cause deflection of the sample leveling by loading in tension at the beginning of the test induce diagonal cracks (with regard to the loading direction) which do not contribute significant for further evaluation. The strain at which the cracks starts to appear perpendicular to the tensile direction gives a measure of the tensile fracture strength of the film. Furthermore, the steady state spacing between the cracks can be analyzed to get the ultimate shear strength of the interface as reported in Refs. [113, 114]. Figure 3.12 reveals clearly higher crack density but finer cracks for the CrN/c-AlN multilayer

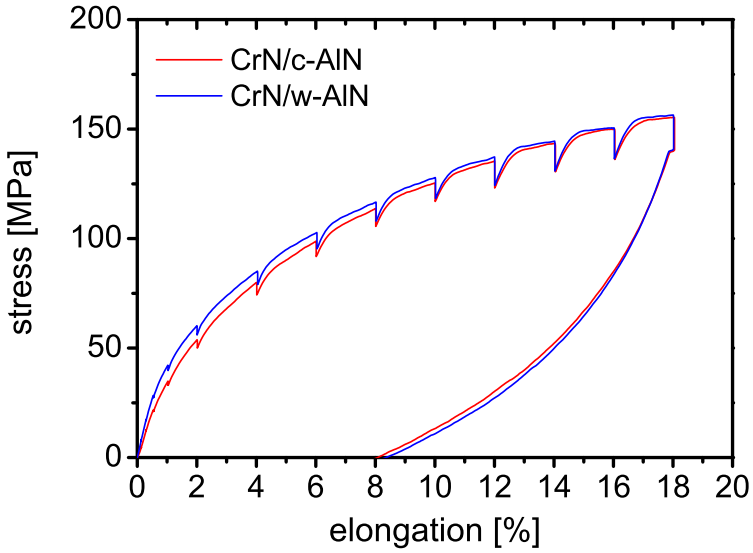


Figure 3.11: Stress–elongation curve recorded during tensile test of CrN/c-AlN and CrN/w-AlN multilayers deposited on polymer substrates.

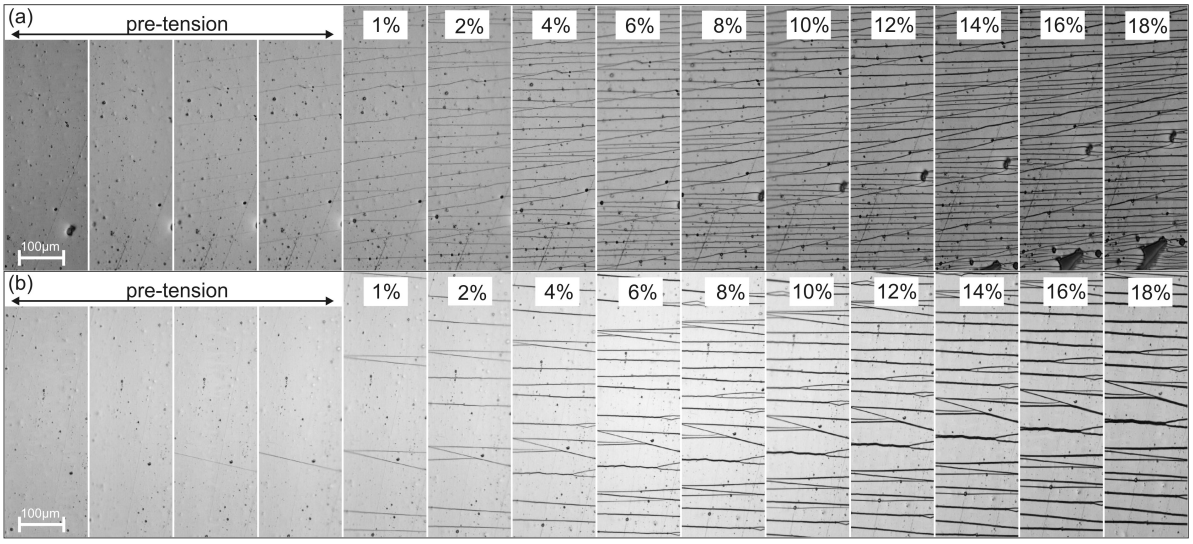


Figure 3.12: Top-view of the surface of (a) CrN/c-AlN and (b) CrN/w-AlN multilayer coatings after 1, 2, 4, 6, 8, 10, 12, 14, 16, and 18% elongation providing cracks perpendicular to the strain direction. The first 4 pictures indicate diagonal cracks resulting from leveling the deflected sample.

(a) compared to the CrN/w-AlN coating (b) which can be attributed to higher energy of crack propagation needed than for crack formation ($E_{\text{form}} < E_{\text{prop}}$). Therefore it can be concluded that the crack propagation is more inhibited in the c-AlN containing multilayer.

Within this work the coating area including cracks of both multilayers was exposed by using a FIB (Leo, XB1540) providing cross sectional observation and the investigation of the crack

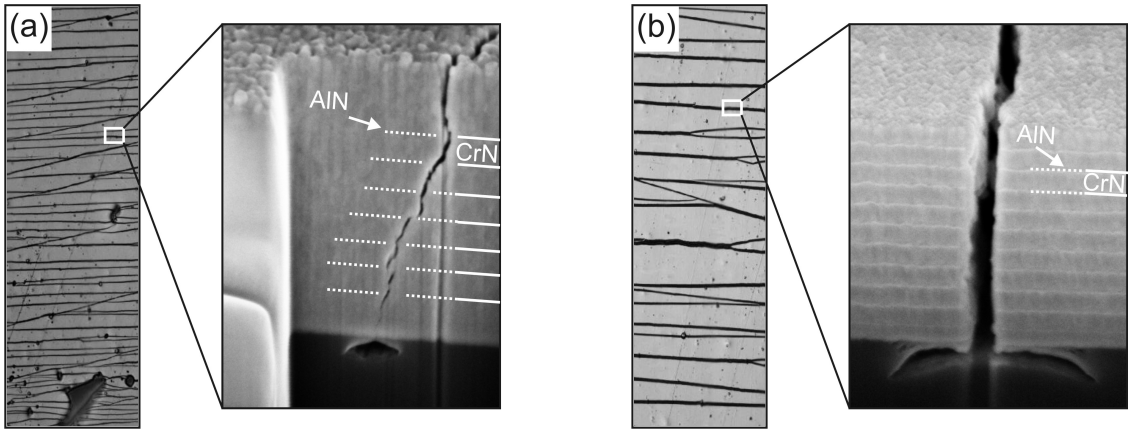


Figure 3.13: Cross sectional SEM images of the fracture pattern of (a) CrN/c-AlN and (b) CrN/w-AlN multilayer coatings on polymer substrate after 18% elongation.

path after the tensile test (18% of elongation) in more detail (Fig. 3.13). The images clearly demonstrate crack deflection of the coatings with c-AlN (Fig. 3.13a) at the interfaces while the CrN/w-AlN multilayer (Fig. 3.13b) seems to have less influence on the crack propagation as this sharp deflection of the crack at the interface could not be observed.

Future investigations by HRTEM may focus on the possible influence of a phase transformation on the crack behavior. Therefore suitable samples for HRTEM investigations providing the crack edges of the strained coatings have to be prepared by FIB.

Chapter 4

# Summary of Publications and Contribution to the Field

### Publication I

CrN/AlN multilayer coatings are well investigated over a wide range of composition and architectural design. However, when focusing on superlattice coatings, with layer thicknesses in the nm range, a thorough study on the structural evolution and mechanical properties influenced by the individual layer thicknesses is missing. Therefore CrN/AlN superlattice coatings with AlN layer thicknesses of 1, 2 and 3 nm and CrN layer thicknesses ranging from 1 to 10 nm were studied in detail on their mechanical and structural evolution as well as on the size-structure relations to stabilize c-AlN. Our investigations indicate a minimum layer ratio of $\geq 1$ for each system to stabilize cubic structured multilayer coatings. Otherwise polycrystalline nanostructured films (mixed cubic and wurtzite phases) will be formed. Hardness measurements indicate maxima of 31 GPa, for the cubic superlattice coatings with 1 and 2 nm AlN, while a slightly lower peak value of $H_{\max} \sim 28.5$ GPa could be obtained for the coatings with 3 nm.

### Publication II

CrN/AlN superlattice coatings are well known for their high strength and hardness. Nevertheless, only few investigations deal with their thermal stability and the thermo-mechanical properties. Hence this work is devoted to the influence of the differences in structure on the thermal behavior of magnetron sputtered CrN/AlN superlattices. Based on HRTEM investigations combined with DSC, XRD and hardness measurements after annealing up to 1500 °C we conclude that the individual layer thicknesses contribute to either cubic (CrN/AlN ratio $\geq 1$) or mixed wurtzite with cubic structure (CrN/AlN ratio $< 1$) and retard the diffusion process of $N_2$. The columnar structure and grain boundaries of the coating with mixed wurtzite and cubic structure are interrupted while cubic stabilized CrN/AlN coatings exhibit

large columnar grains and long grain boundaries providing optimal diffusion paths. This is also confirmed by an earlier and highly pronounced endothermic reaction detected during DSC for the fully cubic structured coating. Hence, these coatings are characterized by a drop in hardness after annealing up to 1000 °C while the coatings having mixed structure provide nearly the same hardness as in the as-deposited state ($H \sim 23.5$ GPa). The results clearly demonstrate improvement of the thermal behavior of CrN/AlN superlattice coatings when adjusting the morphology by individual layer thicknesses and structure.

### Publication III

High thermal stability and oxidation resistance as well as increased mechanical properties make ceramic-like hard coatings to a very valuable material class for various industrial applications. Here we study various multilayer architectures of CrN/AlN, $Cr_{0.4}Al_{0.6}N$/AlN and $Cr_{0.37}Al_{0.6}Y_{0.03}N$/AlN and the effect of the AlN layer thickness (3 or 10 nm, hence mainly cubic or wurtzite structure) while keeping the overall AlN-layer content below 14%, on their mechanical and thermal properties. While the hardness of the Cr-based nitride layers is not influenced by the addition of thin c-AlN layers, due to the small overall content, the formation of wurtzite AlN for the $\sim$ 10 nm thin layers results in loss of coherency and formation of smaller domains during growth also in the Cr-based nitride layers. Thereby, the hardness is slightly increased to 26, 30, and 33 GPa of as deposited CrN/AlN, $Cr_{0.4}Al_{0.6}N$/AlN and $Cr_{0.37}Al_{0.6}Y_{0.03}N$/AlN coatings when compared to the monolithic Cr-based nitrides. Although, especially the thicker AlN layers are inclined to fully transform to the stable wurtzite structure upon annealing, which also triggers the formation of $Cr_2N$ of the Cr-based nitride layers, their hardness remains at the as deposited value up to $T_a = 900$ °C and even increases for the $Cr_{0.37}Al_{0.6}Y_{0.03}N$/AlN multilayers up to 36 GPa. This study clearly shows the importance of a well adjusted coating architecture for optimized performance.

### Publication IV

Ceramic-like coatings in particular, transition metal nitrides, such as CrN are well known and investigated with respect to their microstructure, morphology, thermal and mechanical properties. However, the brittleness of such ceramic-like coatings often negatively influences their performance especially when used in conditions with an increased need for crack resistance. Therefore, this work is devoted to a new design of ceramic like coatings to increase their fracture toughness. Single-layered CrN and multi-layered CrN/AlN, with either cubic (c) or wurtzite (w) AlN layers, were investigated for their fracture toughness using in-situ scanning electron microscopy (SEM) compression tests. Therefore, coating material pillars ($1 \times 1 \times 2$ µm$^3$) were prepared by focused ion beam out of the $\sim$ 1µm thin coatings. Our investigations show that the CrN coating as well as the CrN/w-AlN multilayer coating exhibit a spontaneous and fatal cracking behavior as soon as the compressively applied load

exceeds 5.3 and 3.8 GPa, respectively. Detailed SEM studies of the CrN/w-AlN coatings exhibit preferred crack propagation along the c-CrN and w-AlN interfaces. Contrary, in-situ SEM observations during compressive loading of the CrN/c-AlN multilayer coating pillars suggest a ductile-like behavior, as an initiated crack only slowly propagates and even experiences deflections. This is based on the displacive (diffusion-less) transformation paths from c-AlN towards wurtzite w-AlN with the connected pronounced volume increase of $\sim 26\%$. This leads to an increase in the maximum allowed, compressively applied loading to 6.8 GPa before failure occurs. The study presents a powerful design allowing for the development of a new class of AlN toughened hard coatings.

### Contribution to the field

CrN/AlN multilayer coatings with layers in the range of few nanometers, called superlattice, provide high thermal stability and superior hardness when having epitaxial structure. Hence the investigations of publication I and II contribute to the cubic stabilization of AlN in CrN/AlN superlattices. Deposition parameters were defined allowing for controlled deposition of uniform layers in the nanometer scale. Here, a clear dependence of the individual layer thickness on the cubic stabilization of AlN and the influence on the microstructure is shown. In a further step mechanical and thermal properties reveal to be also influenced by the microstructure as the cubic stabilized AlN provide highest hardness while the mixed structured AlN layers increase the thermal stability due to retarding the nitrogen diffusion. Thus, the study clearly demonstrates that a sophisticated knowledge on layer-structure property is necessary to allow for deposition of high performance hard protective and thermal stable coatings.

Recently published studies showed increased thermal and mechanical behavior from CrN to CrAlN and CrAlYN coatings. Therefore publication III focused on the influence of 3 and 10 nm thin AlN layer thicknesses within these CrN-based coatings on structure, thermal and mechanical properties. This experimental study provides fundamental knowledge for subsequent fracture mechanisms as the AlN layers below 3 nm were stabilized by coherency strains to its cubic metastable phase otherwise mixed cubic and wurtzite structure were observed.

Research in the field of fracture toughness especially for ceramic coatings becomes more important in the last years. Hence different options of coating modifications and architectures were found and investigated with regard to increased fracture toughness in numerous publications. Based on the results from publication III further investigations concentrate on the effect of a stress-induced-phase-transformation on fracture toughening which is well known from yttria toughening zirconia. In publication IV AlN is presented as a high potential material allowing for promising results for increased fracture toughness in ceramic coatings. In

order to investigate the influence of epitaxial stabilized AlN layers on the fracture toughness of CrN-based coatings basic knowledge has been gained by testing CrN/AlN multilayers.

The development of suitable testing methods for generating significant results for the fracture mechanism of multilayer coatings represents an essential point of this thesis. Therefore, numerous information about the preparation of small freestanding micro samples and the execution of micro-mechanical in-situ compression, bending and tensile tests using FIB and SEM were gathered. The results in compression mode demonstrate crack arrest effects and higher fracture stresses for CrN/AlN multilayers when having a fully cubic structure compared to monolithically grown CrN coatings while w-AlN layers cause shearing at the interface exhibiting lowest stresses. For the observation of the fracture mechanism during bending tests a notch has to be introduced. Nevertheless, also bending tests reveal higher fracture stresses for the cubic stabilized CrN/AlN multilayer coatings. A novel design was shown for the tensile tests. Here the crack path after tension of the multilayer coatings is presented on polymer substrates excluding possible substrate effects.

Future investigations may focus on the fracture toughening by stress induced phase transformation in CrN/AlN multilayers in more detail. Therefore, downscaling to in-situ micro-mechanical tests using TEM is a further step to provide essential fundamentals for increased fracture toughness in ceramic coatings.

# Bibliography


[1] M. Ashby, Scr. Mater. **68**, 4 (2013).

[2] P. Hovsepian, D. Lewis, and W. Münz, Surf. Coat. Technol. **133-134**, 166 (2000).

[3] J. Lin, N. Zhang, Z. Wu, W. D. Sproul, M. Kaufman, M. Lei, and J. J. Moore, Surf. Coat. Technol. , in press; doi: 10.1016/j.surfcoat.2011.11.037 (2011).

[4] J. Lin, J. Moore, B. Mishra, M. Pinkas, and W. Sproul, Surf. Coat. Technol. **204**, 936 (2009).

[5] G. S. Kim, S. Y. Lee, and J. H. Hahn, Surf. Coat. Technol. **171**, 91 (2002).

[6] P. H. Mayrhofer, C. Mitterer, and H. Clemens, Adv. Eng. Mater. **7**, 1071 (2005).

[7] H. Holleck, M. Lahres, and P. Woll, Surf. Coat. Technol. **41**, 179 (1990).

[8] F. Rovere, *Materials Chemistry*, 1st ed. (Shaker Verlag GmbH, Aachen, 2010) p. 224.

[9] S. Vepřek, J. Vac. Sci. Technol. A **17**, 2401 (1999).

[10] G. Dehm, C. Motz, C. Scheu, H. Clemens, P. H. Mayrhofer, and C. Mitterer, Adv. Eng. Mater. **8**, 1033 (2006).

[11] S. Vepřek and M. J. Veprek-Heijman, Surf. Coat. Technol. **202**, 5063 (2008).

[12] I. Petrov, P. B. Barna, L. Hultman, and J. E. Greene, J. Vac. Sci. Technol. A **21**, S117 (2003).

[13] S. Vepřek, R. Zhang, M. Veprek-Heijman, S. Sheng, and A. Argon, Surf. Coat. Technol. **204**, 1898 (2010).

[14] R. Rachbauer, S. Massl, E. Stergar, D. Holec, D. Kiener, J. Keckes, J. Patscheider, M. Stiefel, H. Leitner, and P. H. Mayrhofer, J. Appl. Phys. **110**, 023515 (2011).

[15] L. Aihua, D. Jianxin, C. Haibing, C. Yangyang, and Z. Jun, Int. J. Refract. Met. Hard Mater. **31**, 82 (2012).

[16] H. Barshilia, N. Selvakumar, B. Deepthi, and K. Rajam, Surf. Coat. Technol. **201**, 2193 (2006).

[17] P. H. Mayrhofer, D. Music, and J. M. Schneider, J. Appl. Phys. **100**, 094906 (2006).

[18] H. Willmann, P. Mayrhofer, P. Persson, A. Reiter, L. Hultman, and C. Mitterer, Scr. Mater. **54**, 1847 (2006).

[19] P. H. Mayrhofer, H. Willmann, and A. Reiter, Soc. Vac. Coat. , 575 (2006).

[20] H. Holleck and V. Schier, Surf. Coat. Technol. **76-77**, 328 (1995).

[21] P. C. Yashar and W. D. Sproul, Vacuum **55**, 179 (1999).

[22] P. Panjan, M. Cekada, and B. Navinsek, Surf. Coat. Technol. **175**, 55 (2003).

[23] P. Mayrhofer, P. Hovsepian, C. Mitterer, and W.-D. Münz, Surf. Coat. Technol. **177-178**, 341 (2004).

[24] A. McHale, *Phase Equilibria Diagrams: Phase Diagrams for Ceramists: Borides, Carbides, and Nitrides Vol. X* (Phase Equilibria Diagrams: Phase Diagrams for Ceramists: Borides, Carbides, and Nitrides, Westerville, Ohio, 1994) p. 415.

[25] K. Inumaru, K. Koyama, N. Imo-oka, and S. Yamanaka, Phys. Rev. B **75**, 1 (2007).

[26] *Powder Diffraction File 03-065-2899* (International Center for Diffraction Data, PDF-2/Release, 2005).

[27] R. Sanjinés, O. Banakh, C. Rojas, P. Schmid, and F. Lévy, Thin Solid Films **420-421**, 312 (2002).

[28] J. M. Venkatraman and J. P. Neumann, *Binary Alloy Phase Diagrams*, 2nd ed. (ASM International Materials Park, Ohio, 1990) p. 1293.

[29] J. Almer, M. Odén, L. Hultman, and G. Håkansson, J. Vac. Sci. Technol. A **18**, 121 (2000).

[30] P. Mayrhofer, F. Rovere, M. Moser, C. Strondl, and R. Tietema, Scr. Mater. **57**, 249 (2007).

[31] W. Ernst, J. Neidhardt, H. Willmann, B. Sartory, P. Mayrhofer, and C. Mitterer, Thin Solid Films **517**, 568 (2008).

[32] R. Meyer and E. Pietsch, *Gmelins Handbuch der Anorganischen Chemie*, vol. 8 ed. (Verlag Chemie, GmbH, Weinheim, 1962) p. 157.

[33] *Powder Diffraction File 01-079-2159* (International Center for Diffraction Data, PDF-2/Release, 2005).

[34] H. Willmann, *Al–Cr–N thin film design for high temperature applications*, Ph.D. thesis, Montanuniversität, Leoben (2007).

[35] J. Lin, W. D. Sproul, and J. J. Moore, Mater. Lett. **89**, 55 (2012).

[36] H. Chen and F. Lu, Thin Solid Films **515**, 2179 (2006).

[37] U. Wiklund, M. Bromark, M. Larsson, P. Hedenqvist, and S. Hogmark, Surf. Coat. Technol. **91**, 57 (1997).

[38] P. Mayrhofer, G. Tischler, and C. Mitterer, Surf. Coat. Technol. **142-144**, 78 (2001).

[39] J. Seok, N. Jadeed, and R. Lin, Surf. Coat. Technol. **138**, 14 (2001).

[40] J. Romero, M. Gómez, J. Esteve, F. Montalà, L. Carreras, M. Grifol, and A. Lousa, Thin Solid Films **515**, 113 (2006).

[41] F. Rovere and P. H. Mayrhofer, J. Vac. Sci. Technol. A **25**, 1336 (2007).

[42] *Powder Diffraction File 00-025-1133* (International Center for Diffraction Data, PDF-2/Release, 2005).

[43] *Powder Diffraction File 00-046-1200* (International Center for Diffraction Data, PDF-2/Release, 2007).

[44] A. Madan, I. Kim, S. Cheng, P. Yashar, V. Dravid, and S. Barnett, Phys. Rev. Lett. **78**, 1743 (1997).

[45] Q. Li, I. Kim, S. Barnett, and L. Marks, J. Mater. Res. **17**, 1224 (2002).

[46] J. Cai and N. Chen, Phys. Rev. B **75**, 1 (2007).

[47] R. Zhang and S. Veprek, Acta Mater. **57**, 2259 (2009).

[48] R. Schwarz, M. Niehus, S. Koynov, L. Melo, J. Wang, S. Cardoso, and P. Freitas, Diam. Relat. Mater. **10**, 1326 (2001).

[49] A. Shah and A. Mahmood, Phys. B **407**, 3987 (2012).

[50] S.-R. Jian, G.-J. Chen, J. S.-C. Jang, and Y.-S. Lai, J. Alloys Compd. **494**, 219 (2010).

[51] U. Helmersson, S. Todorova, S. A. Barnett, J.-E. Sundgren, L. C. Markert, and J. E. Greene, J. Appl. Phys. **62**, 481 (1987).

[52] M. Larsson, P. Hollman, P. Hedenqvist, S. Hogmark, U. Wahlström, and L. Hultman, Surf. Coat. Technol. **86-87**, 351 (1996).

[53] M. Kot, W. Rakowski, Ł. Major, R. Major, and J. Morgiel, Surf. Coat. Technol. **202**, 3501 (2008).

[54] D. Cameron, R. Aimo, Z. Wang, and K. Pischow, Surf. Coat. Technol. , 567 (2001).

[55] J. Paulitsch, P. Mayrhofer, W.-D. Münz, and M. Schenkel, Thin Solid Films **517**, 1239 (2008).

[56] Y. Cheng, T. Browne, B. Heckerman, C. Bowman, V. Gorokhovsky, and E. Meletis, Surf. Coat. Technol. **205**, 146 (2010).

[57] M. Ohring, *The material science of thin films* (Academic Press, San Diego, California, 1991).

[58] J. Park and Y. Baik, Surf. Coat. Technol. **200**, 1519 (2005).

[59] P. Hovsepian, D. Lewis, Q. Luo, W.-D. Münz, P. Mayrhofer, C. Mitterer, Z. Zhou, and W. Rainforth, Thin Solid Films **485**, 160 (2005).

[60] M. Tomlinson, S. Lyon, P. Hovsepian, and W.-D. Munz, Vacuum **53**, 117 (1999).

[61] C. Ducros and F. Sanchette, Surf. Coat. Technol. **201**, 1045 (2006).

[62] A. D. Porter and K. E. Easterling, *Phase Transformations in Metals ad Alloys* (Van Nostrand Reinhold (UK), 1981).

[63] V. Chawla, D. Holec, and P. H. Mayrhofer, J. Phys. D: Appl. Phys. **46**, 045305 (2013).

[64] J. A. Thornton, Annu. Rev. Mater. Sci. **7**, 239 (1977).

[65] E. O. Hall, Proc. Phys. Soc. B **64**, 747 (1951).

[66] P. Anderson and C. Li, Nanostr. Mat. **5**, 349 (1995).

[67] E. R. Kreidler and P. M. Anderson, MRS Proc. **434**, 159 (1996).

[68] P. M. Anderson and E. R. Kreidler, MRS Proc. **505**, 571 (1997).

[69] P. Anderson, T. Foecke, and P. Hazzledine, MRS Bulletin **24**, 27 (1999).

[70] C.-C. Ma and H.-T. Lu, Phys. Rev. B **73**, 1 (2006).

[71] S. J. Suresha, S. Math, V. Jayaram, and S. K. Biswas, Phil. Mag. **87**, 2521 (2007).

[72] D. Barnett and J. Lothe, Int. J. Solid Struct. **32**, 291 (1995).

[73] J. Pacaud and M. F. Denanot, Surf. Coat. Technol. **175**, 273 (2003).

[74] M. Stoudt, R. Ricker, and R. Cammarata, Int. J. Fatigue **23**, 215 (2001).

[75] X. Chu and S. A. Barnett, J. Appl. Phys. **77**, 4403 (1995).

[76] P. Haasen, *Physical Metallurgy* (Cambridge University Press, London, UK, 1978).

[77] J. Koehler, Phys. Rev. B **2**, 547 (1970).

[78] J. Lin, J. J. Moore, B. Mishra, M. Pinkas, X. Zhang, and W. D. Sproul, Thin Solid Films **517**, 5798 (2009).

[79] P. H. Mayrhofer, C. Mitterer, L. Hultman, and H. Clemens, Prog. Mater. Sci. **51**, 1032 (2006).

[80] S.-K. Tien, C.-H. Lin, Y.-Z. Tsai, and J.-G. Duh, J. Alloys Compd. **489**, 237 (2010).

[81] J. Lin, J. J. Moore, J. Wang, and W. D. Sproul, Thin Solid Films **519**, 2402 (2011).

[82] S. Tien and J. Duh, Thin Solid Films **494**, 173 (2006).

[83] S.-k. Tien, J.-g. Duh, and J.-w. Lee, Mater. Sci. **201**, 5138 (2007).

[84] J. Pope, *Rules of thumb for mechanical engineers* (Gulf Publishing Company, Houston, Texas, 1997) p. 400.

[85] C.-j. Li, W.-z. Wang, and Y. He, J. Am. Ceram. Soc. **39**, 1437 (2003).

[86] G. Jaeger, Thin Solid Films **377-378**, 382 (2000).

[87] A. Riedl, R. Daniel, M. Stefenelli, T. Schöberl, O. Kolednik, C. Mitterer, and J. Keckes, Scr. Mater. **67**, 708 (2012).

[88] H. Hirakata, M. Kitazawa, and T. Kitamura, Acta Mater. **54**, 89 (2006).

[89] R. Springer and D. Catlett, Thin Solid Films **54**, 197 (1978).

[90] B. Movchan, A. Demchishin, G. Badilenko, R. Bunshah, C. Sans, C. Deshpandey, and H. Doerr, Thin Solid Films **97**, 215 (1982).

[91] Y. Huang and H. Zhang, Acta Metall. Mater. **43**, 1523 (1995).

[92] S. Zhang, D. Sun, Y. Fu, and H. Du, Surf. Coat. Technol. **198**, 2 (2005).

[93] K. Chan, M. He, and J. Hutchinson, Mater. Sci. Eng. A **167**, 57 (1993).

[94] M. Stueber, H. Holleck, H. Leiste, K. Seemann, S. Ulrich, and C. Ziebert, J. Alloys Compd. **483**, 321 (2009).

[95] S. Wang, X. Huang, J. Guo, and B. Li, Mater. Lett. , 43 (1996).

[96] N. Bamba, J. Eur. Ceram. Soc. **23**, 773 (2003).

[97] L. Sestakova, R. Bermejo, Z. Chlup, and R. Danzer, Int. J. Mat. Res. **102**, 613 (2011).

[98] K. Hwu and B. Derby, Acta Mater. **47**, 545 (1999).

[99] B. Mayer, *Influence of the bilayer period on the structure of AlN and the mechanical properties of CrN/AlN superlattice coatings*, Master's thesis, Montanuniversität, Leoben (2012).

[100] A. Fischer-Cripps, *Nanoindentation* (Springer Science and Business Media LLC, New York, 2004).

[101] W. Oliver and G. Pharr, J. Mater. Res. **7**, 1564 (1992).

[102] A. Cavaleiro and J. De Hosson, *Nanostructured Coatings* (Springer Science and Business Media LLC, New York, 2006).

[103] L. Qian, Surf. Coat. Technol. **173**, 178 (2003).

[104] S. Zhang, D. Sun, Y. Fu, and H. Du, Thin Solid Films **469-470**, 233 (2004).

[105] J. Elambasseril, R. Ibrahim, and R. Das, Compos. B: Eng. **42**, 1596 (2011).

[106] A. Ray, J. Eur. Ceram. Soc. **19**, 2097 (1999).

[107] J. Carneiro, J. Alpuim, and V. Teixeira, Surf. Coat. Technol. **200**, 2744 (2006).

[108] K. Khor, Y. Gu, and Z. Dong, Surf. Coat. Technol. **139**, 200 (2001).

[109] S. Bhowmick, R. Bhide, M. Hoffman, V. Jayaram, and S. K. Biswas, Phil. Mag. **85**, 2927 (2005).

[110] H. Zaidi, A. Djamai, K. Chin, and T. Mathia, Tribol. Int. **39**, 124 (2006).

[111] A. S. Argon, *Strengthening mechanisms in crystal plasticity* (Oxford University Press, Oxford, 2008).

[112] K. Matoy, T. Detzel, M. Müller, C. Motz, and G. Dehm, Surf. Coat. Technol. **204**, 878 (2009).

[113] M. J. Cordill, A. Taylor, J. Schalko, and G. Dehm, Metall. Mater. Trans. A **41**, 870 (2009).

[114] D. Agrawal and R. Raj, Acta Metall. **37**, 1265 (1989).

Chapter 5

# Papers

## 5.1 Publications included into this Thesis

### Publication I

*Influence of CrN and AlN layer thicknesses on structure and mechanical properties of CrN/AlN superlattices*
**M. Schlögl**, B. Mayer, J. Paulitsch, P.H. Mayrhofer
Manuscript submitted to Thin Solid Films.

### Publication II

*Influence of the CrN and AlN thicknesses on the thermal and mechanical properties of CrN/AlN superlattice coatings*
**M. Schlögl**, J. Paulitsch, P.H. Mayrhofer
Manuscript in final preparation.

### Publication III

*Publication Influence of AlN Layers on Mechanical Properties and Thermal Stability of Cr-Based Nitride Coatings*
**M. Schlögl**, J. Paulitsch, J. Keckes, P.H. Mayrhofer
Thin Solid Films (2012), article in press.
doi: 10.1016/10.1016/j.tsf.2012.12.057

### Publication IV

*Effects of structure and interfaces on fracture toughness of CrN/AlN multilayer coatings*
**M. Schlögl**, C. Kirchlechner, J. Paulitsch, J. Keckes, P.H. Mayrhofer
Manuscript submitted to Scripta Materialia.

## 5.2 (Co)Supervised Diploma Thesis

*Influence of the bilayer period on the structure of AlN and the mechanical properties of CrN/AlN superlattice coatings*
Bernhard Mayer, finished in October 2012.

# Publication I

*Influence of CrN and AlN layer thicknesses on structure and mechanical properties of CrN/AlN superlattices*

**M. Schlögl**, B. Mayer, J. Paulitsch, P.H. Mayrhofer

Manuscript submitted to Thin Solid Films.

# Influence of CrN and AlN layer thicknesses on structure and mechanical properties of CrN/AlN superlattices

M. Schlögl,[1,2] B. Mayer,[1] J. Paulitsch,[2] and P.H. Mayrhofer[2]

[1] *Department of Physical Metallurgy and Materials Testing, Montanuniversität Leoben, A-8700 Leoben, Austria*

[2] *Institute of Materials Science and Technology, Vienna University of Technology, A-1040 Vienna, Austria*

Based on their outstanding chemical, physical and mechanical properties, CrN/AlN multilayer coatings are the topic of many research activities. Our results for CrN/AlN superlattice coatings with AlN layer thicknesses of 1, 2 and 3 nm combined with CrN layer thicknesses ranging from 1 to 10 nm suggest that the CrN layer thicknesses need to be at least as thick as the targeted AlN layer thicknesses to provide sufficient strength for a fully stabilization of the AlN layers in their metastable cubic structure by epitaxial strain. Otherwise, the AlN layers tend to crystallize in their stable hexagonal (wurtzite type) structure leading to the loss of coherency between alternating CrN and AlN layes. Hardness maxima of 31.0 GPa are obtained at a bilayer period $\Lambda$ of 3 and 5.5 nm, for the fully cubic superlattice coatings composed of 1 and 2 nm thin AlN layers, respectively. Due to the reduced number of interfaces per coating thickness, only a hardness maximum of $\sim 28.5$ GPa at $\Lambda = 6.3$ nm can be obtained for the coatings composed of 3 nm thin AlN layers.

Our study clearly demonstrates that the structural and mechanical properties of superlattice CrN/AlN coatings not just depend on the bilayer period but on the individual layer thicknesses.

Keywords: magnetron sputtering, superlattice coating, CrN/AlN, wurtzite, cubic, hardness, structure

## I. INTRODUCTION

Multilayer coatings composed of different metal nitrides such as CrN or TiN and AlN are widely used for numerous applications [1–7], as they allow for optimized properties, e.g. thermal stability or fracture toughness [8, 9], by simply varying the individual layer materials and their thicknesses. Especially, synthesizing multilayer coatings with epitaxially grown layers having thicknesses in the nanometer range–so-called superlattice coatings– are able to provide superior hardness values [7, 10–12]. Such an increase in mechanical properties, as compared to their individual single-layered counterparts, can only be obtained if the alternating layers show a significant difference in their elastic constants, bonding energies and their dislocation-line energies [3, 13]. Furthermore, the layer with the lower dislocation-line energy has to be thin enough to inhibit dislocation-generation mechanisms [13]. The results of Kim and Lin et al. indicate that CrN/AlN superlattice coatings exhibit a 1.6 times higher hardness value as their single-layered counterpart coatings. The peak hardness value of $\sim 42$ GPa was obtained for a bilayer period $\Lambda$ of 4.1 nm [7, 12]. However, such an increase in hardness can only be obtained if the AlN layer is stabilized in its (metastable) cubic (face centered cubic, NaCl prototype, B1) structure, for simplicity abbreviated with c-AlN. Within the TiN/AlN and CrN/AlN multilayer systems the AlN layers can only be stabilized in their metastable cubic structure up to layer thicknesses of $\sim 3$ nm. For thicker layers the stable hexagonal (hexagonal close packed, ZnS-wurtzite prototype, B4) w-AlN phase is preferred [12, 14]. However, variations in the strain and interface energy can also lead to a reduction of the critical AlN layer thickness (e.g., to 1.95 nm for TiN/AlN [15]) before w-AlN is preferred. Chawla *et al.* [16] showed, that the stabilization of c-AlN within multilayers strongly depends on the elastic properties, the crystallographic orientation and lattice parameters of the other layer material, as well as the strength of the substrate.

Although there are many studies on the influence of the bilayer period $\Lambda$ on the mechanical properties of CrN/AlN multilayer coatings, the effect of the individual layer thicknesses of CrN or AlN is still not explored in detail. Consequently, the aim of this work is to investigate the influence of the individual CrN and AlN layer thicknesses on the structure and mechanical properties. Therefore, CrN/AlN multilayer coatings with AlN layer thicknesses of 1, 2 and 3 nm combined with variations of the CrN layer thicknesses from 1 to 10 nm were prepared and investigated for their morphology, structure and mechanical properties.

## II. EXPERIMENTAL

CrN/AlN superlattice coatings were deposited on Si 1 0 0 strips ($20 \times 7 \times 0.38\,\mathrm{mm}^3$), using an AJA Orion 5 lab scale deposition unit equipped with one 3" Cr (99.9% purity) and two 2" Al (99.9% purity) targets. The base pressure of the chamber was always below 0.1 mPa. Prior to all depositions the Si substrates were thermally-cleaned at 500 °C for 20 min as well as Ar ion etched at a pressure of $4 \cdot 10^{-2}$ mbar (4 Pa). The depositions were carried out in a mixed $Ar/N_2$ glow discharge at a working gas pressure of $4 \cdot 10^{-3}$ mbar (0.4 Pa). The Ar to $N_2$ flow ratio was kept constant for all runs at 2/3 and the temperature was set to 470 °C. CrN/AlN superlattice coatings were prepared by using a computer controlled powering device allowing for alternately dc-powering of

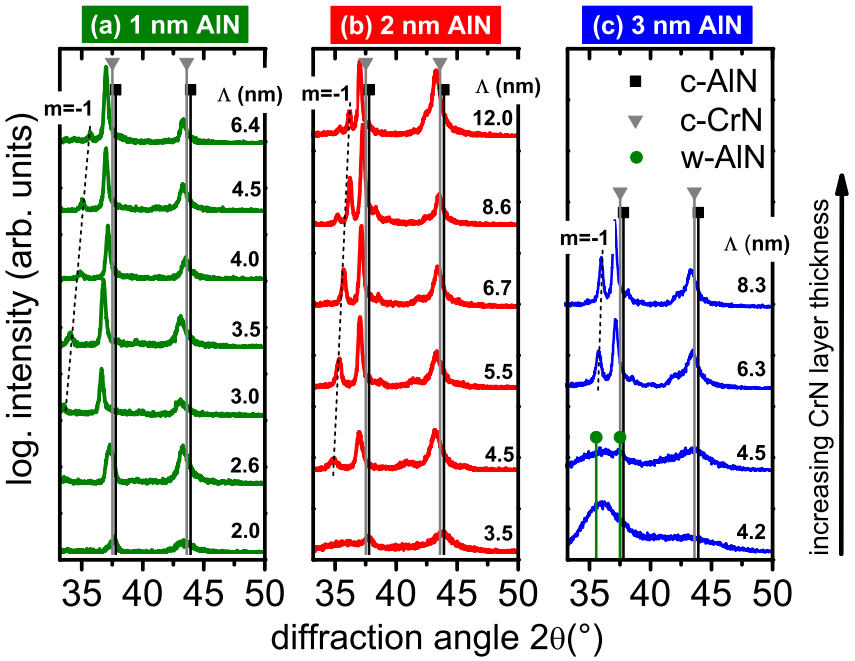


FIG. 1. XRD scans in Bragg Brentano configuration of CrN/AlN multilayer coatings with (a) 1 nm, (b) 2 nm and (c) 3 nm thin AlN layers and increasing CrN layer thicknesses (represented by the labeled bilayer period Λ, in nm). The 1st order satellite peaks are marked with $m = -1$. The standard peak positions for c-AlN, c-CrN and w-AlN are added, as given in the ICDD data base [17].

the Cr and Al targets for different time periods at 250 W. During deposition a −70 V rf-biasing of the substrates was used to ensure dense coating morphologies.

Structural investigations and bilayer measurements of the as deposited films were conducted by high angle X-ray diffraction (XRD) in the Bragg-Brentano mode using a Bruker AXS D8 diffractometer equipped with a Cu $K_\alpha$ radiation source ($\lambda = 1.5456$ nm).

Detailed characterizations of our multilayers were conducted by transmission electron microscopy (TEM), within a Phillips CM12 microscope, operating at 120 kV as well as by high resolution transmission electron microscopy (HRTEM) using a Tecnai F20 operating at 200 kV.

Measurements of the indentation hardness ($H$) of the coatings on Si substrates were conducted with a CSIRO ultra micro indentation system equipped with a Berkovich-tip and evaluated using the loading and unloading segments according to Oliver and Pharr [18]. Residual stresses $\sigma$ of our coatings were determined by biaxial residual stress measurements using the substrate-curvature method [19].

## III. RESULTS AND DISCUSSION

### A. Structure and Morphology

Structural investigations of our CrN/AlN multilayer coatings by XRD analysis in Bragg Brentano configuration are shown in Figs. 1a, b and c for AlN layer thicknesses of 1, 2 and 3 nm, respectively, and variations for their CrN layer thicknesses resulting in the given bilayer periods Λ. The latter are calculated after Yashar et al. [4] using the first order satellite peak positions, marked in Fig. 1 with $m = -1$. These satellite peaks suggest the formation of a superlattice structure of our CrN/AlN multilayers. The calculated bilayer periods are in excellent agreement with our TEM investigations (next paragraph) which were furthermore used to identify the individual AlN layer thicknesses. The results demonstrate a single phase cubic structure for all multilayer coatings with 1 nm thin AlN layers, see Fig. 1a, independent of the bilayer period (i.e., CrN layer thickness variation). The XRD patterns also suggest–by the narrowing of the XRD peaks–an increase in grain size with increasing bilayer period. Such an increase in grain size is expected based on the transition from competitive to preferential crystal

growth with increasing layer thickness and furthermore, the grain size for thin layers is also limited by the layer thickness. However, the structures of CrN/AlN superlattice coatings composed of 2 and 3 nm thin AlN layers are more sensitive to the CrN layer thicknesses, see Figs. 1b and c, respectively. Keeping the bilayer period $\Lambda \leq 3.5$ and 4.5 nm (hence, the CrN layers thinner than 1.5 nm), Figs. 1b and c, respectively, result in a decrease of the cubic crystallinity degree. The results suggest even an XRD amorphous structure, or at least for a dual-phase mixed wurtzite-cubic structure. For these systems the CrN layer thicknesses are too thin to allow for a fully epitaxial-strain-induced stabilization of the AlN phase in its metastable cubic structure. Increasing the bilayer period to values above 4.5 and 6.3 nm (hence, CrN layers thicker than 2.5 and 3.3 nm), Figs. 1b and c, respectively, results in a well-defined cubic structure of the CrN/AlN multilayers. The results obtained clearly show that a fully stabilization of the AlN layers in their metastable cubic structure is only obtained if the CrN layers are at least as thick as the AlN layers combined with the condition that the AlN layers need to be thinner than 3 nm.

To investigate the influence of the CrN layer thicknesses on the structure of the AlN layers in more detail, HRTEM investigations of our coatings with bilayer periods of 2 and 3 nm (1 nm thin AlN layers), 3.5 nm (2 nm thin AlN layers) as well as 4.2 and 6.3 nm (3 nm thin AlN layers) were carried out, Figs. 2, 3 and 4, respectively. The images clearly show the multilayer architecture of our coatings and confirm the bilayer periods calculated from the satellite peaks obtained by XRD investigations, Fig. 1. The multilayers exhibit a dense morphology and columnar grains, elongated in the growth direction. The images of the CrN/AlN coatings with 1 nm thin AlN layers and $\Lambda = 2$ nm, Figs. 2a and b, and $\Lambda = 3$ nm, Figs. 2c and d, indicate continuing lattice fringes throughout the CrN and AlN layers, as well as sharp interfaces between them. Fast Fourier Transformation (FFT) of these coatings, insets in Figs. 2b and d, proof the face centered cubic structure of the AlN layers and suggest 1 1 1 and 2 0 0 lattice-plane distances of 2.37 and 2.06 Å, respectively [20]. For these coatings, the CrN layers are strong enough to provide a template effect for the AlN layers. For the coating with the smallest bilayer period of 2 nm combined with a 1 nm thin AlN layer, hence a CrN layer thickness of $\sim 1$ nm, the data suggest that the only 1 nm thin AlN layer does not provide a sufficiently high strain to break coherency to the cubic CrN layer. Hence, also for this combination with an extremely thin CrN layer of only $\sim 1$ nm a fully cubic structure is obtained.

If the AlN layer thickness is increased to 2 nm, Figs. 3a and b for $\Lambda = 3.5$ nm, the results are a bit different. A bilayer period of 3.5 nm, which corresponds to CrN layer thicknesses of 1.5 nm, is not sufficient to fully stabilize the 2 nm thin AlN layers in their metastable cubic structure. Hence, epitaxial growth of the layers is interrupted– as now the AlN layers prefer a different structure as the underlying CrN layers–leading to necessary re-nucleation

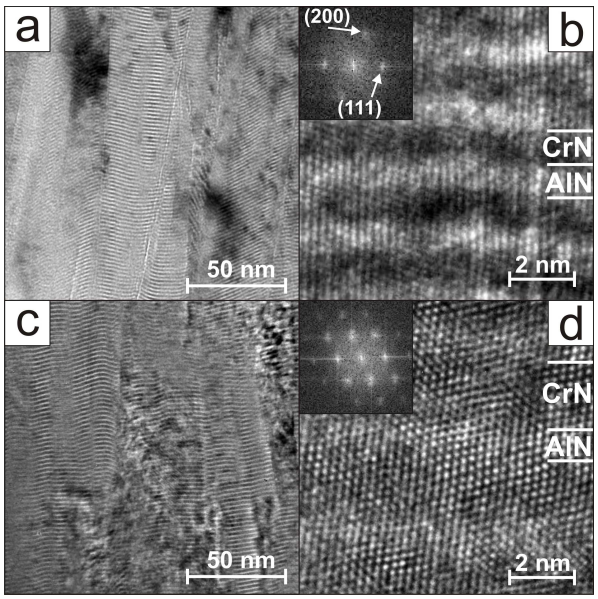


FIG. 2. TEM and HRTEM cross section images of CrN/AlN multilayer coatings with 1 nm thin AlN layers and a bilayer period $\Lambda$ of 2 nm (a and b) and 3 nm (c and d), respectively.

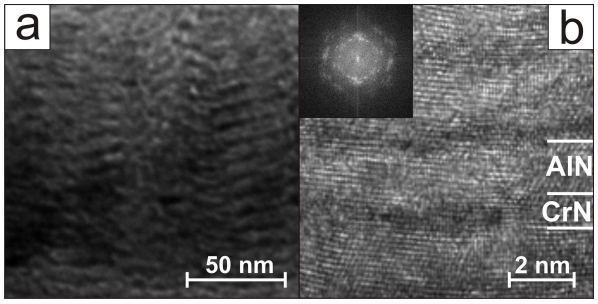


FIG. 3. TEM (a) and HRTEM (b) cross section images of CrN/AlN multilayer coating with 2 nm thin AlN layers and a bilayer period of $\Lambda = 3.5$ nm.

events for the subsequent CrN layers. This results in the observed discontinuity of the columnar growth, Fig. 3a. FFT analyses of the AlN layers, inset in Fig. 3b, confirm the XRD findings, Fig. 1b, of additional non-cubic structural contributions and suggest hexagonal additions. The alternation of preferably cubic (c-CrN) and hexagonal (w-AlN) layers, leads to an inhibited crystal growth and the formation of a more polycrystalline nanostructured nature of the CrN/AlN coating.

However, increasing the bilayer period to 5.5 nm which corresponds to an increase of the CrN layer thicknesses to 2.5 nm, allows for fully stabilizing the AlN layers in their metastable cubic structure as shown by XRD, Fig. 1b. Hence, a structure corresponding to the results obtained for the CrN/AlN superlattice coatings composed of 1 nm

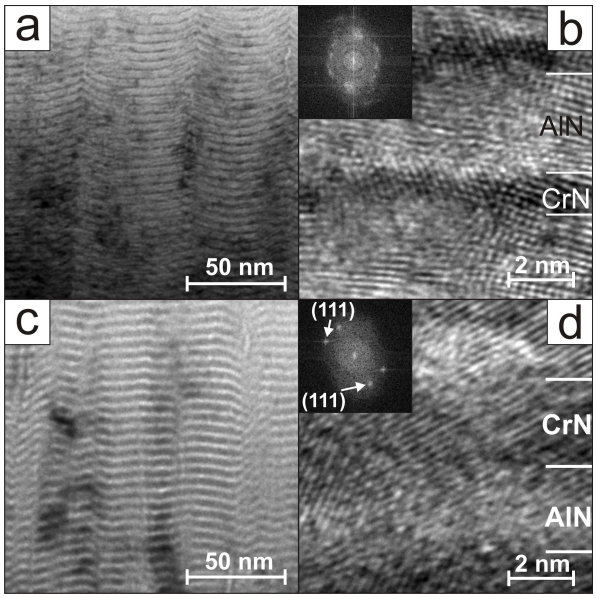


FIG. 4. TEM and HRTEM cross section images of CrN/AlN multilayer coatings with 3 nm thin AlN layers and a bilayer period Λ of 4.2 nm (a and b) and 6.3 nm (c and d), respectively.

thin AlN layers with a fully epitaxial growth of the CrN and AlN layers will be formed, Figs. 2a and c.

TEM and HRTEM cross sectional investigations of CrN/AlN multilayers with AlN layer thicknesses of around 3 nm, Figs. 4a and b for Λ = 4.2 nm and Figs. 4c and d for Λ = 6.3 nm, further confirm the previous suggestions and findings. If the CrN layers are thinner than the AlN layers they are not able to provide the necessary strength to stabilize the AlN layers in their metastable cubic structure by epitaxial strain, Figs. 4a and b. The competitive growth of cubic and hexagonal structured AlN grains leads to a loss of coherency and a more randomly oriented mixed crystalline structure, see the FFT inset in Fig. 4b. If the CrN layers are thicker than the AlN layers, a fully epitaxial relation between these layers can be obtained leading to a complete stabilization of AlN in the metastable cubic structure, FFT inset of Fig. 4d. Consequently, the growth of crystals during deposition is not interrupted leading to a well-defined columnar morphology, Fig. 4c.

### B. Mechanical Properties

The hardnesses of our CrN/AlN multilayer coatings with 1, 2 and 3 nm thin AlN layers exhibit a pronounced and comparable dependence on their bilayer periods, Fig. 5, which is typical for superlattice coatings as presented for CrN/AlN, CrN/CrAlN and TiN/VN in Refs. [2, 10, 21]. The coating systems with 1, 2 and 3 nm

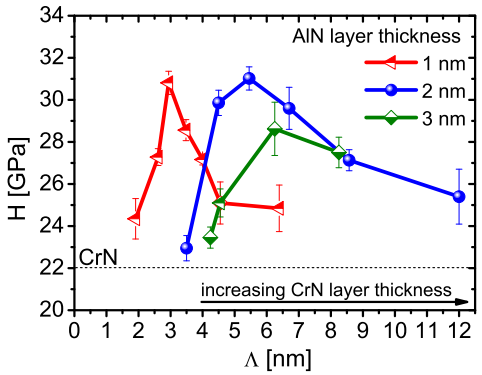


FIG. 5. Hardness measurements ($H$) of our CrN/AlN superlattice coatings with 1 nm (triangle), 2 nm (balls) and 3 nm (diamond) thin AlN layers as a function of their bilayer period Λ.

thin AlN layers, yield their peak hardness values of 31.0, 31.0 and 28.5 GPa at Λ = 3, 5.5 and 6.3 nm respectively. When compared with the corresponding single-layered boundary systems, with $H \sim 22$ GPa for CrN and $H = 14$–$20$ GPa for w-AlN [22], an increase in hardness by around 40% can be obtained due to the superlattice effect. In addition, also the stabilization of AlN in its metastable cubic structure plays an important role. The pronounced hardness increase due to the superlattice structure is mainly based on the hindered dislocation generation and motion by the nm-sized alternating layers providing different shear moduli and dislocation-line energies. Hence, propagation of dislocations across the different layers of CrN and AlN is extremely difficult, as reported by Koehler *et al.* [13, 23–25]. To propagate dislocations from the lower-shear-moduli-layer to the higher-shear-moduli-layer (i.e., from c-CrN to c-AlN) additional strains are necessary, to be reflected by the increased hardnesses. The result obtained are in good agreement with ab initio calculations, indicating comparable shear moduli $G$ for c-CrN ($\sim 140$ GPa [26]) and w-AlN ($\sim 116$ GPa [27]), whereas for c-AlN a nearly twice as high value is obtained with $G \sim 220$ GPa [28]. Consequently, for coatings with thin CrN layers–which do not provide the required strength to fully stabilize the AlN layers in their metastable cubic structure–the hardness increase is not as pronounced as for thicker CrN layers, which allow for a fully cubic stabilization of the AlN layers.

However, a further increase in CrN layer thicknesses results in a decline of the hardness towards that of single-layered CrN ($H \sim 22$ GPa) for all multilayer systems investigated with 1, 2 and 3 nm thin AlN layers. This can be explained by the reduction of the interface density (i.e., number of interfaces along the coating thickness) and consequently changes in the stress/strain state with increasing the layer thicknesses as described by the 2D

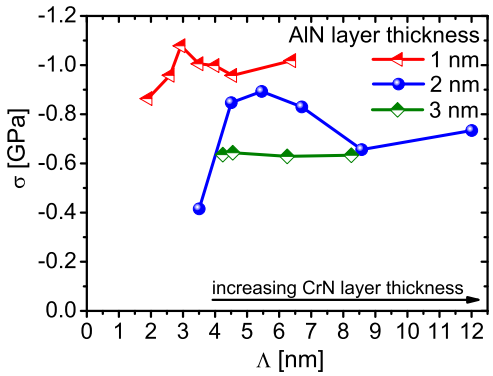


FIG. 6. Biaxial residual stresses ($\sigma$) of our CrN/AlN superlattice coatings with 1 nm (triangle), 2 nm (balls) and 3 nm (diamond) thin AlN layers as a function of their bilayer period $\Lambda$.

model of dislocation pile-ups from Anderson and Li [29], and by the reduction of the grain size hardening effect (i.e., Hall-Patch effect [30]). An increased layer thickness allows not only for generation of new dislocations–as now dislocation sources such as Frank-Read sources [31] can be active–but also enables them to move long distances [4]. Therefore, a layer should be thin to hinder the generation of dislocations but thick enough to avoid that also the number of dislocation loops per layer decreases. If there are too few dislocation loops also less strain is necessary to operate the dislocation sources, resulting in lower hardness values [4, 29]. The combination of these effects can explain the lower hardness maximum for the fully cubic superlattice coatings composed of 3 nm thin AlN layers when compared to their counterparts with 1 and 2 nm thin AlN layers. Also the hardness decrease with decreasing bilayer period below 3, 5.5 and 6.3 nm for the three systems with 1, 2 and 3 nm thin AlN layers, respectively, is based on the combination of their effects. The layer should be thin to hinder dislocation-generation but thick enough to allow for dislocation-interaction. For the coatings with CrN/AlN layer thickness-ratios (in nm) of 1.5/2, 1.2/3 and 1.5/3 the hardness reduction is further influenced by the additional effect of losing the epitaxial relationship between the CrN and AlN layers and the thereby connected preference of AlN to crystallize in the wurtzite phase exhibiting a lower shear moduli, as described above. Please remember, this occurs if the CrN layer is thinner than the AlN layer.

A comparable dependence on the bilayer period as obtained for the hardnesses exhibit also the stresses of the coatings as obtained from cantilever beam bending methods, Fig. 6. The coatings which show the highest hardnesses also have the highest compressive stresses. This is also indicated by the XRD (Fig. 1) as highest peak position deviations from the standard position are observed for the coatings having also the highest hardnesses. With decreasing AlN layer thicknesses the peak-formation of stresses becomes sharper as a function of the bilayer period and the stress-profiles are shifted to lower bilayer periods and higher compressive stress values. This dependence can be attributed to the increasing number of layers and consequently the increasing number of interfaces. For the superlattice coatings composed of 3 nm thin AlN layers the variation of compressive stresses is almost within the error of measurement as a function of the different bilayer periods.

## IV. CONCLUSIONS

The influence of the individual layer thicknesses of CrN and AlN on structural and mechanical properties of CrN/AlN superlattices prepared by DC reactive magnetron sputtering is studied in detail. We used AlN layer thicknesses of 1, 2 and 3 nm and varied the corresponding CrN layers between 1 and 10 nm. Based on XRD, TEM and HRTEM we can conclude that a fully stabilization of the AlN layers in their metastable cubic structure can be achieved up to an AlN layer thickness of 3 nm with the condition that the CrN layers neeed to be at least as thick as the AlN layers. For thinner CrN layers, especially the 2 and 3 nm thin AlN layers tend to crystallize in their stable wurtzite structure. CrN/AlN layer-thickness ratios above 1 allow for a fully cubic structure and a pronounced hardness maximum of $H = 31$ GPa for 1 and 2 nm thin AlN layers combined with a bilayer period $\Lambda$ of 3 and 5.5 nm, respectively, and $H = 28.5$ GPa for 3 nm thin AlN layers combined with $\Lambda = 6.3$ nm.

The study clearly demonstrates that especially for superlattice coatings containing AlN layers it is extremely important to concentrate on the individual layer thicknesses as well as on the bilayer period. The layers providing epitaxial relationship to stabilize the AlN layer in the targeted metastable cubic structure need to be strong and thick enough, but at the same time thin enough to allow for a pronounced hardness increase by the superlattice effect.

## ACKNOWLEDGMENTS

The authors highly acknowledge financial support by the START project (Project No. Y371) and the LISE MEITNER Program (Project No. M1233) of the Austrian Science Fund (FWF). Further acknowledgements are given to Dr. Daniel Kiener, Matthias Nöhrer and Dr. Krystyna Spiradek-Hahn and Manfred Brabetz of ADG Seibersdorf for supporting with HRTEM and TEM investigations.

[1] H. Holleck, J. Vac. Sci. Technol., A **4**, 2661 (1986).
[2] U. Helmersson, S. Todorova, S. A. Barnett, J.-E. Sundgren, L. C. Markert, and J. E. Greene, J. Appl. Phys. **62**, 481 (1987).
[3] X. Chu and S. A. Barnett, J. Appl. Phys. **77**, 4403 (1995).
[4] P. C. Yashar and W. D. Sproul, Vacuum **55**, 179 (1999).
[5] S. Vepek and S. Reiprich, Thin Solid Films **268**, 64 (1995).
[6] S. Veprek, R. Zhang, M. Veprek-Heijman, S. Sheng, and A. Argon, Surf. Coat. Technol. **204**, 1898 (2010).
[7] G. S. Kim, S. Y. Lee, and J. H. Hahn, Surf. Coat. Technol. **171**, 91 (2002).
[8] S. Zhang, D. Sun, Y. Fu, and H. Du, Surf. Coat. Technol. **198**, 2 (2005).
[9] G. Was and T. Foecke, Thin Solid Films **286**, 1 (1996).
[10] J. Park and Y. Baik, Surf. Coat. Technol. **200**, 1519 (2005).
[11] J. Lin, J. Moore, B. Mishra, M. Pinkas, and W. Sproul, Surf. Coat. Technol. **204**, 936 (2009).
[12] J. Lin, J. J. Moore, B. Mishra, M. Pinkas, X. Zhang, and W. D. Sproul, Thin Solid Films **517**, 5798 (2009).
[13] J. Koehler, Phys. Rev. B **2**, 547 (1970).
[14] M. Setoyama, A. Nakayama, M. Tanaka, N. Kitagawa, and T. Nomura, Surf. Coat. Technol. **86-87**, 225 (1996).
[15] D. Chen, X. Ma, and Y. Wang, Acta Mater. **53**, 5223 (2005).
[16] V. Chawla, D. Holec, and P. H. Mayrhofer, J. Phys. D: Appl. Phys. **46**, 045305 (2013).
[17] *Powder Diffraction File 03-065-2899 (c-CrN), 01-076-0702 (w-AlN), 00-025-1495 (c-AlN)* (International Center for Diffraction Data, PDF-2/Release, 2005).
[18] W. Oliver and G. Pharr, J. Mater. Res. **7**, 1564 (1992).
[19] A. Brenner and S. Senderoff, J. Res. **42**, 105 (1949).
[20] *Powder Diffraction File 00-025-1495* (International Center for Diffraction Data, PDF-2/Release, 2007).
[21] Y. Kim, T. Byun, and J. Han, Superlattice Microst. **45**, 73 (2009).
[22] S.-R. Jian, G.-J. Chen, J. S.-C. Jang, and Y.-S. Lai, J. Alloys Compd. **494**, 219 (2010).
[23] J. Koehler, Phys. Rev. **86**, 52 (1952).
[24] J. Gilman, Philos. Mag. A **76**, 329 (1997).
[25] J. Koehler and T. Blewitt, Phys. Rev. Lett. , 1952 (1949).
[26] L. Zhou, D. Holec, and P. H. Mayrhofer, submitted in J. Appl. Phys. (2012).
[27] S. Łepkowski, J. Majewski, and G. Jurczak, Phys. Rev. B **72**, 245201 (2005).
[28] D. Holec, M. Friák, J. Neugebauer, and P. Mayrhofer, Phys. Rev. B **85**, 064101 (2012).
[29] P. Anderson and C. Li, Nanostr. Mat. **5**, 349 (1995).
[30] E. O. Hall, Proc. Phys. Soc. B **64**, 747 (1951).
[31] G. Dehm, C. Motz, C. Scheu, H. Clemens, P. H. Mayrhofer, and C. Mitterer, Adv. Eng. Mater. **8**, 1033 (2006).

# Publication II

*Influence of the CrN and AlN thicknesses on the thermal and mechanical properties of CrN/AlN superlattice coatings*

**M. Schlögl**, J. Paulitsch, P.H. Mayrhofer

Manuscript in final preparation.

# Influence of the CrN and AlN thicknesses on the thermal and mechanical properties of CrN/AlN superlattice coatings

M. Schlögl,[1,2] J. Paulitsch,[2] and P.H. Mayrhofer[2]

[1] *Department of Physical Metallurgy and Materials Testing, Montanuniversität Leoben, A-8700 Leoben, Austria*

[2] *Institute of Materials Science and Technology, Vienna University of Technology, A-1040 Vienna, Austria*

CrN/AlN superlattice coatings are well known for their high strength and hardness. Nevertheless, only few investigations deal with their thermal stability and the thermo-mechanical properties. Recently we showed that the structural evolution of AlN layers during growth of CrN/AlN superlattices not only depends on its own layer thickness but also strongly on the thickness of the CrN layers. Fully cubic stabilized multilayers are obtained when the AlN layers are thinner than 3 nm combined with CrN/AlN layer thickness ratios above 1. Here we show that with increasing AlN layer thickness the thermal stability of the CrN/AlN superlattice coatings increases. Furthermore, higher thermal stability and thermo-mechanical properties are obtained when the CrN layer thickness is reduced to a minimum, regardless of the AlN layer thickness and structure. Even after vacuum annealing to 1100 °C their hardness is almost at the as as-deposited value of 23.5 GPa. The results are supported by differential scanning calorimetry and thermo gravimetric measurements combined with X-ray diffraction after various annealing steps.

## I. INTRODUCTION

Ceramic-like hard coatings such as CrN and TiN are highly valued for a wide range of applications in high temperature, abrasive and corrosive environments [1–5]. Alloying Al to these binary coating systems indicated increased mechanical properties and moreover thermal stability and oxidation resistance due to the formation of a dense protective aluminium oxide layer [6–14]. However, the metastable solubility limit of AlN within the $Cr_{1-x}Al_xN$ and $Ti_{1-x}Al_xN$ coatings, to form face centered cubic (c, NaCl) structures, limits the optimization of these coatings by simply increasing the AlN content [10, 15]. In addition to monolithically grown coatings also multilayer coating architectures became increasingly important, as they allow to combine individual layers creating numerous interfaces which can act as obstacles for the inward and outward diffusion of ion species [16]. This is important to effectively increase the thermal stability. Cubic structured CrN/AlN multilayer coatings with an optimized bilayer thickness in the nanometer range (superlattice coatings) exhibit superior mechanical properties when compared to monolithically grown CrN or $Cr_{1-x}Al_xN$ coatings [16–20]. While the structure of ternary $Cr_{1-x}Al_xN$ coating systems is mainly influenced by the content of Al, the structure and consequently the mechanical properties of the CrN/AlN multilayer coatings are mainly affected by the individual layer thicknesses of AlN and CrN, as shown by several research groups [16, 21, 22].

Even though structural and mechanical properties of CrN/AlN superlattice coatings are investigated in detail, only few publications concentrate on the thermal behavior of such coatings. Lin et al. observed for wurtzite AlN containing CrN/AlN multilayer coatings a poor oxidation resistance when annealing up to 1100 °C in ambient air [23]. However, stabilizing CrN/AlN in the cubic structure with increased AlN layer thicknesses should result in enhanced thermal properties due to the formation of a protective alumina outer-layer, as well as due to the layered structure and stabilization against decomposition at elevated temperatures [18, 19].

Recently we investigated the influence of CrN layer thickness on the stabilization of c-CrN/AlN superlattice coatings and their resulting mechanical properties [22]. Here we study the influence of the different bilayer periods and structure obtained within our CrN/AlN superlattice coatings on their thermal behavior.

Our results clearly indicate that superior properties in the as deposited state do not also guarantee for increased thermal resistance, and demonstrate the need of detailed knowledge on the field of application.

## II. EXPERIMENTAL DETAILS

CrN/AlN superlattice coatings were deposited in a laboratory scaled unbalanced magnetron deposition unit (AJA Orion 5) equipped with one Cr (99.9% purity) and two Al (99.9% purity) targets with a diameter of 3" (76.2 mm) and 2" (50.8 mm), respectively, on sapphire ($10 \times 10 \times 0.53\ mm^3$) and Si platelets ($7 \times 21 \times 0.35\ mm^3$) as well as on copper foil ($\varnothing 114 \times 0.05\ mm^3$). After evacuating the chamber to a back pressure of below $1 \cdot 10^{-7}$ mbar (0.1 mPa) the sapphire was thermal-cleaned at 500 °C for 20 min as well as rf Ar ion etched for 5 min at a total pressure of $4 \cdot 10^{-4}$ mbar (0.04 Pa). The depositions were carried out in an $Ar/N_2$ gas mixture (ratio of 40/60%) at a working pressure of $4 \cdot 10^{-3}$ mbar (0.4 mPa) and the temperature were set to 470 °C. During deposition a −70 V rf-biasing of the substrates was used. The layer thickness in the CrN/AlN superlattice coatings were adjusted by a computer controlled device which alternately dc-powered the Cr and Al targets for different periods at 250 W. Due to the different thick-

nesses of CrN and AlN layer the number of layers varied from 250 to 580 to provide constant total coating thickness of $\sim 1.5$ µm for all coatings.

The investigation of phase transformation and thermal resistance of our multilayer coatings were conducted on grinded coating powder (after chemical removal of their Cu-substrates using a diluted nitric acid) by combining differential scanning calorimetry (DSC) and thermal gravimetric analyzes (TGA) in a SETSYS Evolution TMA (Setaram instrumentation) calorimeter. The measurements were accomplished in He atmosphere at temperatures up to 1500 °C with a constant heating rate of 20 °C/min.

The crystal structure of the coated Si (as deposited state) and powdered coating (as deposited and annealed state) was investigated by X-ray diffraction (XRD) analysis, using a Bruker AXS D8 diffractometer equipped with a Cu $K_\alpha$ ($\lambda = 1.54056$ nm) radiation source in the Bragg-Brentano configuration. A Tecnai F20 high resolution transmission electron microscope (HRTEM) operating at 200 kV was used to examine the bilayer period and the crystal structure of the multilayers. The annealing of the coated sapphire and the thin film powder was executed in a vacuum furnace (HTM Reetz GmbH, base pressure $< 5 \cdot 10^{-4}$ Pa) from 700 to 1500 °C in steps of 100 °C with a heating and cooling rate of 20 °C/min and a holding time of 20 min. The hardness ($H$) measurements of coated sapphire in the as-deposited state and after annealing up to 1100 °C were accomplished in a CSIRO ultra micro indentation system equipped with a Berkovich-tip and evaluated after the Oliver and Pharr method [24]. The maximum load was set to 20 mN and the indentation depth was kept below 10% of the film thickness in order to minimize possible substrate interference.

## III. RESULTS AND DISCUSSION

Investigations of variations in the individual layer thicknesses of CrN/AlN multilayer coatings showed a significant influence on the structure (especially of the AlN layers) and hence mechanical evolution in the as deposited state [22]. For detailed thermal investigations six CrN/AlN multilayer systems, indicating the minimum hardness values (CrN/AlN layer thicknesses of 1/1, 1.5/2 and 1/3 nm, Fig. 1a-c, respectively) as well as the maximum hardness values (CrN/AlN layer thicknesses of 2/1, 3.5/2 and 3/3 nm, Fig. 2a-c, respectively) are vacuum annealed up to 1300 °C and further investigated. As already pointed out in [22] the coatings with 2 and 3 nm thin AlN layers having a CrN/AlN ratio ¡ 1 exhibit no well-defined XRD peaks in the as-deposited state (Figs. 1b and c), while all other coatings show a clear overall cubic structure, see Fig. 1a and Figs. 2a, b and c. The XRD pattern of our coatings with CrN/AlN ratios $\leq 1$ shown in Fig. 1, indicate a slight shift to higher angles of the individual reflexes after annealing up to

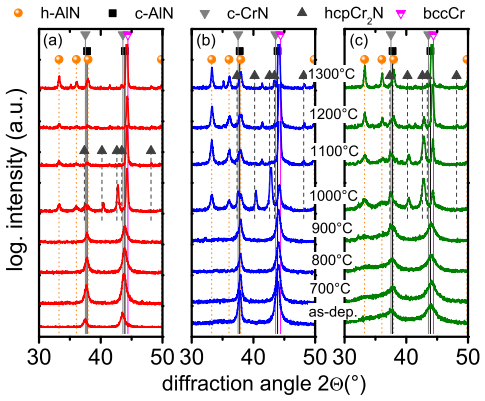


FIG. 1. XRD pattern of CrN/AlN superlattice coatings in the as deposited state and annealed up to 1300 °C with CrN/AlN layer thicknesses of (a) 1/1 nm, (b) 1.5/2 nm and (c) 1/3 nm. The standard peak positions for h-AlN, c-AlN, c-CrN, hcp-$Cr_2N$ and bcc-Cr are added, as given in the ICDD data base [25–27].

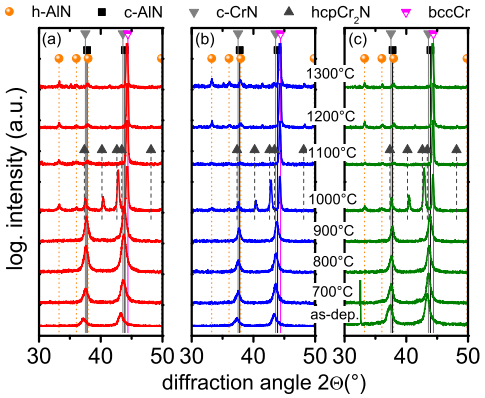


FIG. 2. XRD pattern of CrN/AlN superlattice coatings in the as deposited state and annealed up to 1300 °C with CrN/AlN layer thicknesses of (a) 2/1 nm, (b) 3.5/2 nm and (c) 3/3 nm. The standard peak positions for h-AlN, c-AlN, c-CrN, hcp-$Cr_2N$ and bcc-Cr are added, as given in the ICDD data base [25–27].

900 °C for the cubic samples (Fig. 1a) while the coatings exhibiting wurtzite (w, which is the stable structure of AlN) and cubic structures (AlN can be stabilized by coherency strains in the metastable cubic structure [16, 22, 23], Figs. 1b and c) suggest separation and growth of cubic CrN and wurtzite AlN domains. Further annealing to 1000 °C is indicated by initial precipitation of w-AlN and the transformation of CrN into hexagonal close packed (hcp) $Cr_2N$, as also shown by Willmann *et al.* [9], for all coating systems investigated. However, at $T_a = 1200$ °C, the mixed structured coating with 3 nm thin AlN layers (Fig. 1c) exhibit still $Cr_2N$ fractions while

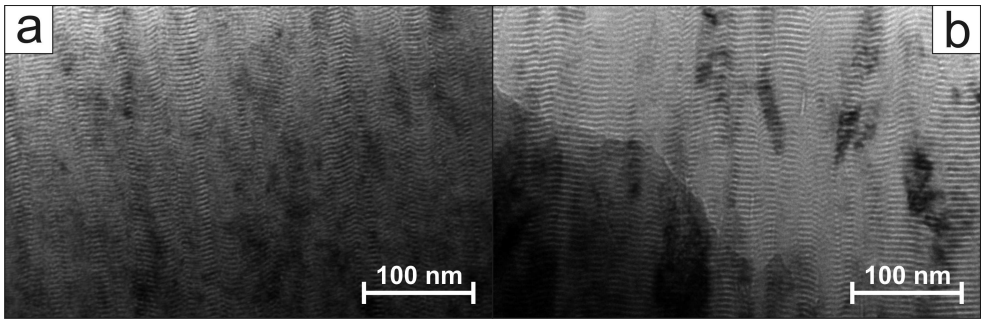


FIG. 3. HRTEM cross section images of as deposited CrN/AlN multilayer coatings with 3 nm AlN and (a) 1 nm and (b) 3 nm CrN layer thickness.

the coatings having smaller amount of AlN (Figs. 1a and b) indicate already fully recrystallized w-AlN and body centered cubic (bcc) Cr (due to completed dissociation of CrN towards Cr and $N_2$).

Even though the multilayers having a CrN/AlN ratio of $> 1$ indicate an overall cubic structure in the as deposited state with the highest hardness values, see also [22], all our multilayers show an early decomposition towards bcc-Cr and w-AlN at $T_a = 1100$ °C.

As our coating with a CrN/AlN layer ratio of 1/3 nm show increased thermal stability within the systems investigated HRTEM investigations in the as-deposited state are carried out and compared with cubic stabilized 3/3 nm CrN/AlN. Here, the fully cubic stabilized coatings (Fig. 3a) demonstrate large columnar grains elongated trough out the individual layers. Hence, decreased thermal stability for this coating can be attributed to the long linear column boundaries towards the growth direction over the whole coating thickness (see Fig. 3a) providing optimal diffusion paths. On the other hand the epitaxial growth is interrupted for the coatings having a CrN/AlN layer ratio of 1/3 nm, as the only 1 nm thin CrN layers are not able to fully stabilize the 3 nm thin AlN layers in their cubic structure by providing the necessary coherency strength. Consequently, the AlN layers tend to crystallize in their stable wurtzite structure which breaks coherency and forces renucleation. Thereby, the easy diffusion channels (especially provided by the column boundaries) with an almost direct access to the ambient atmosphere are blocked. Consequently, the nitrogen, formed by dissociation of CrN towards bcc-Cr and $N_2$, cannot that easily escape leading to an increase in internal $N_2$-pressure which retards the dissociation process.

Additional DSC and TGA investigations of superlattices with CrN/AlN layer-thickness ratios of 1/3 and 3/3 nm are presented in Figs. 4a and b, respectively. The DSC measurements clearly exhibit exothermic features up to $\sim 900$ °C which are replaced or superimposed by pronounced endothermic contributions at higher temperatures. These endothermic contributions are connected with a pronounced mass loss, as detected by TGA,

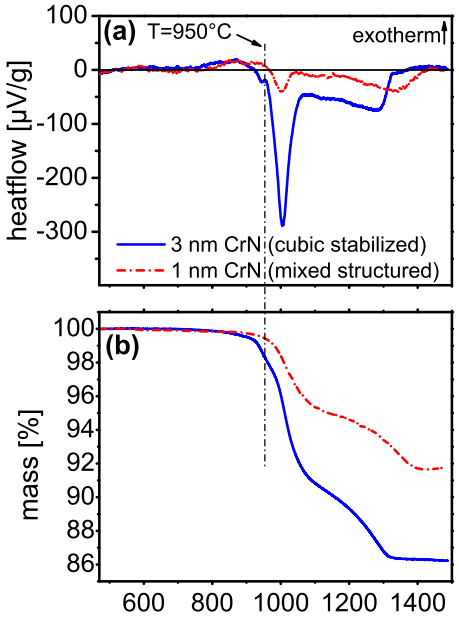


FIG. 4. (a) DSC and (b) TGA curves up to 1500 °C in inert atmosphere (He) of CrN/AlN superlattice coatings with 3 nm thin AlN combined with 1 nm thin CrN (dashed red line) or 3 nm thin CrN (solid blue line).

Fig. 4b, and are more pronounced for the superlattices composed of 3 nm thin CrN layers. The obtained mass loss due to dissociation of CrN to bcc-Cr and $N_2$ is in perfect agreement to the CrN content of the individual CrN/AlN superlattices. The theoretical mass loss of the superlattices with CrN/AlN layer-thicknesses of 1/3 and 3/3 nm is 8 and 14%, respectively, if the CrN layers fully dissociate into bcc-Cr and $N_2$. The onset of the endothermic reaction is at slightly higher temperatures ($\sim 950$ °C) for the coatings composed of 1 nm thin CrN layers. This is mainly attributed to the more complex

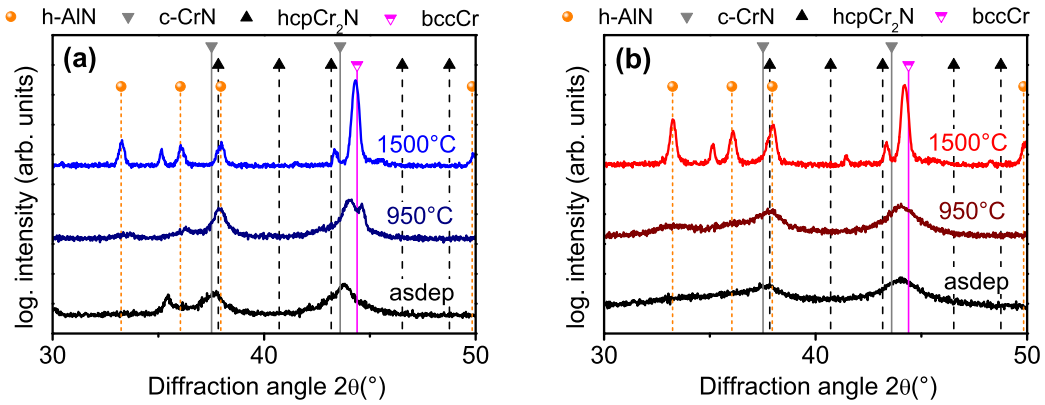


FIG. 5. XRD patterns of CrN/AlN superlattice coatings with 2 nm thin AlN layers and (a) 3.5 nm and (b) 1.5 nm thin CrN layers in the as-deposited state and after annealing in inert atmosphere (He) at $T_a$ = 950 and 1500 °C. The standard peak positions for h-AlN, c-AlN, c-CrN, hcp-$Cr_2N$ and bcc-Cr are added, as given in the ICDD data base [25–27].

diffusion pathways for the coatings composed of 1 nm thin CrN layers, as these have no pronounced columnar growth, see previous paragraph.

However, for a better understanding also XRD analyzes after DSC measurements up to 950 and 1500 °C were conducted, see Fig. 5. The coating with 3 nm thin CrN layers exhibit already for $T_a$ = 950 °C clear indications for the formation of $Cr_2N$ and even Cr, whereas the coating composed of 1 nm thin CrN layers exhibits mainly growth of the w-AlN phases. This is in perfect agreement to the afore mentioned reduced dissociation process for the coating composed of 1 nm thin CrN layers, as here $N_2$-release is inhibited due to the more complex diffusion pathways. XRD analysis for $T_a$ = 1500 °C show for both coating types the expected structure composed of bcc-Cr and w-AlN.

Figure 6 demonstrates the hardness of our CrN/AlN multilayer coatings with (a) 1, (b) 2 and (c) 3 nm thin AlN layers combined with variations of CrN layer thickness from 1 to 10 nm deposited on sapphire in the as-deposited state (as already shown in [22]) and after annealing up to 1100 °C. As our hardness curves indicate comparable trends within the variations the main discussion will focus on the six systems (CrN/AlN layer-thicknesses of 1/1, 1.5/2 and 1/3 nm, red circles; 2/1, 3.5/2 and 3/3 nm, blue squares) discussed in this manuscript. The measurements reveal a hardness maximum in the as-deposited state of 31 GPa for the superlattice coatings with 1 and 2 nm thin AlN layers and 28.5 GPa for the coating composed of 3 nm thin AlN layers, as already shown in [22]. Contrary, the coatings composed with the thinnest CrN layer thicknesses exhibit the lowest hardnesses as a function of the bilayer period, see [22] for more details. Therefore we will concentrate on these two coating-systems of the superlattices composed of 1, 2, and 3 nm thin AlN layers. Due to the thermal expansions mismatch between coatings and sapphire substrates spallation of some coatings occurred due to the thermal annealing up to 1100 °C. The hardness profiles for the superlattice coatings with CrN/AlN layer thicknesses of 2/1, 3.5/2, and 3/3 nm, which are all fully cubic structured and exhibit the peak-hardness in the as deposited state, (full lines) indicate a pronounced hardness reduction for $T_a \geq$ 1000 °C. This is especially pronounced for the coating with CrN/AlN layer thicknesses of 2/1 nm. After annealing at $T_a$ = 1100 °C the coatings with CrN/AlN layer thicknesses of 2/1, 3.5/2, and 3/3 nm exhibit only hardness of $H \sim$ 6.5, 11 and 14 GPa, respectively. However, such a pronounced hardness reduction is not observed for the coating with CrN/AlN layer thicknesses of 1/1 nm and for the coatings having CrN/AlN layer-thickness ratios < 1. Especially the coat-

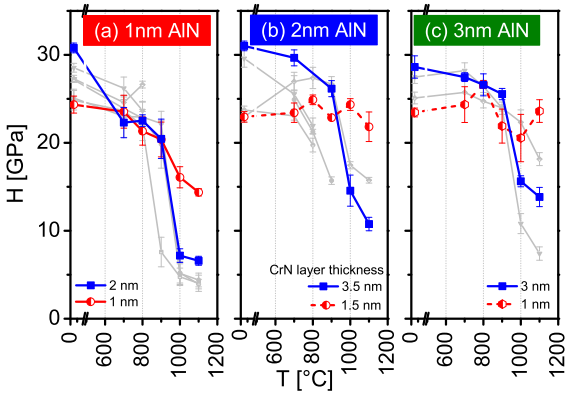


FIG. 6. Hardness characteristics of CrN/AlN superlattice coatings with (a) 1 nm, (b) 2 nm and (c) 3 nm thin AlN layers combined with CrN layers with thicknesses of 1 to 10 nm for $T_a$ up to 1100 °C.

ings composed of CrN/AlN layer thicknesses of 1/1, 1.5/2 and 1/3 nm still exhibit hardness values in the range of $\sim 23.5$ GPa after $T_a = 1100$ °C.

## IV. CONCLUSIONS

The thermal stability and the thermo-mechanical properties of CrN/AlN superlattice coatings with AlN layer thicknesses of 1, 2 and 3 nm combined with CrN layer thickness variations from 1 to 10 nm were investigated. HRTEM investigations indicate large grains elongated in the growth direction throughout the layers for the cubic stabilized multilayers, whereas the films with wurtzite und cubic phases show shorter columns and a more equiaxed growth morphology. Based on our results from DSC, TGA and XRD measurements up to $T_a = 1500$ °C and hardness measurements of coatings of sapphire up to $T_a = 1100$ °C we can conclude that the coatings with an interrupted columnar growth and minimum CrN layer thickness exhibit the highest thermal stability. The columnar structure and especially the column boundaries provide ideal pathways for diffusion processes. These coatings provide almost no resistance against the dissociation of CrN towards bcc-Cr and $N_2$. The coatings with a more equiaxed morphology, which is especially obtained for thin CrN layers–these are too weak to fully support a cubic stabilization of the alternatingly grown AlN layers–exhibit a more retarded CrN dissociation. The hardness curves as a function of $T_a$ support these findings as especially the coatings with a more equiaxed morphology and thin CrN layers demonstrate enhanced mechanical properties with hardness values of around 23.5 GPa even after annealing at temperatures as high as 1100 °C.

## ACKNOWLEDGMENTS

The authors highly acknowledge financial support by the START project (Project No. Y371) of the Austrian Science Fund (FWF).

[1] T. Matsue, T. Hanabusa, and Y. Ikeuchi, Vacuum **74**, 647 (2004).
[2] M. Huang, Y. Liu, F. Meng, L. Tong, and P. Li, Vacuum , 10 (2011).
[3] L. Cunha, M. Andritschky, K. Pischow, and Z. Wang, Thin Solid Films **355-356**, 465 (1999).
[4] P. Mayrhofer, F. Rovere, M. Moser, C. Strondl, and R. Tietema, Scr. Mater. **57**, 249 (2007).
[5] H. Barshilia, N. Selvakumar, B. Deepthi, and K. Rajam, Surf. Coat. Technol. **201**, 2193 (2006).
[6] O. Banakh, Surf. Coat. Technol. **163-164**, 57 (2003).
[7] R. Rachbauer, S. Massl, E. Stergar, D. Holec, D. Kiener, J. Keckes, J. Patscheider, M. Stiefel, H. Leitner, and P. H. Mayrhofer, J. Appl. Phys. **110**, 023515 (2011).
[8] P. H. Mayrhofer, D. Music, and J. M. Schneider, J. Appl. Phys. **100**, 094906 (2006).
[9] H. Willmann, P. Mayrhofer, P. Persson, A. Reiter, L. Hultman, and C. Mitterer, Scr. Mater. **54**, 1847 (2006).
[10] P. H. Mayrhofer, A. Horling, L. Karlsson, J. Sjolen, T. Larsson, C. Mitterer, and L. Hultman, Appl. Phys. Lett. **83**, 2049 (2003).
[11] T. Polcar and A. Cavaleiro, Surf. Coat. Technol. , 8 (2011).
[12] G. Kim, S. Lee, and J. Hahn, Surf. Coat. Technol. **193**, 213 (2005).
[13] M. Du, L. Hao, X. Liu, L. Jiang, S. Wang, F. Lv, Z. Li, and J. Mi, Phys. Procedia **18**, 222 (2011).
[14] L. Aihua, D. Jianxin, C. Haibing, C. Yangyang, and Z. Jun, Int. J. Refract. Met. Hard Mater. **31**, 82 (2012).
[15] P. H. Mayrhofer, H. Willmann, and A. Reiter, Soc. Vac. Coat. , 575 (2006).
[16] J. Lin, J. Moore, B. Mishra, M. Pinkas, and W. Sproul, Surf. Coat. Technol. **204**, 936 (2009).
[17] J. Park and Y. Baik, Surf. Coat. Technol. **200**, 1519 (2005).
[18] S.-k. Tien, J.-g. Duh, and J.-w. Lee, Mater. Sci. **201**, 5138 (2007).
[19] S. Tien and J. Duh, Thin Solid Films **494**, 173 (2006).
[20] U. Bardi, S. Chenakin, F. Ghezzi, C. Giolli, A. Goruppa, A. Lavacchi, E. Miorin, C. Pagura, and A. Tolstogouzov, Appl. Surf. Sci. **252**, 1339 (2005).
[21] G. S. Kim, S. Y. Lee, and J. H. Hahn, Surf. Coat. Technol. **171**, 91 (2002).
[22] M. Schlögl, B. Mayer, J. Paulitsch, and P. H. Mayrhofer, to be published in Thin Solid Films (2012).
[23] J. Lin, J. J. Moore, B. Mishra, M. Pinkas, X. Zhang, and W. D. Sproul, Thin Solid Films **517**, 5798 (2009).
[24] W. Oliver and G. Pharr, J. Mater. Res. **7**, 1564 (1992).
[25] *Powder Diffraction File 03-065-2899 (c-CrN), 01-076-0702 (h-AlN), 00-025-1495 (c-AlN)* (International Center for Diffraction Data, PDF-2/Release, 2005).
[26] *Powder Diffraction File 01-079-2159* (International Center for Diffraction Data, PDF-2/Release, 2005).
[27] *Powder Diffraction File 01-071-4644* (International Center for Diffraction Data, PDF-2/Release, 2005).

# Publication III



*Publication Influence of AlN Layers on Mechanical Properties and Thermal Stability of Cr-Based Nitride Coatings*

**M. Schlögl**, J. Paulitsch, J. Keckes, P.H. Mayrhofer

Thin Solid Films, doi: 10.1016/10.1016/j.tsf.2012.12.057, article in press.

# Influence of AlN Layers on Mechanical Properties and Thermal Stability of Cr-Based Nitride Coatings

M. Schlögl,[1] J. Paulitsch,[1] J. Keckes,[2] and P.H. Mayrhofer[1]

[1] *Department of Physical Metallurgy and Materials Testing, Montanuniversität Leoben, Austria*
[2] *Department of Materials Physics, Montanuniversität Leoben, Austria*

Based on their excellent thermal stability and mechanical properties ceramic-like hard coatings are highly valued for various industrial applications. Here we study the effect of additional AlN layers (3 or 10 nm thin) on the mechanical and thermal properties of cubic CrN, $Cr_{0.4}Al_{0.6}N$ and $Cr_{0.37}Al_{0.6}Y_{0.03}N$. To focus our research on the influence of the additional layers, but minimizing the influence of the additional phase, we kept the overall AlN-layer content at a minimum ($< 14\%$). The hardness of the cubic Cr-based nitride layers is not influenced by the addition of coherently grown 3 nm thin AlN layers, due to their small overall content. The formation of wurtzite AlN, for the $\sim$ 10 nm thin layers, breaks the coherency to the cubic Cr-based nitride layers. Thereby renucleation is promoted, resulting in a smaller grain size and consequently an actual hardness increase of about 3 GPa for CrN/AlN, $Cr_{0.4}Al_{0.6}N$/AlN and $Cr_{0.37}Al_{0.6}Y_{0.03}N$/AlN coatings, respectively, when compared to the monolithically grown cubic Cr-based nitrides or the multilayers containing c-AlN. Both multilayer types, with 3 and 10 nm thin AlN layers, exhibit a similar dependence of their hardness on the annealing temperature. The hardness maximum of 36 GPa was obtained for the $Cr_{0.37}Al_{0.6}Y_{0.03}N$/AlN multilayers after annealing at 900 °C. This study clearly demonstrates that even a small addition of thin AlN layers to CrN and $Cr_{0.37}Al_{0.6}Y_{0.03}N$ nitride layers increases their mechanical response to annealing treatments.

Keywords: magnetron sputtering; multilayer coatings; CrN/AlN, CrAlN/AlN, CrAlYN/AlN coating; hardness; thermal stability



## I. 1. INTRODUCTION

CrN based protective coatings are widely used for molds, tools, dies as well as automotive and aerospace applications due to their high hardness and outstanding corrosion as well as oxidation resistance [1–8]. Consequently, there are numerous reports on the microstructure, morphology, thermal and mechanical properties of such coatings [9–11]. The ever growing demand on improved properties led to the development of ternary and multinary coatings like $Cr_{1-x}Al_xN$, $Ti_{1-x}Cr_xN$, $Cr_{1-x-y}Al_xY_yN$ as well as multilayered coatings such as TiN/CrN, CrN/AlN and CrN/$Cr_{1-x}Al_xN$, just to name some Cr-based nitride layers [12–21].

Especially by the alloying and combination with Al and AlN, the chemical and mechanical properties of transition metal nitrides like CrN and TiN (to name the most prominent representatives) could further be improved and optimized [22–27]. For example, ternary $Cr_{1-x}Al_xN$ and $Ti_{1-x}Al_xN$ coatings, where Al substitutes for Cr or Ti in their CrN and TiN based face centered cubic (c) lattice (B1, $Fm\bar{3}m$), respectively, exhibit improved hardness, oxidation resistance and thermal stability as compared to their binary counterparts CrN and TiN. Further improvement (towards increased thermal stability) of such ternary nitrides have been obtained by alloying with Yttrium [12, 24, 25, 28–31]. Not only due to alloying, properties of coatings can be modified and improved, but also due to their architecture as shown by reports dealing with multilayer and superlattice coatings [32–40]. Especially for superlattice coatings, the mechanical properties are strongly influenced by the layer thickness of the individual alternating layers and consequently their bilayer period [41–44]. For example superlattice CrN/AlN coatings exhibit a peak-hardness of around 45 GPa when the bilayer period is $\sim$ 3 nm [18, 20].

Whereas $Cr_xN$ crystallizes in the cubic NaCl or in the hexagonal close packed $Fe_2N$ (hcp, $P6_3/mmc$) structure for a Cr/N ratio $x$ of $\sim$ 1 and $\sim$ 2, respectively, depending on the $N_2$ partial pressure used during deposition [45, 46] the stable configuration of the AlN line compound is the hexagonal wurtzite (w) ZnS (B4, $P6_3mc$) structure. By coherency strains AlN can also be stabilized in its metastable cubic NaCl high pressure polymorph [47], as shown by Lin *et al.* [18] for AlN layer thicknesses below 3.3 nm in a CrN/AlN multilayer arrangement [18]. The formation of a CrN/AlN multilayer with either cubic or hexagonal AlN layers strongly depends on the strain energy available and the energy for dislocation formation [48].

The development of multilayers, especially with AlN layers is additionally highly motivated based on *ab initio* data suggesting that there exist displacive (diffusionless) transformation paths [49] from cubic AlN towards wurtzite AlN with the connected pronounced volume increase of $\sim$ 26% [50]. This effect can be used to influence the propagation of cracks, resulting in a type of transformation toughening effect. Consequently we study the influence of additional cubic and hexagonal structured AlN layers (by simply changing the AlN layer thickness from 3 to 10 nm) on the structure development, mechanical and thermal properties of CrN, $Cr_{1-x}Al_xN$ and $Cr_{1-x-y}Al_xY_yN$ coatings. Furthermore, keeping the additional AlN layer content at a minimum ($< 14\%$) of the overall coating volume fraction allows a comparison be-

tween the monolithically grown Cr-based nitride coatings and their multilayer arrangements. Contrary, literature reports basically concentrate on multilayer or superlattice coatings composed of comparable layer thicknesses.

## II. 2. EXPERIMENTAL DETAILS

CrN/AlN, $Cr_{1-x}Al_xN$/AlN and $Cr_{1-x-y}Al_xY_yN$/AlN multilayer coatings and their Cr-based monolithic coatings were deposited onto sapphire $(1\,\bar{1}\,0\,2)$ ($10 \times 10 \times 0.53$ mm$^3$), Si $(1\,0\,0)$ ($20\times7\times0.38$ mm$^3$), and low-carbon-steel foil ($\varnothing114 \times 0.05$ mm$^3$) using an AJA Orion 5 lab scaled magnetron sputter deposition unit, equipped with 2-inch (50.8 mm) Al, Cr, $Cr_{0.4}Al_{0.6}$ and $Cr_{0.39}Al_{0.59}Y_{0.02}$ targets (purity 99.99%, PLANSEE SE, Lechbruck). Prior to the depositions the targets were sputter-cleaned (14.8 W/cm$^2$) for 3 minutes and the substrates were rf-etched for 5 minutes in an Ar glow discharge at a total pressure of 3 Pa after evacuating the chamber to a back-pressure of below $1 \cdot 10^{-5}$ Pa. The depositions were carried out at a total pressure of 0.3 Pa, using a mixed $Ar/N_2$ glow discharge with a gas flow ratio of 40/60 (4 sccm Ar and 6 sccm $N_2$), a continuous substrate holder rotation of 50 revolutions/min, and keeping the substrate temperature at 500 °C. The multilayers were prepared by operating the Cr, $Cr_{0.4}Al_{0.6}$ or $Cr_{0.39}Al_{0.59}Y_{0.02}$ cathodes with 300 W dc and the Al cathode simultaneously with 200 W rf. A computer controlled shutter system (directly above the targets) allowed for a periodical arrangement of alternating Cr-containing nitride layers (shutter open for 600 s, 10 layers) and AlN (shutter open for 120 or 600 s, for two individual deposition series, 10 layers). During deposition a 70 V rf-biasing of the substrates was used.

The hardness ($H$) was obtained from coated sapphire using a CSIRO ultra micro indentation system equipped with a Berkovich-tip and analyzing the unloading curve by the Oliver and Pharr method [51]. Multiple indents with maximum normal loads varying from 20 to 10 μN in steps of 0.5 μN were carried out to allow statistically relevant hardness values. Furthermore due to this the indentation depth was kept below 10% of the film thickness to minimize any influence by the substrate. The overall thicknesses of our coatings were evaluated by the ball-crater-technique using a CSM CaloTest. Structural and phase analyses of as-deposited and annealed samples (see next paragraph) were conducted by X-ray diffraction (XRD) in Bragg Brentano mode using a Bruker AXS D8 diffractometer equipped with a Cu $K_\alpha$ radiation source ($\lambda = 1.54056$ nm, scan speed = 1.2 s/step, step size = 0.02°).

Coated sapphire substrates (for hardness measurements) and coating materials (after removal from their low-carbon-steel foils using a diluted nitric acid, and crunched to a fine powder) were annealed in a Reetz vacuum furnace for 20 min at temperatures $T_a$ up to 1500 °C using a heating and cooling rate of 20 °C/min.

Scanning electron microscopy (SEM) and energy dispersive X-ray analysis (EDX) for the evaluation of the coating morphology as well as composition, respectively, were conducted by a Zeiss EVO 50 microscope, using an operating voltage of 20 kV. More detailed investigation on the coating morphologies were conducted by transmission electron microscopy (TEM) with a Phillips CM12 operating at 120 kV and high resolution transmission electron microscopy (HRTEM) with a Tecnai F20 operating at 200 kV. To prepare TEM transparent samples coated Si substrates, mechanically polished to a thickness of around 50 μm, were ion etched using a GATAN precision ion polishing system PIPS, with an incident angle of 4° and an acceleration voltage of 3.5 keV. A final low ion energy ($\sim$ 2.5 eV) polishing step was conducted for around 10 min to reduce the ion damaging areas.

X-ray elastic strains $\varepsilon_{200}$ were determined by measuring the positions of CrN 200 reflections. Since the X-ray elastic constants of the newly designed coatings are not known, the residual stresses were not evaluated.

## III. RESULTS AND DISCUSSIONS

### A. Structure and Morphology

The single layer (monolithic) nitride coatings prepared from the Cr, $Cr_{0.4}Al_{0.6}$ and $Cr_{0.39}Al_{0.59}Y_{0.02}$, and Al targets (using identical deposition conditions as for the multilayers) exhibit a chemical composition corresponding to CrN, $Cr_{0.4}Al_{0.6}N$ and $Cr_{0.37}Al_{0.6}Y_{0.03}N$ and AlN, respectively. All coatings investigated exhibit a dense morphology with a fibrous structure and smooth surfaces. Cross sectional TEM investigations of the two sets of CrN/AlN, $Cr_{0.4}Al_{0.6}N$/AlN and $Cr_{0.37}Al_{0.6}Y_{0.03}N$/AlN multilayers (prepared with either 120 or 600 s of open shutter above the Al target, see experimental) suggest AlN layer thicknesses of either 3 or 10 nm, shown here for $Cr_{0.37}Al_{0.6}Y_{0.03}N$/AlN in Fig. 1. Already the TEM investigations indicate (by the continuing grain contrast throughout the AlN layers) that the $\sim$ 3 nm thin AlN layers are epitaxial to the cubic Cr-based nitride layers, Figs. 1a and b show as an example $Cr_{0.37}Al_{0.6}Y_{0.03}N$/AlN. The cross-sectional HRTEM image, Fig. 1c, nicely presents the continuing lattice fringes throughout the AlN layer. The small inset gives a Fast Fourier Transformation (FFT) of the AlN layer with 2.05 Å for the $(2\,0\,0)$ lattice spacing.

Continuing crystalline domains throughout the AlN layers cannot be observed for the multilayers having thicker ($\sim$ 10 nm) AlN layers, Figs. 1d and e. Whereas at the interface to the Cr-based nitride layers continuing lattice fringes may suggest for epitaxial like behavior, within the AlN layers the random orientation, indicate loss of epitaxy and a hexagonal structure, Fig. 1f. The FFT image (small inset) points towards a wurtzite structure with 2.485 and 2.663 Å for the $(0\,0\,2)$ and $(1\,0\,0)$ lattice spacings. These observations are in good agree-

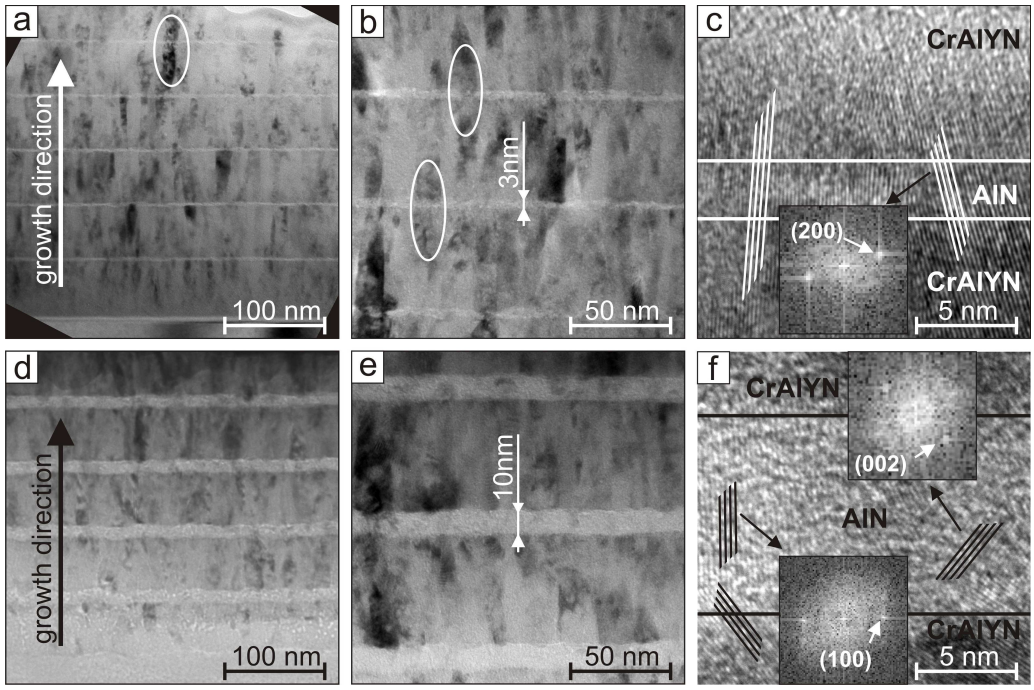


FIG. 1. TEM and HRTEM cross section images of as-deposited $Cr_{0.37}Al_{0.6}Y_{0.03}N$/AlN multilayer coatings with (a–c) 3 nm and (d–f) 10 nm AlN layer thicknesses and small FFT insets of the AlN layers indicating (c) cubic and (f) wurtzite structure.

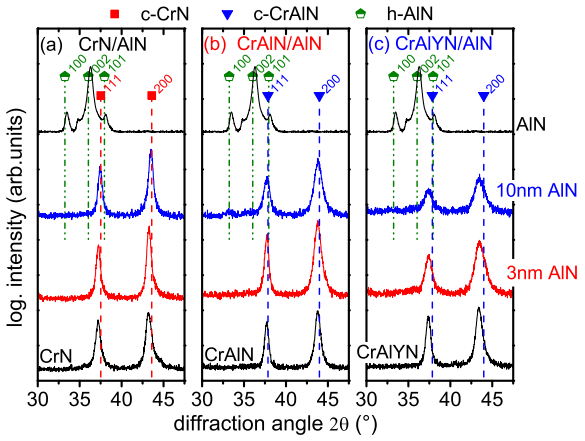


FIG. 2. XRD scans of as-deposited (a) CrN/AlN, (b) $Cr_{0.4}Al_{0.6}N$/AlN and (c) $Cr_{0.37}Al_{0.6}Y_{0.03}N$/AlN multilayer coatings with 3 nm and 10 nm AlN layer thickness. The standard peak positions for cubic Cr, $Cr_{0.4}Al_{0.6}N$ (calculated from the lattice parameter $a = 4.11$ Å [15]) and cubic CrN as well as for hexagonal w-AlN are added, as given in the ICDD data base [52]. The small peak in the uppermost diffraction pattern on the left-hand side of 0 0 2 from w-AlN originates from the aperture of the XRD system (as proven by using different aperture sizes).

ment with literature showing that AlN layers can be epitaxially stabilized in their metastable cubic structure for layer thicknesses $\leq 3$ nm [18, 53].

The XRD patterns of the CrN/AlN, $Cr_{0.4}Al_{0.6}N$/AlN and $Cr_{0.37}Al_{0.6}Y_{0.03}N$/AlN multilayer systems with 3 and 10 nm AlN layers compared with their respective individual monolithic layers are given in Fig. 2. Corresponding to the TEM and HRTEM investigations the XRD data confirm a solely cubic structure for the Cr-based nitride layers and multilayers composed of 3 nm thin AlN layers and indications of a w-AlN phase for the multilayers having 10 nm thin AlN layers. For the CrN/AlN with 10 nm thin AlN layers the w-AlN phase can almost not be detected as here the cubic Cr-based nitride layer content is around 1.5 times higher than for the $Cr_{0.4}Al_{0.6}N$/AlN and $Cr_{0.37}Al_{0.6}Y_{0.03}N$/AlN multilayers. This is based on our experimental setup where we kept the numbers of layers constant and for identical deposition conditions CrN (layer thickness $\sim$ 100 nm) shows an around 1.5 times higher deposition rate than $Cr_{0.4}Al_{0.6}N$ and $Cr_{0.37}Al_{0.6}Y_{0.03}N$.

As the lattice parameter a of CrN ($\sim$ 4.15 Å) deceases with the addition of Al to $\sim$ 4.11 Å for $Cr_{0.4}Al_{0.6}N$ [15] their cubic XRD peaks are shifted towards larger diffraction angles as compared to the standard CrN position (from the ICDD data base [52]). The addition of Y leads to an increase of a to 4.13 Å for $Cr_{0.37}Al_{0.6}Y_{0.03}N$ [15], and hence the cubic XRD peaks are shifted to smaller diffraction angels as compared to $Cr_{0.4}Al_{0.6}N$.

### B. Mechanical Properties

While CrN has elastic strains of approximately $1.15 \cdot 10^{-3}$, the $Cr_{0.4}Al_{0.6}N$ and $Cr_{0.37}Al_{0.6}Y_{0.03}N$ coatings have elastic strains of around $-2.58 \cdot 10^{-3}$ and $-2.86 \cdot 10^{-3}$, respectively, in the as-deposited state, Fig. 3a. The formation of multilayers with 3 and 10 nm thin AlN layers only slightly decreases the elastic strains for CrN from approximately $1.15 \cdot 10^{-3}$ to around $6.69 \cdot 10^{-4}$, respectively. Contrary, the elastic strains of $Cr_{0.4}Al_{0.6}N$ and $Cr_{0.37}Al_{0.6}Y_{0.03}N$ are strongly influenced by their multilayer arrangements and increase from $-2.58 \cdot 10^{-3}$ to $-5.23 \cdot 10^{-3}$ and from $-2.86 \cdot 10^{-3}$ to $-7.47 \cdot 10^{-3}$, respectively by adding 3 nm thin AlN layers. This increase is attributed to coherency strains between the Cr-based layers and the cubic stabilized 3 nm thin AlN layers. As the lattice parameter difference is larger between c-$Cr_{0.37}Al_{0.6}Y_{0.03}N$ ($\sim$ 4.13 Å) and c-AlN ($\sim$ 4.06 Å) [54] than between c-$Cr_{0.4}Al_{0.6}N$ ($\sim$ 4.11 Å) and c-AlN, the increase in elastic strains, due to the multilayer arrangement with 3 nm thin c-AlN, is more pronounced for c-$Cr_{0.37}Al_{0.6}Y_{0.03}N$, see Fig.3a. A further increase of the AlN layer thickness from 3 to 10 nm leads to a further increase in elastic strains to $-6.15 \cdot 10^{-3}$ and $-7.73 \cdot 10^{-3}$ for $Cr_{0.4}Al_{0.6}N$/AlN and $Cr_{0.37}Al_{0.6}Y_{0.03}N$/AlN, respectively. Here, the loss of epitaxy between Cr-based layers and AlN, due to the increased AlN layer thickness, would lead to a reduction of the strains which is more than compensated by the formation of hexagonal AlN with its $\sim$ 26% larger volume as compared to c-AlN [50]. The different behavior in strains of the monolithically grown CrN coating as compared to $Cr_{0.4}Al_{0.6}N$ and $Cr_{0.37}Al_{0.6}Y_{0.03}N$, Fig. 3a, can be explained by their different morphology. While CrN exhibits a pronounced columnar structure with underdense regions at the column boundaries (responsible for even tensile strains [55]) the $Cr_{0.4}Al_{0.6}N$ and $Cr_{0.37}Al_{0.6}Y_{0.03}N$ coatings exhibit a fully dense fine columnar structure (not shown here, but we refer to [15]). Therefore, the latter two exhibit even compressive strains.

The different behavior in strains of CrN to $Cr_{0.4}Al_{0.6}N$ and $Cr_{0.37}Al_{0.6}Y_{0.03}N$ can be explained by the morphology and the fact of an increased amount of the CrN phase as the layer thickness of CrN is $\sim$ 1.5 times higher compared to the other ones.

The hardnesses H indicate a slightly different dependency on the AlN layer thicknesses used, as shown in Fig. 3. Whereas the hardness of CrN, $Cr_{0.4}Al_{0.6}N$ and $Cr_{0.37}Al_{0.6}Y_{0.03}N$ with $\sim$ 23, 26 and 30 GPa, respectively, is almost unaffected by the additions of 3 nm thin AlN layers, it increases to $\sim$ 26, 30 and 33 GPa by the addition of 10 nm AlN layers. The small difference between monolithically grown Cr-based layers and their corresponding multilayers with 3 nm thin cubic stabilized AlN layers is mainly based on following reasons. The overall volume fraction of AlN is rather small with $\sim$ 2.9% for the CrN/AlN multilayer and $\sim$ 4.8% for

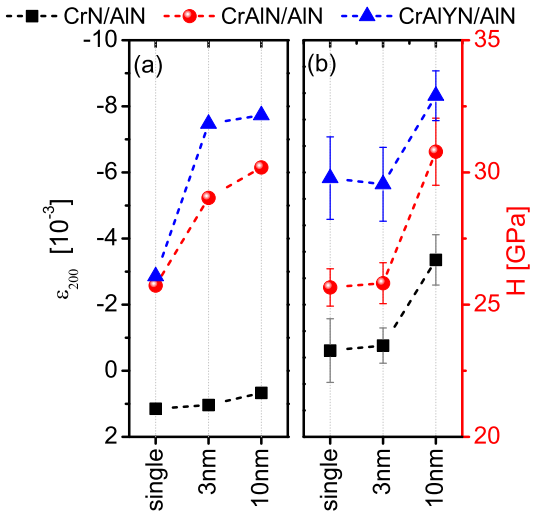


FIG. 3. (a) Elastic strains ($\varepsilon$) and (b) hardness ($H$) of CrN, $Cr_{0.4}Al_{0.6}N$ and $Cr_{0.37}Al_{0.6}Y_{0.03}N$ and their multilayer arrangements with 3 nm and 10 nm thin AlN layers.

the $Cr_{0.4}Al_{0.6}N$/AlN and $Cr_{0.37}Al_{0.6}Y_{0.03}N$/AlN multilayers. Furthermore, due to the coherent growth of the thin AlN layer on the Cr-based nitride layers, the grain size is almost not influenced, compare Fig. 1a. When increasing the AlN layer thickness to 10 nm, their volume fraction increases to 9.1 and 14.3%, respectively, but also their structure changes from cubic to hexagonal. This causes breaking of coherency to the Cr-based layers during growth leading to a smaller crystalline grain size also within the Cr-based layers. This is confirmed by TEM investigations, Fig. 1d, and the XRD patterns, Fig. 2, exhibiting lower peak intensities connected with a larger broadening for the multilayers with 10 nm thin AlN layers. Hence, the coatings provide more obstacles against dislocation movement leading to an increase in hardness.

### C. Thermal Stability

Figures 4 to 6 show XRD patterns of powdered coatings of monolithically grown CrN, $Cr_{0.4}Al_{0.6}N$ and $Cr_{0.37}Al_{0.6}Y_{0.03}N$ and their multilayer arrangements with 3 and 10 nm thin AlN layers, in the as-deposited state and after annealing in vacuum up to 1500 °C. For easier reading we refer to the multilayers with 3 nm thin AlN layers with CrN/c-AlN, $Cr_{0.4}Al_{0.6}N$/c-AlN and $Cr_{0.37}Al_{0.6}Y_{0.03}N$/c-AlN and to those with 10 nm thin AlN layers with CrN/w-AlN, $Cr_{0.4}Al_{0.6}N$/w-AlN and $Cr_{0.37}Al_{0.6}Y_{0.03}N$/w-AlN, based on their major as-deposited phases.

For the CrN coatings (Fig. 4a) a pronounced peak-shift to larger angles due to annealing at $T_a = 600$ °C can be observed suggesting thermal relaxation. Generally the

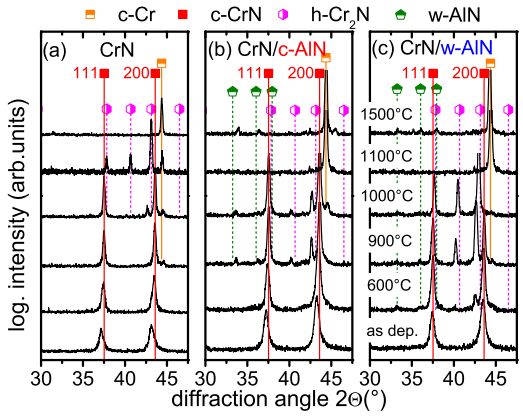


FIG. 4. XRD powder scans of (a) monolithic CrN, (b) CrN/c-AlN and (c) CrN/w-AlN multilayer coatings after annealing at temperatures $T_a$ up to 1500 °C.

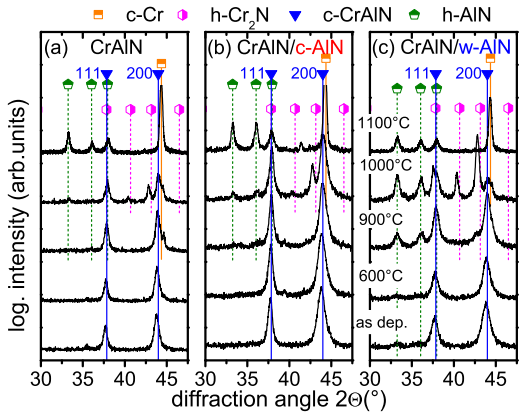


FIG. 5. (XRD powder scans of (a) monolithic $Cr_{0.4}Al_{0.6}N$, (b) $Cr_{0.4}Al_{0.6}N$/c-AlN and (c) $Cr_{0.4}Al_{0.6}N$/w-AlN multilayer coatings after annealing at temperatures $T_a$ up to 1100 °C.

density of defects (like point, line and area) decreases. For example, annihilation of point and line defects takes place as well as dislocation polygonization and rearrangement to lower energy sites [56]. Annealing at 900 °C causes a further shift of the peaks towards the standard position of c-CrN and a reduction of the peak broadening, indicative for further relaxation processes (reduction of macro- and micro-strains) and grain growth. Around the 2 0 0 peak (at 43.8°) small indications for additional phases like h-$Cr_2N$ and body-centered cubic (bcc) Cr point towards the onset of a CrN dissociation. This can clearly be seen after annealing at $T_a = 1000$ and 1100 °C. For $T_a = 1500$ °C only bcc Cr can be detected, in agreement to previous studies [7].

The XRD studies of the CrN/c-AlN multilayers (Fig.4b) suggest an earlier onset for this dissociation. Already after annealing at 900 °C h-$Cr_2N$ can be detected accompanied by the transformation of c-AlN towards w-AlN. With increasing temperature, these transformations proceed and at 1100 °C the Cr-N phase cannot be detected anymore. Due to the small content of AlN in these coatings almost no w-AlN peak can be detected. The CrN/w-AlN multilayer (Fig. 4c) shows an earlier onset for the CrN dissociation towards h-$Cr_2N$ and bcc-Cr. Furthermore, w-AlN can be detected by XRD already after annealing at $T_a = 600$ °C. In the as-deposited state, w-AlN could only be identified by HRTEM and selected area electron diffraction studies. These results suggest that the additional interfaces present in the multilayer coatings and the transformation of c-AlN towards w-AlN, with the connected increase in specific volume, promotes the dissociation of CrN towards h-$Cr_2N$ and bcc-Cr.

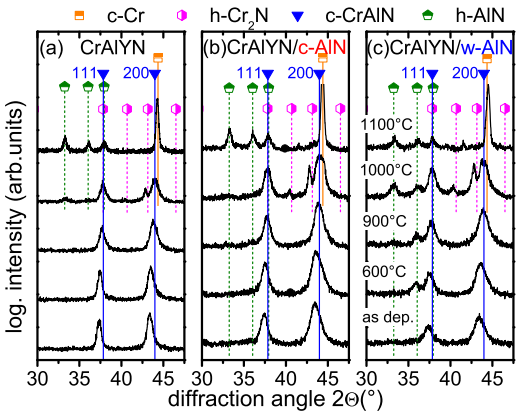


FIG. 6. XRD powder scans of (a) monolithic $Cr_{0.37}Al_{0.6}Y_{0.03}N$, (b) $Cr_{0.37}Al_{0.6}Y_{0.03}N$/c-AlN and (c) $Cr_{0.37}Al_{0.6}Y_{0.03}N$/w-AlN multilayer coatings after annealing at temperatures $T_a$ up to 1100 °C.

Corresponding observations are obtained for $Cr_{0.4}Al_{0.6}N$ (Fig. 5a) and the multilayers with c-AlN (Fig. 5b) and w-AlN (Fig. 5c) as well as for $Cr_{0.37}Al_{0.6}Y_{0.03}N$ (Fig. 6a) and the multilayers with c-AlN (Fig. 6b) and w-AlN (Fig. 6c). However, after annealing at 1100 °C the XRD data show only bcc-Cr in addition to w-AlN, for all these coatings, indicating a completed decomposition towards their stable constituents of $Cr_{0.4}Al_{0.6}N$ and $Cr_{0.37}Al_{0.6}Y_{0.03}N$ and their multilayers, and completed dissociation of the Cr-N bonds. Nevertheless, no earlier onset of the $Cr_2N$ formation for the $Cr_{0.4}Al_{0.6}N$ and $Cr_{0.37}Al_{0.6}Y_{0.03}N$ multilayers, compared to their monolithic coatings as shown for the CrN-based coatings were observed. The formation of h-$Cr_2N$ can be detected after annealing at 1000 °C, with indications for h-$Cr_2N$ already at $T_a = 900$ °C for $Cr_{0.4}Al_{0.6}N$/w-AlN (Fig. 5c) as shown by the small shoulder at the left side of the 2 0 0 peak. This again points towards the observed results for CrN/AlN, that especially the formation of w-AlN, with the connected volume increase, promotes the dissociation of Cr-N bonds. The decomposition process of $Cr_{0.4}Al_{0.6}N$ and $Cr_{0.37}Al_{0.6}Y_{0.03}N$ towards the stable

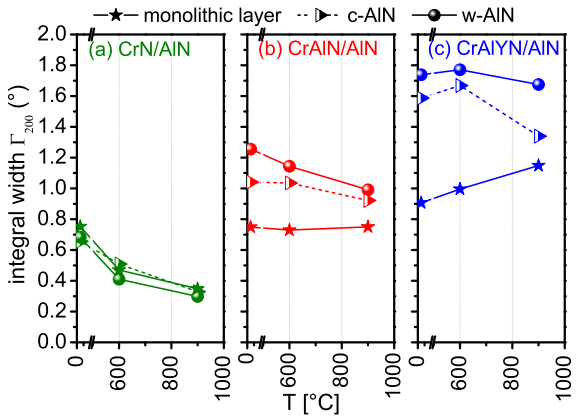


FIG. 7. Integral peak broadening $\Gamma_{200}$ of the 200 XRD peak ($\sim 44°$) for (a) CrN, (b) $Cr_{0.4}Al_{0.6}N$ and (c) $Cr_{0.37}Al_{0.6}Y_{0.03}N$ coatings compared to their corresponding multilayer arrangements with c-AlN (dashed lines) and w-AlN (solid lines) for annealing temperatures $T_a$ up to 900 °C. The error bars are in the range of the symbol size.

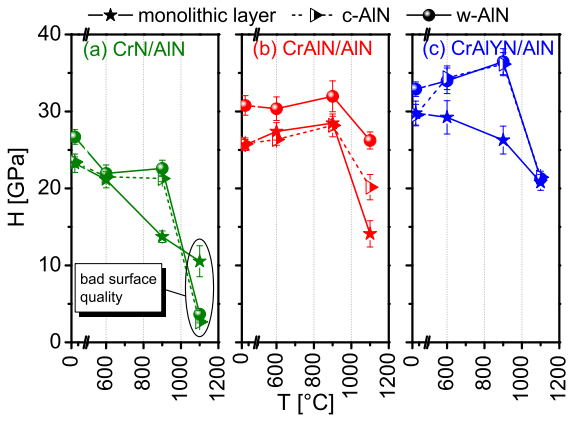


FIG. 8. Hardnesses $H$ of (a) CrN, (b) $Cr_{0.4}Al_{0.6}N$ and (c) $Cr_{0.37}Al_{0.6}Y_{0.03}N$ coatings compared to their corresponding multilayer arrangements with c-AlN (dashed lines) and w-AlN (solid lines) for annealing temperatures $T_a$ up to 1100 °C.

constituents is presented in more detail in [57].

Based on the XRD studies we can further conclude, that the CrN based layers and the $Cr_{0.4}Al_{0.6}N$ and $Cr_{0.37}Al_{0.6}Y_{0.03}N$ based layers exhibit different XRD peak broadening (which is an indication for the inherent microstrains and domain sizes [58]). Figure 7 shows the integral width, $\Gamma_{200}$, of the 200 peak of the various coatings as a function of the annealing temperature up to 900 °C. The integral width rapidly decreases with $T_a$ for the CrN based layers (Fig. 7a) to values below 0.4° due to the already mentioned stress relaxation and grain growth. While the $Cr_{0.4}Al_{0.6}N$/w-AlN (Fig.7b) also shows decreasing $\Gamma_{200}$ values from $\sim$ 1.25 to $\sim$ 1°, the monolithic $Cr_{0.4}Al_{0.6}N$ and their multilayer with c-AlN exhibit almost constant $\Gamma_{200}$ at $\sim$ 0.8 and $\sim$ 1°. Nevertheless, the multilayer arrangements of $Cr_{0.4}Al_{0.6}N$ and $Cr_{0.37}Al_{0.6}Y_{0.03}N$ (Fig.7c) with w-AlN layers exhibit the largest values for $\Gamma_{200}$ throughout the annealing treatment indicating smallest domain sizes and largest strains. The $Cr_{0.37}Al_{0.6}Y_{0.03}N$/w-AlN exhibit even after annealing at $T_a$ = 900 °C $\Gamma_{200}$ values above 1.6°. Furthermore, $\Gamma_{200}$ increases for the monolithic $Cr_{0.37}Al_{0.6}Y_{0.03}N$ to 1.15° but decreases for the multilayer with c-AlN to $\sim$ 1.35°.

Corresponding to the structural changes, also the hardness values of the coatings investigated change with annealing temperature. The hardness for the monolithically grown CrN rapidly decreases upon annealing and is $14 \pm 0.75$ GPa for $T_a$ = 900 °C, Fig. 8a. This reduction, based on the XRD studies, is caused by pronounced relaxation, grain growth processes and the onset of CrN dissociation and agrees to the integral width $\Gamma_{200}$ dependence on $T_a$, Fig. 7a. When forming a multilayer arrangement with either c-AlN ( 3 nm thin) or w-AlN ( 10 nm thin) layers the $H$ vs. $T_a$ curve deviates significantly from that of CrN. Up to 900 °C the hardness for both multilayer types remains at a high level of 23 GPa, although the overall AlN content is relatively low < 14 vol%. For higher annealing temperatures the pronounced CrN dissociation towards $Cr_2N$ and Cr results in a very rough surface and open coating morphology, leading to unreliable hardness values (indicated in Fig. 8a).

The hardnesses for $Cr_{0.4}Al_{0.6}N$ and $Cr_{0.4}Al_{0.6}N$/AlN multilayers remain at their high as-deposited values (within the error of measurements) upon annealing to 900 °C, Fig. 8b. For higher temperatures the dissociation of Cr-N bonds again results in a pronounced hardness loss, but especially for the multilayers, the surface quality and coating morphology is sufficient for reasonable hardness measurements. In agreement to the XRD studies, indicating a more stable structure upon annealing and larger $\Gamma_{200}$ values for the multilayers with w-AlN, their hardnesses for the entire annealing range are highest, with values ranging from 30 to 32 GPa for $T_a \leq$ 900 °C.

The $Cr_{0.37}Al_{0.6}Y_{0.03}N$ multilayers (Fig. 8c) even exhibit an increased hardness upon annealing to $T_a$ = 900 °C. Such an increase in hardness, especially for the coatings with c-AlN, can be attributed to the first onset of w-AlN formation hence changed stress/strains field at the interface near regions, which is in excellent agreement to earlier reports [59–61]. Both multilayer arrangements, with c-AlN or w-AlN, show comparable $H$ vs. $T_a$ curves, with $H$ = 36 GPa for $T_a$ = 900 °C. These coatings show also the largest $\Gamma_{200}$ values (above 1°) over the entire annealing range, compare Fig. 7c. The hardness of monolithic $Cr_{0.37}Al_{0.6}Y_{0.03}N$ is indicated by a slight decrease up to 900 °C to $H$ = 26 GPa. Further annealing to $T_a$ = 1100 °C causes a drop in hardness to $21 \pm 1.03$ GPa for all $Cr_{0.37}Al_{0.6}Y_{0.03}N$ based coatings according to their structural changes (see Fig. 6).

## IV. SUMMARY AND CONCLUSIONS

Within this work monolithic cubic structured CrN, $Cr_{0.4}Al_{0.6}N$ and $Cr_{0.37}Al_{0.6}Y_{0.03}N$ as well as their multilayer arrangements with 3 and 10 nm thin AlN layer thicknesses were deposited and investigated with respect to their structural, thermal and mechanical properties. Based on XRD and HRTEM studies the 3 nm thin AlN layers exhibit a cubic structure whereas the 10 nm thin AlN layers exhibit also a wurtzite structure. The 3 nm thin AlN layer grow epitaxially between the cubic CrN, $Cr_{0.4}Al_{0.6}N$ and $Cr_{0.37}Al_{0.6}Y_{0.03}N$ layers, whereas incoherent interfaces and a wurtzite structure for the 10 nm thin AlN layers is observed. Due to the small overall AlN volume fraction of only 5% for the c-AlN and 14% for the w-AlN multilayer arrangements, the hardness and elastic constants are dominated by the CrN, $Cr_{0.4}Al_{0.6}N$ and $Cr_{0.37}Al_{0.6}Y_{0.03}N$ layers, and the effect of the AlN layers on the growth behavior of these Cr-containing nitride layers. Especially the thicker AlN layers, due to the formation of non cubic areas, interrupt the crystal growth of the cubic Cr-based nitride layers during growth. Therefore, their overall microstructure is finer. This is of course not so pronounced for epitaxial growth of cubic AlN layers.

Consequently, the multilayers with thicker w-AlN layers exhibit higher hardness values of $\sim$ 26, 30, and 33 GPa, in the as-deposited state compared to the monolithically grown CrN, $Cr_{0.4}Al_{0.6}N$ and $Cr_{0.37}Al_{0.6}Y_{0.03}N$ and their multilayers with thin c-AlN layers with $H \sim$ 22, 26, 30 GPa, respectively. Upon annealing, the phase transformation of the AlN layers towards the stable wurtzite structure, with the connected volume expansion by $\sim$ 26%, triggers the dissociation of the Cr-based nitride layers and the formation of $Cr_2N$. The latter can be observed for $Cr_{0.4}Al_{0.6}N$/AlN and $Cr_{0.37}Al_{0.6}Y_{0.03}N$/AlN for $Ta \geq 1000\,^{\circ}C$. Decomposition of the Cr-based nitride layers connected with small domain sizes especially for the coatings with w-AlN layers, and large inherent microstrains lead to high constant hardness values even when annealed to $T_a = 900\,^{\circ}C$. The highest hardness values are obtained for $Cr_{0.37}Al_{0.6}Y_{0.03}N$/w-AlN exhibiting an increase from the as-deposited 33 GPa to 36 GPa upon annealing to $T_a = 900\,^{\circ}C$.

## ACKNOWLEDGMENTS

The work was supported by the START project (Project No. Y371) of the Austrian Science Fund (FWF). Further acknowledgements are given to Dr. Krystyna Spiradek-Hahn and Manfred Brabetz of ADG Seibersdorf for supporting with HRTEM investigations.

[1] B. Navinšek, P. Panjan, and I. Milošev, Surf. Coat. Technol. **97**, 182 (1997).
[2] J. W. Seok, N. M. Jadeed, and R. Y. Lin, Surf. Coat. Technol. **138**, 14 (2001).
[3] B. Navinšek and P. Panjan, Surf. Coat. Technol. **74-75**, 919 (1995).
[4] Y. L. Su and S. H. Yao, Wear **205**, 112 (1997).
[5] W. Ernst, J. Neidhardt, H. Willmann, B. Sartory, P. H. Mayrhofer, and C. Mitterer, Thin Solid Films **517**, 568 (2008).
[6] P. Mayrhofer, C. Mitterer, and H. Clemens, Advanced Engineering Materials **7**, 1071 (2005).
[7] P. Mayrhofer, F. Rovere, M. Moser, C. Strondl, and R. Tietema, Scr. Mater. **57**, 249 (2007).
[8] A. Kumar, H. L. Chan, J. J. Weimer, and L. Sanderson, Thin Solid Films **309**, 406 (1997).
[9] J.-E. Sundgren, Thin Solid Films **128**, 21 (1985).
[10] I. Petrov, L. Hultman, and J. E. Sundgren, J. Vac. Sci. Technol. A **10**, 265 (1992).
[11] J. Vetter, Surf. Coat. Technol. **76-77**, 719 (1995).
[12] O. Banakh, Surf. Coat. Technol. **163-164**, 57 (2003).
[13] Y. Otani and S. Hofmann, Thin Solid Films **287**, 188 (1996).
[14] S. PalDey and S. C. Deevi, Mater. Sci. Eng. **342**, 58 (2003).
[15] F. Rovere and P. H. Mayrhofer, J. Vac. Sci. Technol. A **25**, 1336 (2007).
[16] Q. Yang, C. He, L. R. Zhao, and J.-P. Immarigeon, Scr. Mater. **46**, 293 (2002).
[17] J. Paulitsch, P. H. Mayrhofer, W.-D. Münz, and M. Schenkel, Thin Solid Films **517**, 1239 (2008).
[18] J. Lin, J. J. Moore, B. Mishra, M. Pinkas, and W. D. Sproul, Surf. Coat. Technol. **204**, 936 (2009).
[19] Y. Kim, T. Byun, and J. Han, Superlattice Microst. **45**, 73 (2009).
[20] S. Tien and J. Duh, Thin Solid Films **494**, 173 (2006).
[21] B. Yang, L. Chen, K. K. Chang, W. Pan, Y. B. Peng, Y. Du, and Y. Liu, Int. J. Refract. Met. Hard Mater. **35**, 235 (2012).
[22] G. Kim, S. Lee, and J. Hahn, Surf. Coat. Technol. **193**, 213 (2005).
[23] K. Kutschej, P. H. Mayrhofer, M. Kathrein, P. Polcik, R. Tessadri, and C. Mitterer, Surf. Coat. Technol. **200**, 2358 (2005).
[24] H. Barshilia, N. Selvakumar, B. Deepthi, and K. Rajam, Surf. Coat. Technol. **201**, 2193 (2006).
[25] M. Brizuela, A. Garcia-Luis, I. Braceras, J. I. Oñate, J. C. Sánchez-López, D. Martínez-Martínez, C. López-Cartes, and A. Fernández, Surf. Coat. Technol. **200**, 192 (2005).
[26] A. E. Reiter, V. H. Derflinger, B. Hanselmann, T. Bachmann, and B. Sartory, Surf. Coat. Technol. **200**, 2114 (2005).
[27] J. Romero, M. A. Gómez, J. Esteve, F. Montalà, L. Carreras, M. Grifol, and A. Lousa, Thin Solid Films **515**, 113 (2006).
[28] M. Kawate, A. Kimura Hashimoto, and T. Suzuki, Surf. Coat. Technol. **165**, 163 (2003).

[29] J. Vetter, E. Lugscheider, and S. Guerreiro, Surf. Coat. Technol. **98**, 1233 (1998).
[30] M. Zhu, M. Li, and Y. Zhou, Surf. Coat. Technol. **201**, 2878 (2006).
[31] F. Rovere, P. H. Mayrhofer, A. Reinholdt, J. Mayer, and J. M. Schneider, Surf. Coat. Technol. **202**, 5870 (2008).
[32] J. Park and Y. Baik, Surf. Coat. Technol. **200**, 1519 (2005).
[33] P. E. Hovsepian and W.-D. Münz, Vacuum **69**, 27 (2002).
[34] Y.-C. Chan, H.-W. Chen, P.-S. Chao, J.-G. Duh, and J.-W. Lee, Vacuum **87**, 195 (2013).
[35] J. Lin, N. Zhang, Z. Wu, W. D. Sproul, M. Kaufman, M. Lei, and J. J. Moore, Surf. Coat. Technol. , in press; doi: 10.1016/j.surfcoat.2011.11.037 (2011).
[36] M. Stueber, H. Holleck, H. Leiste, K. Seemann, S. Ulrich, and C. Ziebert, J. Alloys Compd. **483**, 321 (2009).
[37] U. Helmersson, S. Todorova, S. A. Barnett, J.-E. Sundgren, L. C. Markert, and J. E. Greene, J. Appl. Phys. **62**, 481 (1987).
[38] C.-L. Liang, G.-A. Cheng, R.-T. Zheng, and H.-P. Liu, Thin Solid Films **520**, 813 (2011).
[39] Y. Zhao, L. Hu, G. Lin, J. Xiao, C. Dong, and B. Yu, Int. J. Refract. Met. Hard Mater. **32**, 27 (2012).
[40] T. A. Rawdanowicz, V. Godbole, J. Narayan, J. Sankar, and A. Sharma, Compos. Part B: Eng. **30**, 657 (1999).
[41] J. Lao, Z. Han, J. Tian, and G. Li, Mater. Lett. **58**, 859 (2004).
[42] G. S. Kim, S. Y. Lee, and J. H. Hahn, Surf. Coat. Technol. **171**, 91 (2002).
[43] V. Braic, C. Zoita, M. Balaceanu, A. Kiss, A. Vladescu, A. Popescu, and M. Braic, Surf. Coat. Technol. **204**, 1925 (2010).
[44] M.-K. Wu, J.-W. Lee, Y.-C. Chan, H.-W. Chen, and J.-G. Duh, Surf. Coat. Technol. **206**, 1886 (2011).
[45] S. Inoue, F. Okada, and K. Koterazawa, Vacuum **66**, 227 (2002).
[46] P. H. Mayrhofer, G. Tischler, and C. Mitterer, Surf. Coat. Technol. **142-144**, 78 (2001).
[47] N. Christensen and I. Gorczyca, Phys. Rev. B **47**, 4307 (1993).
[48] V. Chawla, D. Holec, and P. H. Mayrhofer, J. Phys. D: Appl. Phys. **46**, 045305 (2013).
[49] R. F. Zhang and S. Vepřek, Acta Mater. **57**, 2259 (2009).
[50] P. H. Mayrhofer, D. Music, and J. M. Schneider, J. Appl. Phys. **100**, 094906 (2006).
[51] W. C. Oliver and G. M. Pharr, J. Mater. Res. **7**, 1564 (1992).
[52] *Powder Diffraction File 03-065-2899 (fccCrN), 01-076-0702 (hcpAlN)* (International Center for Diffraction Data, PDF-2/Release, 2005).
[53] J. Lin, J. J. Moore, B. Mishra, M. Pinkas, X. Zhang, and W. D. Sproul, Thin Solid Films **517**, 5798 (2009).
[54] Q. Li, I. W. Kim, S. A. Barnett, and L. D. Marks, J. Mater. Res. **17**, 1224 (2002).
[55] R. Daniel, K. Martinschitz, J. Keckes, and C. Mitterer, Acta Mater. **58**, 2621 (2010).
[56] M. Ohring, *The material science of thin films* (Academic Press, San Diego, California, 1991).
[57] F. Rovere and P. H. Mayrhofer, J. Vac. Sci. Technol. A **26**, 29 (2008).
[58] L. Spieß, G. Teichert, R. Schwarzer, H. Behnken, and C. Genzel, *Moderne Röntgenbeugung* (Vieweg+Teubner, Wiesbaden, 2009) p. 564.
[59] H. Willmann, P. H. Mayrhofer, L. Hultman, and C. Mitterer, J. Mater. Res. **23**, 2880 (2008).
[60] R. Rachbauer, S. Massl, E. Stergar, D. Holec, D. Kiener, J. Keckes, J. Patscheider, M. Stiefel, H. Leitner, and P. H. Mayrhofer, J. Appl. Phys. **110**, 023515 (2011).
[61] D. Rafaja, C. Wüstefeld, M. Dopita, V. Klemm, D. Heger, G. Schreiber, and M. Šíma, Surf. Coat. Technol. **203**, 572 (2008).

# Publication IV



*Effects of structure and interfaces on fracture toughness of CrN/AlN multilayer coatings*
**M. Schlögl**, C. Kirchlechner, J. Paulitsch, J. Keckes, P.H. Mayrhofer
Manuscript submitted to Scripta Materialia.

# Effects of structure and interfaces on fracture toughness of CrN/AlN multilayer coatings

M. Schlögl,[1] C. Kirchlechner,[2] J. Paulitsch,[3] J. Keckes,[2,4] and P.H. Mayrhofer[3]

[1] *Department of Physical Metallurgy and Materials Testing, Montanuniversität Leoben, A-8700 Leoben, Austria*
[2] *Department of Materials Physics and Erich Schmid Institute of Materials Science, Montanuniversität Leoben, A-8700 Leoben, Austria*
[3] *Institute of Materials Science and Technology, Vienna University of Technology, A-1040 Vienna, Austria*
[4] *Materials Center Leoben Forschung GmbH, A-8700 Leoben, Austria*

In-situ scanning electron microscopy compression tests clearly demonstrate that a multi-layered arrangement of CrN and AlN–when stabilized by coherency strains to its cubic metastable phase for AlN layer thicknesses below 3 nm–exhibits increased fracture toughness as compared to single-layered CrN. This allows increasing the maximum loading from ∼ 5.25 to 6.8 GPa. If the AlN layers mainly crystallize in their stable wurtzite structure–for thicknesses above 3 nm–spontaneous and fatal cracking occurs already for 3.8 GPa loads.

Keywords: sputtering, CrN/AlN multilayers, fracture, crack, coating



Ceramic hard coatings are widely used for various industrial applications because of their outstanding properties like high thermal stability, oxidation resistance and abrasion resistance [1, 2]. Particularly, transition metal nitrides, such as CrN are well known and investigated with respect to their microstructure, morphology, thermal and mechanical properties [3–8]. However, the brittleness of these ceramic like coatings often reduces their field of application due to spontaneous failure as soon as a crack is initiated. Therefore, many investigations focus on enhancing the film ductility by architectural approaches or variations in chemical compositions [2]. Recent studies showed self-healing abilities of MAX phases after crack-initiation due to the formation of an oxide phase at the crack tip [9–11]. However, deposition of a multilayer arrangement indicated to be promising as due to the interfaces and their differences in elasticity or morphology, blunting of the crack tip by plastic deformation, crack branching or inhibiting of dislocation movement can be obtained [12–14].

CrN/AlN multilayer coatings are well investigated, as they show high mechanical properties and oxidation resistance, which are main requirements for advanced machining and high temperature applications [15, 16]. Furthermore, AlN can be easily stabilized in its metastable cubic (c) structure within a CrN/AlN multilayer system by keeping the AlN layer thicknesses below ∼ 3 nm, otherwise the stable wurtzite (w) phase will be formed [17]. Deposition of CrN/AlN multilayer coatings results, due to the lattice-mismatch of c-CrN ($a = 4.149$ Å [18]) and the metastable c-AlN ($a = 4.06$ Å [19]), in compressive stresses at the interface near regions of the CrN layers. Allowing the c-AlN to transform into its stable w-AlN structure by e.g. an open surface area due to a crack, the specific volume of AlN will increase by around 26% [20, 21]. Such an increase at the free surface of a crack can influence its propagation by absorbing energy, deflecting or even stopping the crack. Such a strain-induced phase-transformation of AlN is similar to that of yttrium stabilized tetragonal zirconia polycrystalline (Y-TZP), exhibiting excellent flexural strength and fracture toughness [22–24]. However, evaluating the properties of a few m thick films is still a challenge. Hence a number of testing methods such as tensile tests, indentation tests, scratch tests or blister tests have been developed in recent years, especially for studying the fracture toughness of thin film materials [25–28].

Within this work a new approach of in-situ scanning electron microscopy (SEM) micro-compression tests were conducted to evaluate the fracture mechanism of CrN and CrN/AlN multilayer coatings. For the latter, the AlN layers are either ∼ 3 or ∼ 10 nm thin to guarantee for a cubic-stabilization or not, respectively. Thereby, not only the influence of cubic-stabilized and non-cubic-stabilized AlN layers on the fracture behavior is investigated but also the influence of either coherent or non-coherent interfaces. Furthermore, in order to minimize the influence of the additional AlN phases on the mechanical properties of the multilayer coatings, we kept the overall AlN-layer rather small (< 14%), see also [29].

Monolithically grown CrN as well as CrN/AlN multilayer coatings, with either 3 or 10 nm thin AlN layers were deposited on Si (1 0 0) platelets ($20 \times 7 \times 0.38$ mm$^3$) in an AJA Orion 5 lab scaled unbalanced magnetron sputtering system. A computer controlled shutter system enabled reproducible deposition of coatings with alternating layers of CrN and AlN. Two inch Cr and Al targets (purity of 99.9%) were used and powered in dc mode at 14.8 W/cm$^2$ and rf mode at 9.87 W/cm$^2$, respectively. The coatings were prepared in an Ar/$N_2$ mixture with a flow-rate ratio of 3/2 at a substrate temperature of 500 °C and a total pressure of 0.4 Pa. Prior to depositions, the substrates were rf-etched for 5 minutes in an Ar glow discharge at a total pressure of 3 Pa and the targets were sputter-cleaned (sputter power density of 14.8 W/cm$^2$ for 3 minutes. During deposition a −70 V rf-biasing of the substrates was used to assure for a dense coating morphology. The multilayer arrangement was

kept similar for all depositions having CrN as starting layer at the substrate interface and as a top-layer.

Preparation of free-standing micro-pillars ($2 \times 1 \times 1\ \mu m^3$) for the micro-compression tests were carried out by a focused ion beam (FIB) workstation (Zeiss, XB1540). Prior to FIB preparation the Si substrates were separated from the $\sim 1\ \mu m$ thick coatings by dissolving in a 60 °C heated stirred potassium hydroxide (30 wt.%) aqueous solution for 1 h.

The fracture behavior of our multilayer coatings was investigated in a field emission scanning electron microscope (Zeiss, LEO 982). The samples were loaded using a conical diamond microindenter (ASMEC, UNAT) with a punch diameter of 20 µm, using a normal loading perpendicular to the growth direction, hence along the interfaces between CrN and AlN layers.

The mechanical loading of the pillars was performed in-situ in displacement controlled mode with a constant loading speed of 85 nm/s [30]. The evaluated load-displacement curves were calculated to engineering stress–displacement values according to [31].

Detailed investigation on the coating morphologies were conducted by a Phillips CM12 transmission electron microscope (TEM) operating at 120 kV and a Tecnai F20 high resolution transmission electron microscope (HRTEM) operating at 200 kV.

All coatings investigated exhibit a dense columnar morphology with smooth surfaces, not shown. Cross-sectional TEM investigations of our multilayer coatings exhibit either $\sim 3$ or 10 nm thin AlN layers (bright contrasts) see Figs. 1a and b respectively. The CrN layers (dark contrast) were kept constant at $\sim 110$ nm for both multilayer types. The coatings with $\sim 3$ nm thin AlN layers exhibit large columnar grains expanding over several CrN and AlN layers (Fig. 1a), suggesting epitaxial growth of the CrN and AlN layers. Hence, the AlN layer should be stabilized in its cubic metastable structure by epitaxial strain. This is confirmed by HRTEM investigations clearly suggesting a cubic structure for the $\sim 3$ nm thin AlN layers, as continuous lattice planes through the c-CrN and AlN layers can be seen, Fig. 1c. Additionally, Fast Fourier Transformation (FFT) evaluations (inset in Fig. 1c) confirm the cubic structure for AlN and indicate a 2 0 0 lattice spacing of 2.06 Å [32]. Increasing the AlN layer thickness to 10 nm leads to a loss of the epitaxial growth of AlN on CrN, Fig. 1d. Although, continuing lattice fringes near the CrN/AlN interfaces can be found, the coherency breaks soon leading to the formation of new crystals. The FFT of an area in the middle of the AlN layer (inset in Fig. 1d) represents a wurtzite-type structure with 0 0 2- and 1 1 1-lattice spacing of 2.485 and 2.663 Å, respectively [33]. Consequently, also the CrN columnar grains are smaller due to the necessary re-nucleation of the cubic CrN structure on top of the AlN layers, see Fig. 1b. For an easier reading we refer to these two multilayers with CrN/c-AlN and CrN/w-AlN, although the $\sim 10$ nm thick AlN layers are not completely wurtzite structured.

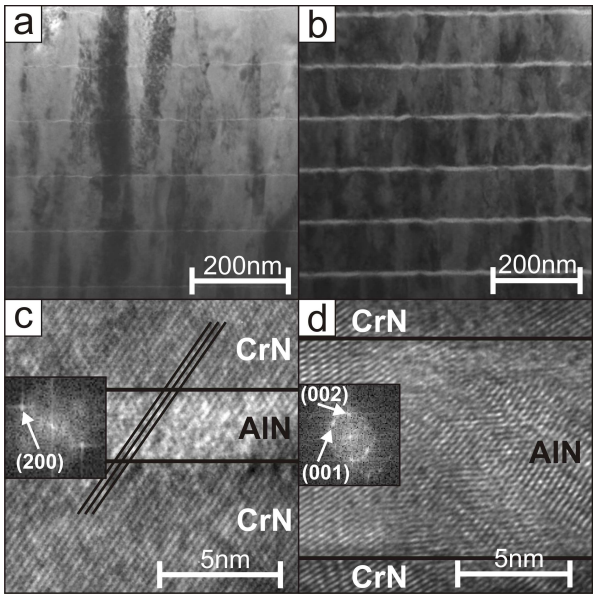


FIG. 1. TEM and HRTEM cross section images of as deposited (a,c) CrN/c-AlN (3 nm AlN layers) and (b,d) CrN/w-AlN (10 nm AlN layers) multilayer coatings. The inset in (c) and (d) is a FFT image indicating cubic and wurtzite structure, respectively.

The hardness of the coatings is $23 \pm 1.20$ GPa for CrN, $23 \pm 0.67$ GPa for CrN/c-AlN and $26 \pm 0.95$ GPa for CrN/w-AlN as also presented in [29].

In-situ SEM observations during compression testing of CrN and CrN/w-AlN multilayer coatings are given in Figs. 2a1-3 and b1-3, respectively. During compression of CrN (Fig. 2a2) no other changes in geometry of the pillar than elastically driven ones can be observed during loading. For comparison, Fig. 2a1 shows the unloaded pillar. However, after a critical load of $\sim 5.25$ GPa the samples immediately crack, Fig. 2a3. The cracking is initiated by shearing processes, which can be identified in Fig. 2a2 (marked by white arrows), which is the very last image-frame detected before cracking occurs.

The CrN/w-AlN multilayer coatings (Fig. 2b) exhibit a very similar behavior during compression as the CrN coating. However, for CrN/w-AlN coatings no shearing can be observed, due to the presence of w-AlN layers, which provide different shearing planes than the c-CrN layers. Hence, the CrN/w-AlN multilayer coating-pillar instantly fails without pre-damage at an even 1.5 GPa lower maximum load ($\sim 3.8$ GPa) than the CrN coating. Detailed SEM investigations of the fracture pattern of the coatings (Fig. 2b4-5) suggest that the crack initiation takes place at the interface between the c-CrN and w-AlN layers.

The CrN/c-AlN multilayer coatings exhibit a completely different behavior during the compression tests, Fig. 3a-d. Applying a certain critical normal load on

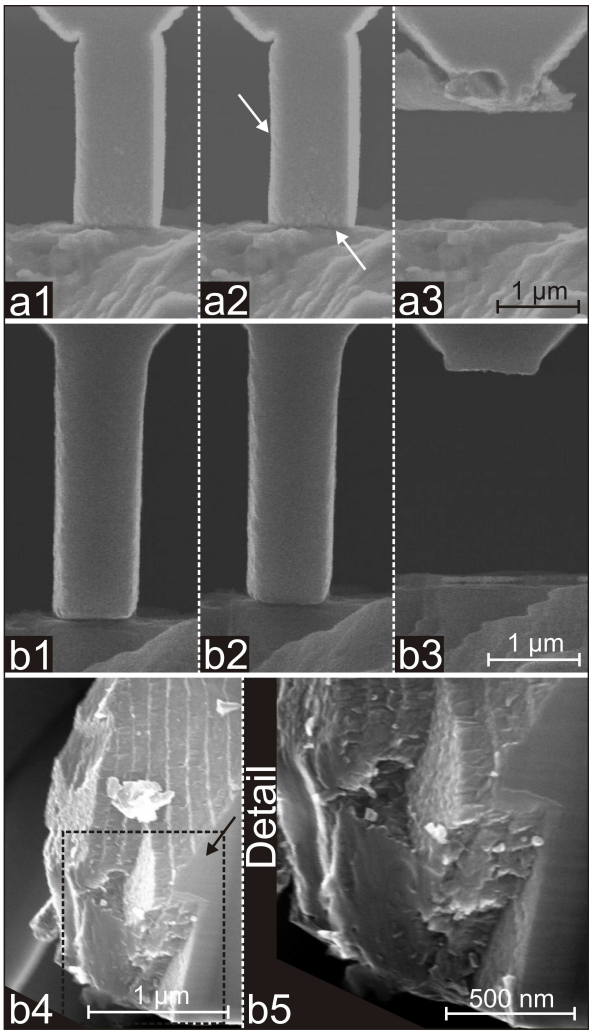


FIG. 2. SEM images during the compression tests of our coating pillars consisting of (a1-a3) monolithically grown CrN and (b1-b5) CrN/w-AlN multilayer. The SEM images given in (a1) and (b1) represent the pillars at the beginning of the test while (a3) and (b3) are taken after the test. The images in (b4) and (b5) show shearing at the interface within fracture fragments of CrN/w-AlN in more detail.

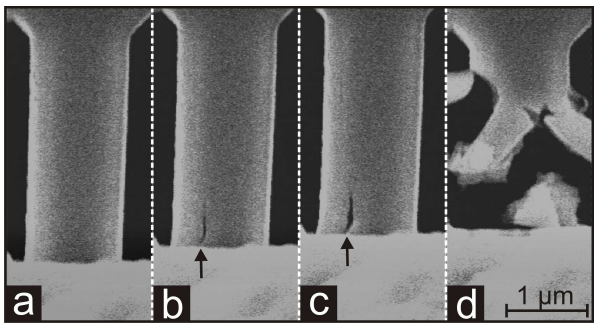


FIG. 3. SEM images during the compression tests of our CrN/c-AlN multilayer coating pillars (a-d). The image in (a) shows the pillar at the beginning of the test and (d) shows the fracture pattern after damage. Image (b) and (c) indicate crack growth during loading (marked by arrows).

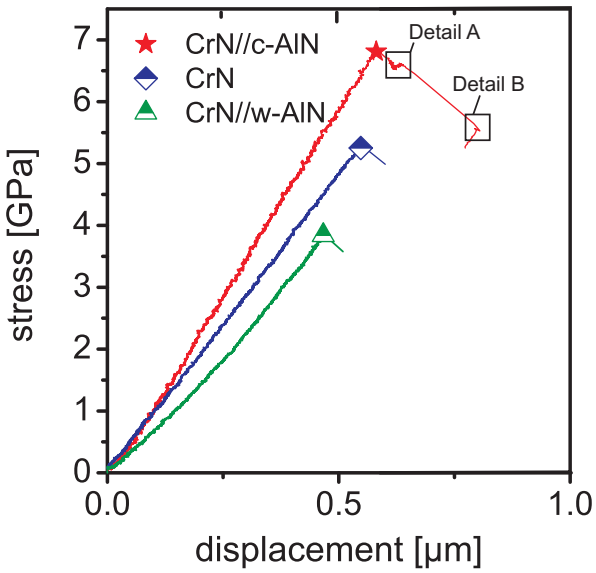


FIG. 4. Stress–displacement curves of our coatings consisting of monolithically grown CrN, CrN/w-AlN and CrN/c-AlN multilayer during compression tests.

the pillar initiates a crack, indicated in Fig. 3b, starting at the indenter contact area. This crack initiation does not cause a significant feature in the recorded stress-displacement curve, Fig. 4, making an identification of the critical load difficult. Further loading of the sample results in crack propagation along the loading direction, being in-plane of the layered coating without its spontaneous breaking (Fig. 3c). Only for a load above 6.8 GPa breaking of the pillar occurs, but the fracture pattern suggests the formation of a crack network, Fig. 3d. This is in contrast to the other coating materials where a critical load resulted in fatal cracking of these generally brittle hard coatings. All of our coatings exhibit a linear elastic behavior in the load-displacement curve, Fig. 4. However, the load-displacement curves of CrN/c-AlN coatings present two discontinuous features after the load-maximum of $\sim 6.8$ GPa, marked as detail A and B. These features suggest that crack propagation is inhibited, and hence also indicate a more ductile-like cracking behavior of the CrN/c-AlN coating. Furthermore, the slopes of the load-displacement curves increase from CrN/w-AlN to CrN to CrN/c-AlN suggesting an increasing stiffness, respectively. Due to the unknown compliance of the measuring system the Youngs modulus of the coatings cannot be evaluated.

The differences in fracture behavior of our coatings can be explained by the contribution of the structural modifications at the interfaces, which are different for the three coating types investigated. The basically single-layer CrN coating serves as a benchmark for comparison. The other two exhibit additional AlN layers, either mainly in their stable structure w-AlN (CrN/w-AlN) or in their metastable structure c-AlN (CrN/c-AlN), cf. Figs. 3b and d. Due to the different crystal structure and their lattice mismatch, the CrN/w-AlN coatings exhibit mainly incoherent interfaces between the w-AlN and the c-CrN layers. Contrary, the CrN/c-AlN coatings are characterized by coherent interfaces between the individual layers. The stabilization of the AlN layers in their cubic metastable structure (which is the high-pressure phase of AlN [16]) is based on the coherent growth onto the cubic CrN layers, which exhibit a very small lattice mismatch of $\sim 2\%$ in the 2 0 0 and 1 1 1 directions. Important to mention is also that a phase transformation from c-AlN to w-AlN is connected with an increase in specific volume of $\sim 26\%$ [20, 21, 34]. Hence, if the c-AlN layers–stabilized by coherency strain–are unstrained, a volume expansion by $\sim 26\%$ is expected. Such a relief of strains can occur if the coating experiences tensile loading or if a crack is formed close to the AlN layers or at the interfaces between CrN and AlN layers. Please remember that the experimental setup was chosen in a way that the compressive loading direction is in-plane of the layered coatings, hence along the interfaces between CrN and AlN layers. Consequently, the lateral contraction leads to an expansion perpendicular to the loading direction. As the CrN/w-AlN coatings mainly exhibit incoherent interfaces between the c-CrN and w-AlN layers, which are generally weaker than the coherent interfaces between c-CrN and c-AlN [35–37], the elastic strains will cause crack initiation at these interfaces. This is easier at such interfaces than within the bulk, as incoherent interfaces are generally areas of a high defect density. Therefore, the CrN/w-AlN coatings exhibit a weaker behavior during the loading experiments than the single layered CrN coatings. The reason for a better behavior of the CrN/c-AlN coatings is at least two-fold; the stronger coherent interfaces between the c-CrN and the c-AlN layers and the driving force of c-AlN to phase-transform to w-AlN under expansion. As mentioned, our material will experience compression in the loading direction but expansion perpendicular to it. Any phase transformation–triggered by the additional tensile strains during loading–of c-AlN towards its stable configuration w-AlN with the connected volume increase of $\sim 26\%$ allows reducing the tensile strains present. Hence, even higher loads are necessary before a crack is initiated, or even if a crack is initiated, its propagation during further loading is reduced. The results obtained for our multilayer coatings open promising prospects in increasing the fracture toughness of generally brittle ceramic materials such as transition metal nitrides by providing mechanisms for tensile strain reduction, crack deflection, crack arrest and crack stop mechanisms.

In conclusion, single-layered CrN and multi-layered CrN/AlN, with either cubic (c) or wurtzite (w) AlN layers, were prepared by magnetron sputtering and investigated for their fraction behavior. Based on our results we can conclude that the CrN/AlN multilayer coatings provide increased resistance against crack initiation and propagation when the AlN layers are stabilized in their metastable cubic structure. In-situ SEM compression tests of CrN and multi-layered CrN/w-AlN coatings exhibit spontaneous failure as soon as a crack is initiated. Simultaneously recorded load-displacement curves present a maximum compressive fracture stress of $\sim 5.25$ and $\sim 3.8$ GPa for CrN and CrN/w-AlN, respectively. Contrary, CrN/c-AlN multilayer coatings only fail if the loading exceeds 6.8 GPa. In-situ SEM observations clearly present a ductile-like behaviour for these CrN/c-AlN multilayers as an initiated crack only slowly propagates and even experiences deflection during loading. Based on the results obtained we propose that the formation of coherent interfaces between c-CrN and c-AlN together with the driving force of c-AlN to phase transform towards its stable w-AlN structure with the connected volume increase of $\sim 26\%$ is responsible for the increased fracture toughness of this type of multilayers. This allows for the development of a new class of AlN toughened hard coatings.

**ACKNOWLEDGMENTS**

This work is supported by the START project (Y371) of the Austrian Science Fund FWF. Matthias Nöhrer and Dr. Daniel Kiener are highly acknowledged for their support with HRTEM investigations.

[1] A. Kumar, H. L. Chan, J. J. Weimer, and L. Sanderson, Thin Solid Films **309**, 406 (1997).
[2] U. Wiklund, P. Hedenqvist, and S. Hogmark, Surf. Coat. Technol. **97**, 773 (1997).
[3] P. Mayrhofer, F. Rovere, M. Moser, C. Strondl, and R. Tietema, Scr. Mater. **57**, 249 (2007).
[4] H. Willmann, P. Mayrhofer, P. Persson, A. Reiter, L. Hultman, and C. Mitterer, Scr. Mater. **54**, 1847 (2006).
[5] P. H. Mayrhofer, C. Mitterer, L. Hultman, and H. Clemens, Prog. Mater. Sci. **51**, 1032 (2006).
[6] L. Hultman, Vacuum **57**, 1 (2000).
[7] L. Cunha, M. Andritschky, K. Pischow, and Z. Wang, Thin Solid Films **355-356**, 465 (1999).
[8] H. Barshilia, N. Selvakumar, B. Deepthi, and K. Rajam, Surf. Coat. Technol. **201**, 2193 (2006).

[9] M. Baben, L. Shang, J. Emmerlich, and J. M. Schneider, Acta Mater. **60**, 4810 (2012).
[10] D. P. Sigumonrong, J. Zhang, Y. Zhou, D. Music, J. Emmerlich, J. Mayer, and J. M. Schneider, Scr. Mater. **64**, 347 (2011).
[11] G. Song, Y. Pei, W. Sloof, S. Li, J. De Hosson, and S. van der Zwaag, Scr. Mater. **58**, 13 (2008).
[12] A. A. Voevodin, Surf. Coat. Technol. **148**, 38 (2001).
[13] H. Holleck and V. Schier, Surf. Coat. Technol. **76-77**, 328 (1995).
[14] C. Subramanian, Wear **241**, 228 (2000).
[15] S. Tien and J. Duh, Thin Solid Films **494**, 173 (2006).
[16] G. Beshkov, G. Vassilev, M. Elizalde, and T. Gomez-Acebo, Mater. Chem. Phys. **82**, 452 (2003).
[17] J. Lin, J. Moore, B. Mishra, M. Pinkas, and W. Sproul, Surf. Coat. Technol. **204**, 936 (2009).
[18] *Powder Diffraction File 03-065-2899* (International Center for Diffraction Data, PDF-2/Release, 2005).
[19] Q. Li, I. W. Kim, S. A. Barnett, and L. D. Marks, J. Mater. Res. **17**, 1224 (2002).
[20] P. H. Mayrhofer, D. Music, and J. M. Schneider, J. Appl. Phys. **100**, 094906 (2006).
[21] P. H. Mayrhofer, H. Willmann, and A. Reiter, Soc. Vac. Coat. , 575 (2006).
[22] P. M. Kelly and L. R. F. Rose, Prog. Mater. Sci. **47**, 463 (2002).
[23] S. Wang, X. Huang, J. Guo, and B. Li, Mater. Lett. , 43 (1996).
[24] N. Bamba, J. Eur. Ceram. Soc. **23**, 773 (2003).
[25] P. Zhao, C. Sun, X. Zhu, F. Shang, and C. Li, Surf. Coat. Technol. **204**, 4066 (2010).
[26] L. Qian, Surf. Coat. Technol. **173**, 178 (2003).
[27] M. Watanabe, S. Kuroda, K. Yokoyama, T. Inoue, and Y. Gotoh, Surf. Coat. Technol. **202**, 1746 (2008).
[28] A. Ray, J. Eur. Ceram. Soc. **19**, 2097 (1999).
[29] M. Schlögl, B. Mayer, J. Paulitsch, and P. H. Mayrhofer, to be published in Thin Solid Films (2012).
[30] C. Kirchlechner, D. Kiener, C. Motz, S. Labat, N. Vaxelaire, O. Perroud, J.-S. Micha, O. Ulrich, O. Thomas, G. Dehm, and J. Keckes, Phil. Mag. **91**, 1256 (2011).
[31] A. S. Argon, *Strengthening mechanisms in crystal plasticity* (Oxford University Press, Oxford, 2008).
[32] *Powder Diffraction File 00-025-1495* (International Center for Diffraction Data, PDF-2/Release, 2007).
[33] *Powder Diffraction File 01-076-0702 (hcpAlN)* (International Center for Diffraction Data, PDF-2/Release, 2005).
[34] P. Mayrhofer, F. Fischer, H. Böhm, C. Mitterer, and J. Schneider, Acta Mater. **55**, 1441 (2007).
[35] S. N. Medyanik and S. Shao, Comp. Mat. Sci. **45**, 1129 (2009).
[36] J. W. Martin, R. D. Doherty, and B. Cantor, *Stability of Microstructure in Metallic Systems*, 2nd ed. (Cambridge University Press, 1997) p. 444.
[37] D. Porter and K. Easterling, *Phase transformations in metals and alloys*, 3rd ed. (CRC Press, New York, 2009) p. 500.